Nonlinear elasticity in nanostructured materials

2011 Rep. Prog. Phys. 74 116501

(http://iopscience.iop.org/0034-4885/74/11/116501)

Rep. Prog. Phys. **74** (2011) 116501 (35pp) doi:10.1088/0034-4885/74/11/116501

Nonlinear elasticity in nanostructured materials

Luciano Colombo[1] **and Stefano Giordano**[2]

[1] Department of Physics, University of Cagliari and CNR-IOM, Unità SLACS Cittadella Universitaria, 09042 Monserrato (Ca), Italy
[2] Joint International Laboratory LEMAC, Institute of Electronics, Microelectronic and Nanotechnology (UMR CNRS 8520) PRES University North of France, ECLille, Avenue Poincaré, BP 60069, 59652, Villeneuve d'Ascq, France

E-mail: luciano.colombo@dsf.unica.it and stefano.giordano@iemn.univ-lille1.fr

Received 6 April 2011, in final form 10 June 2011
Published 14 October 2011
Online at stacks.iop.org/RoPP/74/116501

Abstract
We elaborate on a blended continuum/atomistic theoretical picture of the nonlinear elastic properties of nanostructured materials, looking at diverse aspects such as dispersions of inhomogeneities within a matrix, random or graded nanograined materials, two-dimensional atomic sheets. In particular, we discuss the possible onset of length-scale effects and we establish the limits and merits of continuum versus atomistics. While most situations here discussed correspond to model systems, the main conclusions have a paradigmatic relevance and indeed apply to most nanomaterials of current interest.

This article was invited by S Washburn.

Contents

List of symbols

x_i, X_i, r_i	position vectors
u_i	displacement vector
$F_{i,j}$, $J_{i,j}$	deformation and displacement gradients
ϵ_{ij}, Ω_{ij}	small-strain and local-rotation tensors
T_{ij}	Cauchy stress tensor
δ_{ij}	Kroenecker symbol
U	strain energy function
$\mathcal{C}_{ijkh}$ or $\mathcal{C}_{pq}$ (Voigt)	second-order elastic constants

C_{ijkhnm} or C_{pql} (Voigt)	third-order elastic constants
λ and μ	Lamè coefficients
E_{3D} and ν_{3D}	Young's modulus and Poisson's ratio (3D)
E and ν	Young's modulus and Poisson's ratio (2D)
K	bulk modulus (3D)
k	bulk modulus (2D)
$\mathcal{S}_{ijhk}$	Eshelby tensor
Λ_1, Λ_2, Λ_3	nonlinear elastic coefficients
A, B, C	nonlinear Landau moduli (3D)
e, f	nonlinear Landau moduli (2D)
κ_l, γ_l, κ_h, γ_h, κ_a, γ_a	interatomic potential parameters
$D_{\vec{n}}$	effective nonlinear modulus (graphene, graphane)
L^{I} and L^{II}	linear and nonlinear longitudinal coefficients
T^{I} and T^{II}	linear and nonlinear transversal coefficients

1. Introduction

In principle, any nanostructured material can be conceptualized as a distribution of nanoscale inhomogeneities, embedded within an otherwise homogeneous hosting matrix. This very general picture, in fact, embodies the specific case of an isolated nanoparticle (such as a buried quantum dot or a hard/soft elastic inclusion), the more general case of a dispersion of inhomogeneities (forming, for instance, a nanograined material or a nanograded interface) or even the case of a fiber-reinforced matrix or a texture of nanograins. The same model also applies to nanoporous systems, as well as to multicracked materials. While in the last two examples the inhomogeneities are indeed represented by void volumes, in the previous ones they rather correspond to a second-phase material with unlike physical properties with respect to the hosting matrix.

Nanostructured materials play a major role in modern materials physics, both for the investigation on fundamental properties of condensed matter at the nanoscale (most of which are affected by the interplay between quantum mechanical features and confinement or length-scale issues) and for their large technological impact (basically due to the fact that their functional and structural properties can be tailored by varying the nanoparticles size and shape). As a matter of fact, nanostructured materials are nowadays investigated in fields as diverse as nano-/opto-electronics or photonics, energy harvesting and production, advanced structural engineering, information and communication technologies and even environmental sciences and biotechnology [1–4].

The elastic properties of nanostructured systems are crucially important since they are central to determine their overall mechanical behavior upon loading, as well as to affect their microstructure evolution during growth or self-assembling [5, 6]. Furthermore, in very many cases of practical relevance nanostructured systems are subjected to deformations (either intentional or accidental) with respect to their reference (i.e. ideally underformed) state and, therefore, the physical properties of interest are those of a strained, rather than pristine, system. It is then very important to develop concepts, formal devices and numerical tools to properly model the elastic features of such complex nanosystems. This review is precisely addressed to this issue.

To a great extent, just few key words are needed to focus the above topics, namely, *nonlinear elastic effects* and *nanoscale structural features*. While the first one addresses the physical properties to be considered, the second defines the actual atomic architecture of the specific nanosystem of interest. These two features are tightly entangled and both are underpinned by a third important notion, namely, the possible onset of *length-scale effects*. Therefore, before developing any formal treatment of nonlinear elasticity in nanostructured materials, the concept of elastic nonlinearity is deserving of further elaboration, together with the concept of elastic constitutive equation and the notion of length scale.

1.1. The concept of elastic nonlinearity

The starting point of elasticity theory is that materials subjected to loads undergo deformations. This rather intuitive statement is phenomenologically grounded on robust empirical evidence and formally described by the mathematical concepts of *stress* (profiling loads) and *strain* (profiling deformations). The full characterization of the elastic behavior of a deformed material is provided by its *constitutive equation*, namely by a material-specific stress–strain relationship.

The concept of nonlinearity can be introduced in elasticity in two different ways [7, 8]. On the one hand, nonlinear elastic features are exploited by means of the complete (i.e. not approximated) strain–stress relation and the exact equilibrium equations for any given material volume element. This approach is needed when considering *large deformations* [9, 10] and it is referred to as *geometrical nonlinearity*. Its formal description is typically based on unspecific balance equations of general validity. The inherently nonlinear character of finite elasticity makes such a theory a nontrivial one, containing several mathematical and conceptual subtleties. On the other hand, nonlinear elastic features occur even under the approximation of *small deformations*, a situation of considerable practical relevance, whenever the material stress–strain constitutive relation is not Hookean or, equivalently, is not linear. This case is referred to as *material nonlinearity* (sometimes called *physical nonlinearity*), since it is related to the actual physical regime of elastic response of the specific material under consideration.

By exploiting the twofold definition of elastic nonlinearity, we can make a distinction between four different types of problems [8], by combining linear (L) or nonlinear (NL) features either for the material response regime (i.e. Hookean versus nonlinear) or referring to the corresponding geometrical deformation (i.e. small versus large deformations). The following enumeration will be used throughout this review: problems characterized by a Hookean elastic response regime and small deformations will be labeled as *L–L problems*; problems where the material response regime is nonlinear, but deformations are nevertheless small will be referred to as

NL–L problems; problems in the Hookean response regime, but where deformations are large will be named *L–NL problems*; finally, the last possible combination of nonlinear material response with large deformations will define the *NL–NL problems*.

L–L problems are the subject of the classical theory of elasticity (small deformations in Hookean materials) [7, 11]. Within this formalism the main results of solid mechanics have been developed, namely, the classical theory of wave propagation [12], fracture mechanics [13], the continuum theory of dislocations [14] and the Eshelby theory for the elastic behavior of linear inhomogeneities [15, 16]. In L–L problems (as well as in NL–L ones) the angles of rotation can be neglected in determining the resulting length variations of the line elements upon loading and in formulating the conditions of equilibrium for volume elements. The balance equations are based on the standard *small-strain tensor* and on the *Cauchy stress tensor*. However, in NL–L problems the Hookean limit of proportionality between stress and strain is exceeded, thus requiring the use of a nonlinear stress–strain constitutive equation. This conceptual framework is intended to model any perfectly reversible nonlinear stress–strain behavior, but it is restricted to infinitesimal strains [17, 18].

In this review we will address the material nonlinear elastic regime, while avoiding problems where deformations are large. In particular, we will focus on NL–L problems by considering several prototypical configurations of paramount relevance in the modern materials science of nanostructured systems. We note that the more general theory of L–NL and NL–NL problems falls beyond the scope of this work, since they require an explicit formulation of finite elasticity, based on the balance equations (for mass distribution, linear momentum and angular momentum) within the Euler (spatial) and the Lagrangian (material) description. Such topics are addressed elsewhere [7, 8].

1.2. The concept of a constitutive equation

The application of the principles of mechanics to bulk matter is conventionally divided into the *mechanics of fluids* and the *mechanics of solids*. The entire subject is often referred to as *continuum mechanics* [9], assuming that matter be continuously divisible, i.e. making no reference to its atomistic (and, therefore, discrete) structure. This will be hereafter referred to as the *continuum picture*.

Solid mechanics is concerned with the stressing, deformation and failure of solid materials and structures. We call a material *solid* provided that it can support a substantial shearing force, in addition to supporting normal ones (incidentally, we note that only the second feature is equally found in liquids). Shearing (normal) forces are parallel (perpendicular) to the material surface on which they act; the force per unit of area is called shear (normal) stress. Therefore, in the elasticity theory of solids we need constitutive equations describing both normal and shear stresses. More specifically, a *constitutive equation* is a direct relationship (linear or nonlinear) between stress and deformation.

Materials behave very differently upon loading. In the simple (but very common) case when a material is loaded by a sufficiently small stress, its deformation is fully recovered upon unloading. We then say that the material is *elastic*. However, some solids can also be deformed permanently or, equivalently, sometimes deformations are only partially recovered upon unloading. In this more general case we describe the permanent deformation as a plastic one and we name the material *elastic–plastic*. Those permanent deformations which strongly depend on the time of exposure to a stress (and typically increase with time of exposure) are called viscous (or creep) deformations. Materials which exhibit this behavior (as well as an elastic response) are called *viscoelastic solids* (or sometimes viscoplastic solids, when we focus more on the permanent deformations than on the partial recovery of strain upon unloading).

The constitutive stress–strain equation must match the specific observed behavior. Typically, they are determined by experiments and eventually conceptualized in phenomenological equations such as the simple Hooke law describing a linear stress–strain relationship. A variety of mechanical testing machines and geometrical configurations of material specimens have been devised to characterize their behavior [19]. These allow simple tensile, compressive or shear stressing; sometimes they can also apply combined stressing with several different components of stress. The material response over a range of temperature, strain rate and loading history can therefore be measured and fully characterized [19]. In this review we are only concerned with fully recoverable strains and, therefore, we will consider purely elastic (but generally non-Hookean) materials. Moreover, for simplicity, the undeformed state will be always taken to be stress free. We note that the theory of plastic materials is a fascinating and wide topic, beyond the scope of this review. A good introduction to plasticity can be found elsewhere [20].

A different perspective on the stress–strain relation is offered by the modern atomistic theory of materials where, actually, there is no need to define a macroscopic constitutive equation. Rather, materials properties are determined by many-body interactions among their elementary constituents (i.e. atoms or molecules) [21, 22], while their observed behavior upon loading is worked out by the collective response of very many particles to imposed strain or stress fields. In other words, the chemical composition (i.e. the basic information about many-body interactions among elementary constituents) combined with the proper information about the atomic architecture (i.e. the disposition of the atoms or molecules in the space) completely characterize the elastic response to an arbitrary loading condition. Although most materials are properly described only by many-body interactions, selected materials can be approximately treated by pair-wise interactions (such as the Lennard-Jones potential). Nevertheless, we note that the two-body interactions are not sufficient to fully describe the arbitrary mechanical behavior of a solid body. In other words, as extensively discussed below, we can say that at least three-body interactions are mandatory to reproduce the complex mechanical behavior of real isotropic materials accurately [11, 22].

1.3. The notion of length scale

The basic parameter characterizing the distribution of atoms within any material is the interatomic distance, which is the linear distance between two next-neighboring atoms. The continuum picture is meaningful provided that stress and strain fields occur over space regions much larger than the interatomic distance: this is typical of the macroscopic engineering description of materials elasticity [19].

Nanomaterials are indeed characterized by structures varying at a length scale only slightly larger than the interatomic distance. Despite this, the continuum picture has been widely, and indeed very successfully, applied to investigating many elastic features of such systems. The reason is that elasticity theory is a very robust theoretical tool of general validity and applicability (even beyond to what expected according to its initial assumptions). For example, the elastic behavior of heterogeneities larger than about 10 nm (see section 4.2) can be easily captured by continuum mechanics. However, there are many other difficulties, both conceptual and practical, in fully characterizing elastic phenomena at the atomic scale with conventional continuum mechanics. A paradigmatic example is provided by brittle fracture: by linear elastic fracture mechanics (LEFM) it is indeed possible to predict the stress and strain fields near a crack, but it is not possible to evaluate the exact atomic behavior at the crack tip where molecular and chemical phenomena represent the most important features. More precisely, LEFM predicts an infinite enhancement of the stress at the tips of the crack with vanishingly small thickness (slit crack). We note that this nonphysical result is only due to the underlying continuum hypothesis, whereas it does not apply provided that the atomic structure of the real material is properly taken into account (as a matter of fact, it is easy to figure out that, in atomic lattices, the minimum radius of curvature of a crack is approximately of the order of the interatomic distance).

Anyway, the standard elasticity theory provides the most general conceptual framework to elaborate new understanding. In fact, it can be used for (i) inspiring new modelling methodologies; (ii) properly defining border conditions for a generic system under load; (iii) and for comparing the atomistic predictions with their continuum counterparts within a multiscale perspective. As stated above, some care should be taken when the system size scales down and the possible onset of length-scale effects is likely to occur. This can be illustrated by the following example, which is one of the central points of this work. Most of the continuum investigations on heterogeneous systems are elaborated by means of a rather simple paradigmatic model system, named the *Eshelby configuration* [23–25], which consists of a single inhomogeneity embedded in a given homogeneous matrix. The results holding for such a simple configuration can, in fact, be generalized to a dispersion of inhomogeneities (but only in the dilute limit), approaching the more realistic case of a nanocomposite system. The main result of the Eshelby model (and, therefore, the key feature of the resulting continuum predictions) is that elastic fields within and near the inhomogeneity do not depend upon the size of the inhomogeneity itself. For instance, the elastic fields induced by a spherical inhomogeneity (such as a hard inclusion in a ceramic matrix or a void within a homogeneous material) do not depend on its radius. Basically, this defines the very striking feature according to which elastic features in nanostructured systems should be length-scale invariant.

This result is counter-intuitive and unlikely. However, there is no way to go beyond it still using the continuum approach. Rather, a different approach should be usefully adopted, more advisedly based on condensed matter theories so as to explicitly take into consideration atomistic features. In this respect, the application of atomistic simulations are better suited to provide the relevant elastic fields directly onto the discrete lattice of atoms defining the nanomaterial. This approach naturally drives the full characterization of the possible dependence of elastic fields outside, inside or near inclusions depending upon their dimensions, the loading conditions and any possible interface-specific feature.

1.4. The continuum versus the atomistic picture

To a great extent the boundary between continuum and atomistic approaches lies at the nanometer length scale. At this scale matter can hardly be described by a continuous mass distribution, thus questioning the overall validity of the continuum picture, as discussed above. On the other hand, however, typical atomistic models are over-rich in terms of physical information, as far as the mere description of elastic properties is concerned. Therefore, their straightforward application could require an exceedingly large computational workload. Interestingly enough, the above boundary does represent the core of modern nanotechnology [5, 6].

Since both continuum and atomistic pictures have advantages and drawbacks, a dilemma follows, namely, which is the best approach when interested in modeling elastic features of nanostructured materials. Currently, the better answer affirms that neither of them is definitely superior and, as a matter of fact, both are indeed necessary in order to elaborate a full meaningful picture. This has driven the scientific community to elaborate the concept of *multiscale modeling*, namely, the idea according to which continuum and atomistics can be blended together hierarchically, concurrently or by the quasi-continuum scheme [26–29]. However, although many achievements have been made by multiscale methods, we are still quite far from a general, robust and transferable formulation. As a matter of fact, several open problems are still challenging researchers, including conceptual problems in defining the relevant mathematical objects near the continuum/atomistic boundary (such as stress force and elastic fields) and numerical instability problems (for instance, fully reversible mesh refinement or elastic wave reflection). At the present time, multiscale methods, although very promising in perspective, cannot be considered a mature computational tool for the predictive modeling of nanostructured systems.

In this work we follow a different approach by giving privilege to continuum elasticity, in recognition of its paradigmatic validity, reserving to atomistic simulations a subsidiary role. More specifically, for any problem discussed

in the following sections, a continuum picture is at first elaborated and a corresponding elastic model is formally developed. When feasible, such a model is directly solved to get physical insight of the problem. Alternatively, the elastic continuum model is used to define the protocol for suitable atomistic simulations. Such simulations are eventually used to actually calculate all the relevant quantities (such as linear and nonlinear elastic moduli) previously defined by the continuum approach and to search for any possible occurrence of phenomena that fall out of reach of methods describing materials as a continuous mass distribution. According to this perspective, the continuum formalism will play the major role and, therefore, it will be carefully outlined.

1.5. Synopsis of open problems in nonlinear elasticity of nanostructured materials

Most of the open problems in the elasticity of nanostructured materials or systems involve, in some way or another, either length-scale issues and/or nonlinear features.

One active field of research deals with the evaluation of the possible scale effects in the elastic behavior of an embedded nanoinhomogeneity. In particular, it is important to understand the behavior of the elastic fields versus a typical measure of the inhomogeneity (such as the radius for a spherical/cylindrical particle or the axes for an ellipsoidal one) as well as versus its shape. From the point of view of the classical theory of elasticity such elastic fields should not depend on the size, but only on the shape [15, 16]. When the size is nanoscopic this result is no more valid and scale effects can be generated by volume, as well as surface features. In the first case the major role is played by the actual spatial distribution of atoms. On the other hand, the embedding of a given inhomogeneity in a hosting homogeneous matrix is deeply affected by the lattice mismatch and by the possible differences (in shape and size) between the external surface of the particle and the internal surface of the hosting cavity. Both the inclusion and the matrix must accomplish an elastic relaxation to accommodate such a mismatch and, therefore, they admit a state of deformation even if no external load is applied. The possible length-scale effects exhibited by a single inhomogeneity can be reflected in the effective behavior of a composite material formed by a dispersion of nanoparticles in a given matrix. In many cases, imperfect interfacial bonding may exist at the matrix/particle boundary and the interfacial bonding condition may significantly affect the effective properties of the overall heterogeneous structure.

Another important open problem is the so-called nonlinear Eshelby problem. The Eshelby theory provides a fundamental result, namely, the strain field within both a linear or a nonlinear (ellipsoidal) inhomogeneity is uniform when the matrix is linear [15, 16]. In these cases the complete analytical solution is well known for all the elastic fields characterizing the system. In this context, it is typically assumed that no bonding failures occur at the interface when the structure is placed in an equilibrated state of infinitesimal elastic strain. Hence, the boundary conditions require that both the vector displacement and the normal stress be continuous across the interface. When the matrix is nonlinear, the continuum theory poses a really hard problem from the mathematical point of view and, still now, no explicit solutions have been proposed. This suggests that a possible alternative approach could be based on atomistic simulations. In this case a conceptual mapping of the constitutive linear and nonlinear equations of the continuum elasticity theory onto a lattice model is needed, exploiting the real atomistic structure of an embedded nanoinhomogeneity. Such a lattice model naturally introduces the notion of length scale and, therefore, opens the possibility to investigate by computer experiments the combination of scale effects with nonlinear elasticity on the elastic behavior of nanostructured materials. These effects play a major role in many complex systems such as dispersions of inhomogeneities or buried quantum dots [30–34], graded structures [35, 36], complex interfaces [37–40] and nanoalloys or -composites [41–43].

Finally, nonlinear features have been recently reported in the elastic behavior of graphene [44]. As a matter of fact, graphene is the mother structure of any other carbon-based nanosystem such as nanotubes, multi-sheet graphitic layers or even fullerene molecules. Furthermore, it displays many peculiar and intriguing physical properties, most of them affected by in-plane strain (for instance, its zero-gap nature and, therefore, its electron transport features [45]). There is, in fact, a large interest in the yet to be completely explored opportunity to control quantum transport by strain engineering and various structural modifications. The mechanical behavior of graphene or its derivatives is therefore very important not only for strictly mechanical reasons but also for electronic motivations. Bending elasticity is interesting as well (see [46] and references therein). Finally, there is also an increasing interest in the hydrogenation of graphene: this is a process where added hydrogen atoms bond to the carbon atoms of the graphene scaffold sharing their only electron. This produces a family of two-dimensional hydrocarbons which are called graphanes [47]: their linear and nonlinear elastic properties affect charge transport.

1.6. Structure of the review

This paper is organized as follows.

In section 2 we provide a brief outline of the elasticity theory within the hypothesis of small deformations. We introduce the concepts of stress and strain and we derive the standard balance equations of solid mechanics. This formalism can be adopted to approach any L–L and NL–L problems as stated in section 1.1. We will then derive the general theory of constitutive equations in the nonlinear response regime, corresponding to the situation previously referred to as material nonlinearity. As already stated, this is the physical situation describing the class of NL–L problems relevant for applications to nanomaterials and structures.

Section 3 is addressed to some specific methodological issues. In particular, we give a brief outline of the linear Eshelby theory for describing the elastic behavior of an embedded inhomogeneity and we introduce its generalization to the nonlinear case within the NL–L formalism. Moreover, we elaborate a fruitful discrete elastic model, based on a

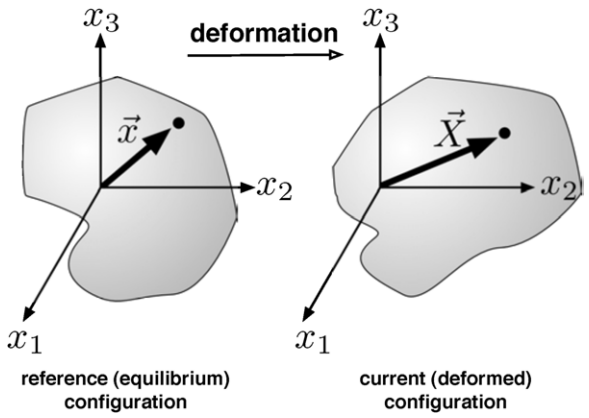

Figure 1. Reference configuration (left) and current configuration (right) after a deformation described by $\vec{f}$.

conceptual mapping of the continuum elasticity onto an atomic lattice, to be used in the following atomistic simulations.

Finally, in section 4 we review a set of applications of the previous methodologies to some paradigmatic nanostructured systems. Firstly, we draw a thorough comparison between the continuum and the atomistic results for a single nonlinear inhomogeneity. In this context, we describe a quantitative analysis of the length-scale effects. Then, we generalize the investigation to the case of a dispersion of nonlinear particles embedded in a given matrix, modeling a wide class of nanocomposite systems. We further describe the results of the atomistic simulations for more complicated structures, such as nanograded materials and two-dimensional atomic sheets, like graphene and graphane.

2. Small-strain elasticity theory

2.1. Formalism

Let $\vec{x}$ be the position vector of a material point within a solid in the reference (or, equivalently, undeformed) configuration and let $\vec{X}$ be its new position in the current (or deformed) configuration generated upon loading, both measured in the same Cartesian coordinate system (see figure 1). Obviously, $\vec{X}$ will be a function of $\vec{x}$ and, therefore, we may write

$$\vec{X} = \vec{f}\,(\vec{x}) = (f_1\,(\vec{x})\,,\, f_2\,(\vec{x})\,,\, f_3\,(\vec{x}))\,, \tag{2.1}$$

where the three axes have been labeled by $\{1, 2, 3\}$. We observe that the function $\vec{f}$ connects the vector $\vec{X}$ with the vector $\vec{x}$, being a vector field. Physically, it describes the deformation experienced by the solid body subjected to load. Of course, the relation $\vec{f}(\vec{x}) \neq \vec{f}(\vec{y})$ is verified for any couple of points $\vec{x} \neq \vec{y}$ of the reference configuration. This means that $\vec{f}$ is a biunivocal vector function and, therefore, the inverse function $\vec{f}^{-1}$ always exists. For the following development we also assume that $\vec{f}$ and $\vec{f}^{-1}$ are differentiable functions. In the theory of elastic materials the deformation gradient $\hat{F} = \{F_{ij},\ i, j = 1, 2, 3\}$,

$$F_{ij} = \frac{\partial f_i}{\partial x_j}, \tag{2.2}$$

is an important quantity. The matrix $\hat{F}$, referred to as the Jacobian matrix of the transformation, has two important properties: (i) it is not singular because of the invertibility of $\vec{f}$ ($\exists\ \hat{F}^{-1}$ such that $\hat{F}\hat{F}^{-1} = \hat{F}^{-1}\hat{F} = \hat{I}$); (ii) its determinant is always strictly positive (det $F > 0$) [7].

Another key quantity is the displacement field $\vec{u}(\vec{x})$ (between $\vec{X}$ and $\vec{x}$) defined as

$$\vec{X} = \vec{f}(\vec{x}) = \vec{x} + \vec{u}(\vec{x}). \tag{2.3}$$

Provided that the displacement vector is known, the Jacobian matrix of the displacement $\hat{J} = \{J_{ij},\ \ i, j = 1, 2, 3\}$ can be expressed as follows:

$$J_{ij} = \frac{\partial u_i}{\partial x_j}. \tag{2.4}$$

From equations (2.2) and (2.4) we easily obtain $\hat{F} = \hat{I} + \hat{J}$.

We now introduce a key feature, namely, *we will assume that the strains are small* or, equivalently, that $\hat{F}$ is very similar to $\hat{I}$ or that $\hat{J}$ is very small. We adopt, as a definition of small deformations, the relation

$$\mathrm{Tr}(\hat{J}\hat{J}^{\mathrm{T}}) \ll 1 \tag{2.5}$$

meaning that in this approximation the trace of the product $\hat{J}\hat{J}^{\mathrm{T}}$ is negligible. Such a hypothesis allows us to introduce a simplified analysis of the dilatation/compression as well as the local rotation of a small element of volume contained in a given material body under deformation [11].

2.2. Strain

Under the hypothesis of small deformations we can introduce the *strain tensor*, which is the most important tool to quantify the deformations in elasticity theory. To this aim we observe that the Jacobian matrix $\hat{J}$ of the displacement can be written as the sum of a symmetric part and a skew-symmetric (emisymmetric) part as follows:

$$J_{ij} = \underbrace{\frac{1}{2}\left(\frac{\partial u_i}{\partial x_j} + \frac{\partial u_j}{\partial x_i}\right)}_{\text{symmetric tensor}} + \underbrace{\frac{1}{2}\left(\frac{\partial u_i}{\partial x_j} - \frac{\partial u_j}{\partial x_i}\right)}_{\text{skew-symmetric tensor}} = \epsilon_{ij} + \Omega_{ij}, \tag{2.6}$$

where we have defined the tensors

$$\epsilon_{ij} = \frac{1}{2}\left(\frac{\partial u_i}{\partial x_j} + \frac{\partial u_j}{\partial x_i}\right), \tag{2.7}$$

$$\Omega_{ij} = \frac{1}{2}\left(\frac{\partial u_i}{\partial x_j} - \frac{\partial u_j}{\partial x_i}\right) \tag{2.8}$$

with the symmetry properties $\epsilon_{ij} = \epsilon_{ji}$ and $\Omega_{ij} = -\Omega_{ji}$. The quantity $\hat{\epsilon} = \{\epsilon_{ij}\}$ is called the *infinitesimal strain tensor* or *small-strain tensor* and the quantity $\hat{\Omega} = \{\Omega_{ij}\}$ is the *local rotation tensor* [18]. Such a decomposition is useful to obtain the three following very important properties of the small-strain tensor.

(i) We note that for a pure local rotation (a volume element is rotated, but not changed in shape and size), we have $\hat{J} = \hat{\Omega}$ and, therefore, $\hat{\epsilon} = 0$. This means that the small-strain tensor does not take into account any local rotation, but only the changes in shape and size (dilatations or compressions) of that element of volume [11]. We stress that the local rotation of a volume element within a body cannot be correlated with any arbitrary force exerted in that region (the forces are correlated with $\hat{\epsilon}$ and not with $\hat{\Omega}$): for this reason the infinitesimal strain tensor is the only relevant object for the analysis of the deformation due to applied loads in the small-strain elasticity theory [7].

(ii) The infinitesimal strain tensor allows for the determination of the length variation of any vector from the reference to the current configuration. By defining ϵ_{nn} as the relative length variation in direction $\vec{n}$, we have

$$\epsilon_{nn} = \vec{n} \cdot \hat{\epsilon}\vec{n}. \tag{2.9}$$

If $\vec{n}$ is a unit vector of any axis of the adopted Cartesian frame of reference, it is straightforward to attribute a geometrical meaning to the components $\epsilon_{11}, \epsilon_{22}, \epsilon_{33}$ of the strain tensor. Since $\epsilon_{nn} = \vec{e}_i \cdot (\hat{\epsilon}\ \vec{e}_i) = \epsilon_{ii}$, they describe the relative length variations along the three Cartesian axes [18].

(iii) The infinitesimal strain tensor allows for the determination of the angle variation between any two vectors from the reference to the current configuration. The variation of the angle defined by the two orthogonal directions $\vec{n}$ and $\vec{t}$ can be obtained from

$$\gamma_{nt} = 2\vec{n} \cdot \hat{\epsilon}\vec{t}. \tag{2.10}$$

The present result is also useful for providing a direct geometrical interpretation of the components ϵ_{12}, ϵ_{23} and ϵ_{13} of the infinitesimal strain tensor. As an example, we take into consideration the component ϵ_{12} and we assume that $\vec{n} = \vec{e}_1$ and $\vec{t} = \vec{e}_2$. The quantity γ_{nt} represents the variation of a right angle on the plane (x_1, x_2). Since $\epsilon_{12} = \vec{e}_1 \cdot (\hat{\epsilon}\ \vec{e}_2)$, we easily obtain the relationship $\gamma_{nt} = 2\epsilon_{12} = (\partial u_1/\partial x_2) + (\partial u_2/\partial x_1)$ [18].

It is also possible to obtain global relations describing the variation of the measure of lines, surfaces and volumes contained in the elastic body. The variation of volume of a subregion V of the body subjected to a strain $\hat{\epsilon}$ is given by the following relation:

$$\Delta \mathrm{V} = \int_{\mathrm{V}} \mathrm{Tr}(\hat{\epsilon})\mathrm{d}V. \tag{2.11}$$

The variation of area of a surface S (with normal unit vector $\vec{n}$) under strain $\hat{\epsilon}$ can be written as

$$\Delta \mathrm{S} = \int_{\mathrm{S}} \left[\mathrm{Tr}(\hat{\epsilon}) - \vec{n} \cdot (\hat{\epsilon}\ \vec{n})\right] \mathrm{d}S. \tag{2.12}$$

Finally, the variation of length of a line γ (with tangent unit vector $\vec{t}$) subjected to a deformation described by $\hat{\epsilon}$ is given by the relation

$$\Delta L = \int_{\gamma} \vec{t} \cdot (\hat{\epsilon}\vec{t})\mathrm{d}l. \tag{2.13}$$

2.3. Stress

In continuum elasticity we must consider two systems of forces acting on a given region of a material [7, 9, 10], namely, *body forces* and *surface forces*. The first ones are due to the external fields acting on the body and they are described by the vector field $\vec{b}(\vec{x})$, representing their volume density in the current configuration. The physical meaning of such a density of forces can be summed up stating that the total force $\mathrm{d}\vec{F}_v$ applied to a small volume $\mathrm{d}\vec{x}$ centered on the point $\vec{x}$ is given by $\mathrm{d}\vec{F}_v = \vec{b}(\vec{x})\mathrm{d}\vec{x}$. In turn, surface forces are due to the interaction between two neighboring portions of any deformable material across their common surface. At a fundamental level, such an interaction originates from a set of interatomic forces; within the continuum picture, however, it is assumed that the net resulting force is adequately represented by a single vector field defined over the surface.

It is useful to introduce the following notation for the surface force $\mathrm{d}\vec{F}_s$ applied to the area element $\mathrm{d}s$ (with unit normal vector $\vec{n}$) of the deformed configuration:

$$\mathrm{d}\vec{F}_s = \vec{\mathcal{F}}\,(\vec{x}, \vec{n}, t)\ \mathrm{d}s, \tag{2.14}$$

where $\vec{\mathcal{F}}$ assumes the meaning of a density of forces distributed over the surface. According to the Cauchy theorem, a stress tensor $\hat{T}$ exists (hereafter referred to as *Cauchy stress tensor*) describing the distribution of the surface forces [7, 48] such that

$$\vec{\mathcal{F}}\,(\vec{x}, \vec{n}, t) = \hat{T}(\vec{x}, t)\vec{n}. \tag{2.15}$$

2.4. Balance equations

The mathematical objects introduced in the previous sections must be linked by means of a set of equations representing the formal structure of the theory of elasticity. The first two important equations can be derived by the principles of linear and angular momentum [7, 48]. When dealing with a system of particles, we can deduce from Newton's laws of motion that the result of the external forces is equal to the rate of change in the total linear momentum of the system. By taking moments about a fixed point, we can also show that the resultant moment of the external forces is equal to the rate of change in the total moment of momentum. Here we define the linear and angular momentum density for a continuum medium and we introduce balance laws for these quantities. We consider a portion V in a material body and we define $\vec{P}$ as its linear momentum, $\vec{F}$ as the result of the applied forces, $\vec{L}$ as the total angular momentum and, finally, $\vec{M}$ as the resultant moment of the applied forces. For a system of particles the above mechanical principles can be written as follows [49]:

$$\frac{\mathrm{d}\vec{P}}{\mathrm{d}t} = \vec{F}, \qquad \frac{\mathrm{d}\vec{L}}{\mathrm{d}t} = \vec{M}. \tag{2.16}$$

We start with the first principle, applied to the portion of body contained to the region V, limited by the closed surface S

$$\frac{\mathrm{d}}{\mathrm{d}t}\int_{\mathrm{V}} \rho \frac{\partial u_j}{\partial t}\mathrm{d}V = \int_{\mathrm{S}} T_{ji}n_i\mathrm{d}S + \int_{\mathrm{V}} b_j\mathrm{d}V, \tag{2.17}$$

where we have used the decomposition of the forces as described in the previous section. We remember that u_j is the jth component of the displacement field. The mass density ρ is assumed to be constant under the small deformation assumption. The previous equation can be simplified by means of the Gauss divergence theorem, by obtaining

$$\frac{\mathrm{d}}{\mathrm{d}t}\int_{\mathtt{V}}\rho\frac{\partial u_j}{\partial t}\mathrm{d}V=\int_{\mathtt{V}}\frac{\partial T_{ji}}{\partial x_i}\mathrm{d}V+\int_{\mathtt{V}}b_j\mathrm{d}V. \tag{2.18}$$

Since the volume V is arbitrary, we easily obtain the first balance equation for the elasticity theory

$$\frac{\partial T_{ji}}{\partial x_i}+b_j=\rho\frac{\partial^2 u_j}{\partial t^2}. \tag{2.19}$$

We now turn to the principle of the angular momentum. For the region V such a balance equation can be written in the following form:

$$\frac{\mathrm{d}}{\mathrm{d}t}\int_{\mathtt{V}}\vec{x}\times\frac{\partial\vec{u}}{\partial t}\rho\mathrm{d}V=\int_{\mathtt{S}}\vec{x}\times\left(\hat{T}\vec{n}\right)\mathrm{d}S+\int_{\mathtt{V}}\vec{x}\times\vec{b}\,\mathrm{d}V. \tag{2.20}$$

As before, the surface integral can be simplified with the application of the Gauss divergence theorem, by obtaining, after some straightforward algebra,

$$\int_{\mathtt{S}}\vec{x}\times(\hat{T}\vec{n})\mathrm{d}S=\int_{\mathtt{V}}\left[T_{kh}+x_h\frac{\partial T_{kp}}{\partial x_p}\right]\eta_{hkj}\vec{e}_j\mathrm{d}V. \tag{2.21}$$

Hence, the second balance equation can be cast in the form

$$\int_{\mathtt{V}}\left\{x_h\left[\frac{\partial^2 u_k}{\partial t^2}\rho-\frac{\partial T_{kp}}{\partial x_p}-b_k\right]-T_{kh}\right\}\eta_{hkj}\vec{e}_j\mathrm{d}V=0. \tag{2.22}$$

The term in the bracket is zero because of the first balance equation and we obtain $\int_{\mathtt{V}}T_{kh}\eta_{hkj}\vec{e}_j\mathrm{d}V=0$ or, equivalently, $T_{kh}\eta_{hkj}=0$. The second principle therefore eventually leads to

$$T_{ij}=T_{ji} \tag{2.23}$$

assuring the symmetry of the stress tensor.

2.5. Nonlinear constitutive equations

The results obtained in the previous section hold for most materials, regardless of their constitution. However, in order to obtain a complete system of equations predicting the material-specific deformation upon stress/strain, we need to introduce the constitutive equations, which characterize the actual elastic behaviour of the investigated system [17, 19]. These equations must be written as a relationship between the components of the stress and the strain

$$T_{ij}=f(\{\epsilon_{ij}\}). \tag{2.24}$$

Equation (2.24) assumes a direct correspondence between stress and strain at any point of the material. In general, the arbitrary constitutive equation of an elastic material can be derived by the strain energy function $U(\hat{\epsilon})$ as [11]

$$T_{ij}=\frac{\partial U(\hat{\epsilon})}{\partial\epsilon_{ij}}. \tag{2.25}$$

It means that an arbitrarily nonlinear constitutive equation can be always written by means of derivatives of the strain energy function [7]: therefore, the strain energy function contains the complete information about the nonlinear elastic response of a given material.

Since equation (2.25) is the most important equation in the theory of nonlinear elastic constitutive equations, we give here a brief outline of its derivation. Let us suppose that a body is subjected to a deformation from configuration A to configuration B. Such a deformation is due to forces which are either internal (due to atomic interactions) or external (due to some external field describing a physical action on the body). Condensed matter theory warrants that internal forces are conservative, a condition that in general is not guaranteed for external ones. Summing up the two contributions, we obtain an energy balance between the configurations A and B in the form

$$\left[U_{\mathrm{p}}(B)+E_{\mathrm{c}}(B)\right]-\left[U_{\mathrm{p}}(A)+E_{\mathrm{c}}(A)\right]=L^{\mathrm{ext}}, \tag{2.26}$$

where L^{ext} is the work done by the external forces, the potential energy U_{p} takes into account the internal forces and E_{c} is the kinetic energy of a given configuration. As before we consider a volume V limited by a surface S. We begin by calculating the work done by the external forces. It can be written as the sum $L^{\mathrm{ext}}=L^{\mathrm{ext}}(\mathtt{V})+L^{\mathrm{ext}}(\mathtt{S})$, where the first term represents the work done by the body forces $\vec{b}(\vec{x},t)$ and the second one represents the work done by the forces $T_{ij}(\vec{x},t)n_j$, applied on the external surface. The term $L^{\mathrm{ext}}(\mathtt{V})$ can be written in the form of a time and volume integral of the applied power (force by velocity), as follows:

$$L^{\mathrm{ext}}(\mathtt{V})=\int_{\mathtt{V}}\left[\int_{t(A)}^{t(B)}\vec{b}\cdot\frac{\partial\vec{u}}{\partial t}\mathrm{d}t\right]\mathrm{d}V, \tag{2.27}$$

where $t(A)$ and $t(B)$ are the initial and the final instant, respectively. Similarly, for the work made on the surface S we obtain

$$\begin{aligned}L^{\mathrm{ext}}(\mathtt{S})&=\int_{\mathtt{S}}\left[\int_{t(A)}^{t(B)}T_{ij}n_j\frac{\partial u_i}{\partial t}\,\mathrm{d}t\right]\mathrm{d}S\\&=\int_{\mathtt{V}}\left[\int_{t(A)}^{t(B)}\frac{\partial}{\partial x_j}\left(T_{ij}\frac{\partial u_i}{\partial t}\right)\mathrm{d}t\right]\mathrm{d}V\\&=\int_{\mathtt{V}}\left[\int_{t(A)}^{t(B)}\left(\frac{\partial T_{ij}}{\partial x_j}\frac{\partial u_i}{\partial t}+T_{ij}\frac{\partial\epsilon_{ij}}{\partial t}\right)\mathrm{d}t\right]\mathrm{d}V,\end{aligned} \tag{2.28}$$

where we have used the divergence theorem and the symmetry of the stress tensor (see equation (2.23)). Therefore, the total external work is

$$L^{\mathrm{ext}}=\int_{\mathtt{V}}\left\{\int_{t(A)}^{t(B)}\left[\left(\frac{\partial T_{ij}}{\partial x_j}+b_i\right)\frac{\partial u_i}{\partial t}+T_{ij}\frac{\partial\epsilon_{ij}}{\partial t}\right]\mathrm{d}t\right\}\mathrm{d}V. \tag{2.29}$$

Using the motion equation given in equation (2.19), we obtain

$$\begin{aligned}L^{\mathrm{ext}}&=\int_{\mathtt{V}}\left\{\int_{t(A)}^{t(B)}\left[\rho\frac{\partial^2 u_i}{\partial t^2}\frac{\partial u_i}{\partial t}+T_{ij}\frac{\partial\epsilon_{ij}}{\partial t}\right]\mathrm{d}t\right\}\mathrm{d}V\\&=\int_{\mathtt{V}}\left\{\int_{t(A)}^{t(B)}\left[\frac{1}{2}\rho\frac{\partial}{\partial t}\left(\frac{\partial u_i}{\partial t}\frac{\partial u_i}{\partial t}\right)+T_{ij}\frac{\partial\epsilon_{ij}}{\partial t}\right]\mathrm{d}t\right\}\mathrm{d}V\\&=\frac{1}{2}\int_{\mathtt{V}}\left\{\left[\rho v_B^2-\rho v_A^2\right]\right\}\mathrm{d}V+\int_{\mathtt{V}}\int_{t(A)}^{t(B)}T_{ij}\frac{d\epsilon_{ij}}{\partial t}\,\mathrm{d}t\,\mathrm{d}V,\end{aligned} \tag{2.30}$$

where $v_A^2 = ((\partial u_i/\partial t)(\partial u_i/\partial t))_A$ and $v_B^2 = ((\partial u_i/\partial t)(\partial u_i/\partial t))_B$ are the scalar velocity fields inside the body in the initial and final configurations, respectively. Since the variation of the kinetic energy can be written as

$$\Delta E_c = \frac{1}{2}\int_V \rho v_B^2 \mathrm{d}V - \frac{1}{2}\int_V \rho v_A^2 \mathrm{d}V \tag{2.31}$$

we easily derive, by means of equation (2.26), the total variation of the elastic potential energy between the initial and the final configurations

$$\Delta U_p = \int_V \int_{t(A)}^{t(B)} T_{ij}\frac{\partial \epsilon_{ij}}{\partial t}\,\mathrm{d}t\,\mathrm{d}V. \tag{2.32}$$

By introducing the volume energy density

$$U_p = \int_V U \mathrm{d}V \tag{2.33}$$

we obtain

$$\Delta U_p = \int_V \int_{t(A)}^{t(B)} \frac{\partial U}{\partial t}\,\mathrm{d}t\,\mathrm{d}V. \tag{2.34}$$

It must be underlined that in equations (2.33) and (2.34) we have implicitly accepted the existence of the energy density as a thermodynamic state variable: however, this assumption is consistent with the basic thermodynamic principles. By drawing a comparison between equations (2.32) and (2.34) we obtain $(\partial U/\partial t) = T_{ij}(\partial \epsilon_{ij}/\partial t)$, which represents the rate of change in the energy density in terms of the strain and the stress tensors. If we write the same equation with explicit arguments $(\mathrm{d}U(\{\epsilon_{kh}\})/\mathrm{d}t) = T_{ij}(\{\epsilon_{kh}\})(\mathrm{d}\epsilon_{ij}/\mathrm{d}t)$ we easily understand that the function U is an exact form which proves equation (2.25), as anticipated.

For the particular case of a nonlinear isotropic material the strain energy function U must depend only upon the invariants of the strain tensor [48]. A constitutive equation may be developed in power series with respect to the components of $\hat{\epsilon}$ (note that everywhere in this review we understand that repeated indices are saturated)

$$U(\hat{\epsilon}) = \tfrac{1}{2}\mathcal{C}_{ijkh}\epsilon_{ij}\epsilon_{kh} + \tfrac{1}{6}\mathcal{C}_{ijkhnm}\epsilon_{ij}\epsilon_{kh}\epsilon_{nm} + \cdots. \tag{2.35}$$

Here the $\mathcal{C}_{ijkh}$ and the $\mathcal{C}_{ijkhnm}$ denote the second-order elastic constants (SEOCs) and the third-order elastic constants (TOECs), respectively (within the small-strain tensor approximation) [17, 18]. Higher order elastic constants are found when expanding equation (2.35) above the third order. Although defined in a formally clean way, higher order elastic constants cannot be provided with a direct and intuitive physical meaning and, therefore, are rarely used. Moreover, their effects are typically negligible within a small-strain regime. In the following we will adopt the compact Voigt notation and, therefore, we will use the symbol $\mathcal{C}_{pq}$ for SOECs and $\mathcal{C}_{pql}$ for TOECs, according to the standard correspondence rule: $p = 1 \to (i, j) = (1, 1)$; $p = 2 \to (i, j) = (2, 2)$; $p = 3 \to (i, j) = (3, 3)$; $p = 4 \to (i, j) = (2, 3)$; $p = 5 \to (i, j) = (1, 3)$; $p = 6 \to (i, j) = (1, 2)$.

As a particular case of equation (2.35), the linear stress-strain constitutive equation is called the *generalized Hooke's law* [17, 18]:

$$T_{ij} = \mathcal{C}_{ijkh}\epsilon_{kh}, \tag{2.36}$$

where $\mathcal{C}_{ijkh}$ are constants (for homogeneous materials). Equation (2.36) is of general validity, including all the possible crystalline symmetry or, in other words, any kind of anisotropy. The tensor of the elastic constants appearing in equation (2.36) satisfies three symmetry properties, determined by general thermodynamics arguments, as well as by the symmetry of the stress and strain tensors: (i) it is symmetric in the first pair of indices, namely, $\mathcal{C}_{ijkh} = \mathcal{C}_{jikh}$; (ii) it is symmetric in the last pair of indices, namely, $\mathcal{C}_{ijkh} = \mathcal{C}_{ijhk}$, and (iii) it is symmetric by exchanging the first pair and the second pair of indices, namely, $\mathcal{C}_{ijkh} = \mathcal{C}_{khij}$ [17, 18]. Because of such properties, $\mathcal{C}_{ijkh}$ has at most 21 independent components. It follows that the energy density can be placed in a very simple form

$$U = \tfrac{1}{2}\mathcal{C}_{ijkh}\epsilon_{ij}\epsilon_{kh}. \tag{2.37}$$

In the case of a linear and isotropic material it can be proved that the constitutive equation has the form [17, 18]

$$\begin{aligned}\hat{T} &= \frac{E_{3D}}{1+\nu_{3D}}\hat{\epsilon} + \frac{\nu_{3D}E_{3D}}{(1+\nu_{3D})(1-2\nu_{3D})}\hat{I}\,\mathrm{Tr}(\hat{\epsilon}) \\ &= 2\mu\hat{\epsilon} + \lambda\hat{I}\mathrm{Tr}(\hat{\epsilon}),\end{aligned} \tag{2.38}$$

where just two elastic moduli appear. In equation (2.38) we made use of two different pairs of moduli, namely, the *Lamé coefficients* μ and λ, or Young's modulus E_{3D} and Poisson's ratio ν_{3D} (we use the symbols E_{3D} and ν_{3D} since E and ν will be used in the following for the two-dimensional case). They are related as follows:

$$\mu = \frac{E_{3D}}{2(1+\nu_{3D})}, \qquad \lambda = \frac{\nu_{3D}E_{3D}}{(1+\nu_{3D})(1-2\nu_{3D})}. \tag{2.39}$$

Another extensively used linear elastic coefficient is the so-called *bulk modulus* K defined as $K = \lambda + 2\mu/3$. The stress–strain relation under the hydrostatic condition can be summarized as $\hat{\epsilon} = (1/3K)\sigma\hat{I}$, where σ represents the (scalar) pressure applied to the system. The further relation $\mathrm{Tr}(\hat{\epsilon}) = (\sigma/K)$ has an important physical meaning because it describes the local volumetric variation under the assumption of hydrostatic stress.

The strain energy function given in equation (2.37) can be further simplified when the material is linear, isotropic and homogeneous. Indeed, it assumes the very compact form [17]

$$U(\hat{\epsilon}) = \tfrac{1}{2}T_{ij}\epsilon_{ij} = \mu\epsilon_{ij}\epsilon_{ij} + \tfrac{1}{2}\lambda\epsilon_{kk}\epsilon_{ii}, \tag{2.40}$$

where we have made use of the Lamé coefficients. Since $\epsilon_{kk} = \epsilon_{ii} = \mathrm{Tr}(\hat{\epsilon})$ and $\epsilon_{ij}\epsilon_{ij} = \mathrm{Tr}(\hat{\epsilon}^2)$ we obtain the tensor form

$$U(\hat{\epsilon}) = \mu\mathrm{Tr}(\hat{\epsilon}^2) + \tfrac{1}{2}\lambda\left[\mathrm{Tr}(\hat{\epsilon})\right]^2 \tag{2.41}$$

which represents the elastic energy density for an isotropic material.

For an elastic solid body at equilibrium, i.e. for $\epsilon_{ij} = 0$ $\forall i, j$, the function $U(\hat{\epsilon})$ must exhibit a minimum (i.e. the equilibrium configuration is stable). Because $U(\hat{\epsilon} = 0) = 0$, we conclude that the quadratic form defined in equations (2.37) or (2.41) is positive definite. In other words, we have proved that the stiffness tensor is always positive definite for real materials. The specific conditions assuring a positive definite

energy density for an isotropic material are $\mu > 0$ and $3\lambda + 2\mu > 0$. By means of standard conversions we obtain the additional relations $K > 0$ and $E_{3D} > 0$. Finally, by means of the expression $\nu_{3D} = ((3K - 2\mu)/(2(3K + \mu)))$ we can easily prove that $-1 < \nu_{3D} < \frac{1}{2}$. It is interesting to observe that the last result admits negative values for Poisson's ratio.

All results of the standard elasticity theory are scale-invariant, i.e. no scale effects can occur within such a theory which does not include any information about internal length scales. It is nevertheless in principle possible to introduce additional features able to treat such scale effects, such as is typically done in integral nonlocal or gradient theories where one (or more) intrinsic length scale(s) is, in fact, explicitly included. Their predictions match those of local continuum theories when the specimen size is much larger than the internal length scale. Briefly, in nonlocal elasticity the algebraic constitutive equations are replaced by integral equations where the stress (or strain) at a given point depends on the strain (or stress) at that point as well as at all neighboring points in the material [50]. More precisely, the constitutive equation is expressed in terms of a nonlocal kernel introduced to account for the effect of long-range interatomic forces. The stress at a given point is a function of the strain at all points in the body, through a weighting kernel. Under certain conditions, an approximation to the true nonlocal material behavior can be mimicked by the so-called strain gradient elasticity. Such a theory takes into account strain gradient contributions in the energy function [51]. Neglecting such terms can lead to artefacts, such as underestimating the stress or size-dependent behaviors in small-scale structures. The major difference between the strain gradient theory and the conventional elastic theory is that the strain energy density U depends on both the conventional strain (the symmetric part of the first-order deformation gradient) and on the second-order deformation gradient $\eta_{ijk} = \partial^2 u_k / \partial x_i \partial x_j$ [52]. While the strain tensor has six independent symmetric components, the second-order deformation gradient tensor has 18 independent components that are symmetric in the first two indices. The common feature of all nonlocal formulations is the elimination of stress field singularities. For instance, the gradient elasticity solutions show no singularity in both stress and strain fields at the core of dislocations or crack tips in fracture mechanics. Furthermore, the strain energy is finite at sites where local elasticity predicts stress singularities and infinite strain energy density. More advanced discussions, based on nonclassical or multipolar continuum theories, can be found elsewhere [53].

3. Methods

The goal of this section is twofold: to set up the general continuum device to cope with an embedded inhomogeneity (section 3.1), the starting point to model nanostructured systems, within the general framework of the Eshelby theory; and to elaborate the concept of constitutive force field, to be used in atomistic simulations (section 3.2).

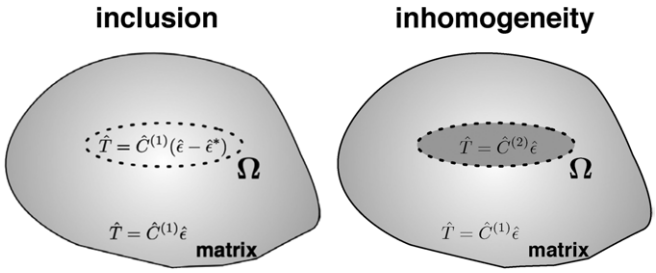

Figure 2. Schematic representation of an inclusion (left) and an inhomogeneity (right) of volume Ω, embedded in a matrix. The inclusion, inhomogeneity and matrix are, respectively, characterized by the stiffness tensor $\hat{C}^{(1)}$, $\hat{C}^{(2)}$ and $\hat{C}^{(1)}$. $\hat{\epsilon}^*$ is the eigenstrain (or stress-free strain) given *a priori* in the inclusion (see text).

3.1. The Eshelby theory

We are going to outline the continuum formalism by investigating the elastic behavior of the Eshelby configuration (see figure 2, right), namely, an ellipsoidal inhomogeneity embedded in a homogeneous matrix subjected to a remotely applied external loading [15, 16]. We aim at calculating general expressions for the elastic stress and strain fields both inside and the outside the ellipsoidal particle for any loading condition and for any elastic contrast between the two media.

3.1.1. The concept of inclusion. Let us consider at first an infinite linear elastic medium with stiffness tensor $\hat{C}^{(1)}$ and let us define an embedded ellipsoidal *inclusion* (figure 2, left) as a region of volume Ω described by the linear constitutive equation $\hat{T} = \hat{C}^{(1)}(\hat{\epsilon} - \hat{\epsilon}^*)$. The strain $\hat{\epsilon}^*$ is *a priori* given and it is called the *eigenstrain* (or stress-free strain) [15]. In other words, throughout this review we will denote as *inclusion* a region containing a distribution of eigenstrain (with the same elastic moduli as the matrix). For instance, $\hat{\epsilon}^*$ could describe the local state of deformation generated by a variation of temperature (i.e. a local heating) or could take into account the strain induced by magneto-/electro-strictive effects. It is important to note that the concept of inclusion is different from that of *inhomogeneity* which instead corresponds to an the ellipsoidal region of volume Ω characterized by a stiffness tensor $\hat{C}^{(2)} \neq \hat{C}^{(1)}$ (figure 2, right).

For the linear elastic isotropic matrix the stiffness tensor can be represented as

$$C^{(1)}_{ijkh} = \left(K_1 - \tfrac{2}{3}\mu_1\right)\delta_{ij}\delta_{kh} + \mu_1(\delta_{ik}\delta_{jh} + \delta_{ih}\delta_{jk}), \tag{3.1}$$

where the elastic moduli are named K_1 (bulk modulus) and μ_1 (shear modulus). The displacement u_i generated by the inclusion (or, equivalently, by the eigenstrain $\hat{\epsilon}^*$) can be evaluated in terms of the so-called harmonic potential $\Phi(\vec{x})$ and biharmonic potential $\Psi(\vec{x})$ [23, 24]:

$$u_i(\vec{x}) = \epsilon^*_{kh}\left[\frac{1}{8\pi\left(1-\nu_{3D,1}\right)}\Psi_{,ikh} - \frac{\delta_{ih}}{4\pi}\Phi_{,k} - \frac{\delta_{ik}}{4\pi}\Phi_{,h} - \frac{\nu_{3D,1}}{1-\nu_{3D,1}}\frac{\delta_{kh}}{4\pi}\Phi_{,i}\right] \tag{3.2}$$

where $\nu_{3D,1}$ is the standard Poisson's ratio of the matrix. Hereafter we use the symbol $f_{,i} = (\partial f/\partial x_i)$ and we extend

this notation to higher order derivatives. Equation (3.2) is valid anywhere. The harmonic potential is defined by the Poisson equation $\nabla^2\Phi = -4\pi$ if $\vec{x} \in \Omega$, 0 if $\vec{x} \notin \Omega$ and the integral form of its solution is $\Phi(\vec{x}) = \int_\Omega (1/\|\vec{r} - \vec{x}\|)\, \mathrm{d}\vec{r}$. Similarly, the biharmonic potential is defined by means of the biharmonic equation $\nabla^4\Psi = -8\pi$ if $\vec{x} \in \Omega$, 0 if $\vec{x} \notin \Omega$ and the standard integral representation is $\Psi(\vec{x}) = \int_\Omega \|\vec{r} - \vec{x}\|\, \mathrm{d}\vec{r}$ [15, 23]. Such harmonic and biharmonic potentials only contain geometrical information about the embedded ellipsoid (i.e. the semi-axes lengths b_1, b_2 and b_3). The explicit form of $\Phi(\vec{x})$ and $\Psi(\vec{x})$ for the elliposidal geometry is found elsewhere [15].

The solution of the elastic problem is given in terms of the strain tensor

$$\epsilon_{ij} = \frac{1}{2}\left(\frac{\partial u_i}{\partial x_j} + \frac{\partial u_j}{\partial x_i}\right) = \mathcal{S}_{ijkh}(\vec{x})\epsilon^*_{kh} \tag{3.3}$$

providing the strain field everywhere in the system (i.e. both in the matrix and within the inclusion). Here $\mathcal{S}_{ijkh}(\vec{x})$ is the *Eshelby tensor*. Its form both inside and outside the inclusion can be written by means of the elastic potentials as follows [15, 16]:

$$\mathcal{S}_{ijkh}(\vec{x}) = \frac{1}{8\pi(1-\nu_{3D,1})}\Psi_{,ijkh} - \frac{\nu_{3D,1}}{1-\nu_{3D,1}}\frac{\delta_{kh}}{4\pi}\Phi_{,ij} - \frac{1}{8\pi}(\delta_{ih}\Phi_{,jk} + \delta_{ik}\Phi_{,jh} + \delta_{jh}\Phi_{,ik} + \delta_{jk}\Phi_{,ih}). \tag{3.4}$$

In order to distinguish between *internal* and *external* points (with respect the inclusion), we adopt the following notation [15, 16]:

$$\mathcal{S}_{ijkh}(\vec{x}) = \begin{cases} \mathcal{S}_{ijkh} & \text{if } \vec{x} \in \Omega \text{ (internal points)}, \\ \mathcal{S}^\infty_{ijkh}(\vec{x}) & \text{if } \vec{x} \notin \Omega \text{ (external points)}. \end{cases} \tag{3.5}$$

Taking a different notation for the *internal* and the *external* region is particularly efficient in order to remind us that the internal Eshelby tensor is constant and, therefore, the internal stress and strain are uniform tensor fields (see figure 2, left).

3.1.2. The equivalence principle. Let us now consider the case of an inhomogeneity embedded in a matrix which is remotely loaded by the stress T^∞_{ij}, as shown in figure 3. This problem is solved by means of the *Eshelby equivalence principle* [23–25] according to which the complete problem (figure 3, left) is solved by combining the solutions of two different simpler problems (figure 3, right). The first one (problem A) corresponds to the application of the remote uniform load to a simple homogeneous elastic system with stiffness tensor $\mathcal{C}^{(1)}_{ijkh}$. The second configuration (problem B) corresponds to an unloaded inclusion with a suitable eigenstrain $\hat{\epsilon}^*$. The solution of problem A is trivial

$$\begin{aligned} \epsilon^{A,\mathrm{in}}_{ij} &= \epsilon^\infty_{ij}, & \epsilon^{A,\mathrm{out}}_{ij} &= \epsilon^\infty_{ij}, \\ T^{A,\mathrm{in}}_{ij} &= T^\infty_{ij}, & T^{A,\mathrm{out}}_{ij} &= T^\infty_{ij}, \end{aligned} \tag{3.6}$$

while the solution of problem B is based on the Eshelby tensor

$$\begin{aligned} \epsilon^{B,\mathrm{in}}_{ij} &= \mathcal{S}_{ijkh}\epsilon^*_{kh}, & \epsilon^{B,\mathrm{out}}_{ij}(\vec{x}) &= \mathcal{S}^\infty_{ijkh}(\vec{x})\epsilon^*_{kh}, \\ T^{B,\mathrm{in}}_{ij} &= \mathcal{C}^{(1)}_{ijkh}(\epsilon^{B,\mathrm{in}}_{kh} - \epsilon^*_{kh}), & T^{B,\mathrm{out}}_{ij}(\vec{x}) &= \mathcal{C}^{(1)}_{ijkh}\mathcal{S}^\infty_{khnm}(\vec{x})\epsilon^*_{nm}, \end{aligned} \tag{3.7}$$

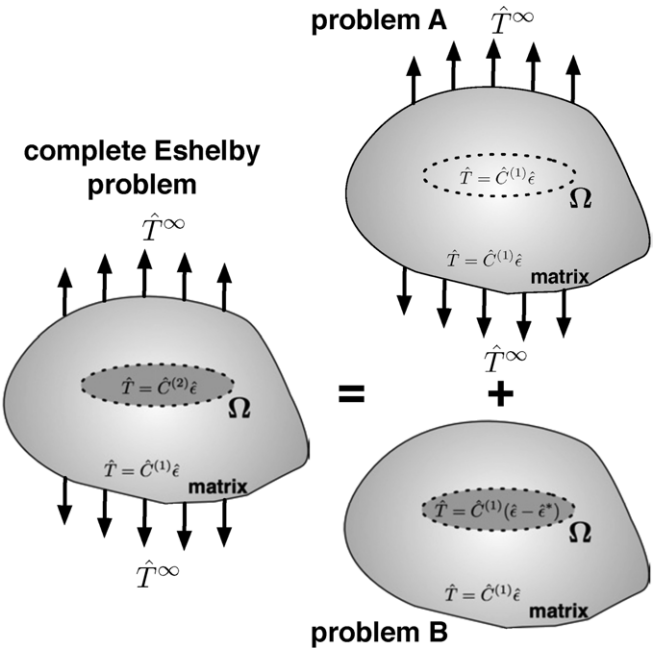

Figure 3. Eshelby equivalence principle: the complete problem of an inhomogeneity under loading (left) is obtained by combining a homogeneous configuration under loading (top right, problem A) with a simple inclusion (bottom right, problem B).

where labels *A* and *B* refer to problem A and B of figure 3, right; labels in and out indicate, respectively, the volume Ω and the outside matrix. By combining the two above equations we eventually obtain

$$\begin{aligned} \hat{\epsilon}^{\mathrm{in}} &= \hat{\epsilon}^{A,\mathrm{in}} + \hat{\epsilon}^{B,\mathrm{in}} = \hat{\epsilon}^\infty + \hat{\mathcal{S}}\hat{\epsilon}^*, \\ \hat{T}^{\mathrm{in}} &= \hat{T}^{A,\mathrm{in}} + \hat{T}^{B,\mathrm{in}} = \hat{\mathcal{C}}^{(1)}\hat{\epsilon}^\infty + \hat{\mathcal{C}}^{(1)}(\hat{\mathcal{S}}\hat{\epsilon}^* - \hat{\epsilon}^*). \end{aligned} \tag{3.8}$$

We note that the constitutive relation $\hat{T}^{\mathrm{in}} = \hat{\mathcal{C}}^{(2)}\hat{\epsilon}^{\mathrm{in}}$ must hold within the inhomogeneity. Therefore, the value of the eigenstrain $\hat{\epsilon}^*$ can be derived by solving the equation obtained by substituting equation (3.8) in $\hat{T}^{\mathrm{in}} = \hat{\mathcal{C}}^{(2)}\hat{\epsilon}^{\mathrm{in}}$. The solution is [15]

$$\hat{\epsilon}^* = \{[\hat{I} - (\hat{\mathcal{C}}^{(1)})^{-1}\hat{\mathcal{C}}^{(2)}]^{-1} - \hat{\mathcal{S}}\}^{-1}\hat{\epsilon}^\infty. \tag{3.9}$$

The internal strain and stress fields are accordingly calculated as

$$\hat{\epsilon}^{\mathrm{in}} = \{\hat{I} - \hat{\mathcal{S}}[\hat{I} - (\hat{\mathcal{C}}^{(1)})^{-1}\hat{\mathcal{C}}^{(2)}]\}^{-1}\hat{\epsilon}^\infty, \tag{3.10}$$

$$\hat{T}^{\mathrm{in}} = \hat{\mathcal{C}}^{(2)}\{\hat{I} - \hat{\mathcal{S}}[\hat{I} - (\hat{\mathcal{C}}^{(1)})^{-1}\hat{\mathcal{C}}^{(2)}]\}^{-1}\hat{\epsilon}^\infty. \tag{3.11}$$

Both $\hat{\epsilon}^{\mathrm{in}}$ and $\hat{T}^{\mathrm{in}}$, as anticipated before, are constant throughout the region Ω. Finally, the solution for the external fields can be obtained by combining the corresponding solutions for problems A and B

$$\hat{\epsilon}^{\mathrm{out}}(\vec{x}) = \hat{\epsilon}^{A,\mathrm{out}}(\vec{x}) + \hat{\epsilon}^{B,\mathrm{out}}(\vec{x}) = \hat{\epsilon}^\infty + \hat{\mathcal{S}}^\infty(\vec{x})\hat{\epsilon}^*, \tag{3.12}$$

$$\hat{T}^{\mathrm{out}}(\vec{x}) = \hat{T}^{A,\mathrm{out}}(\vec{x}) + \hat{T}^{B,\mathrm{out}}(\vec{x}) = \hat{\mathcal{C}}^{(1)}[\hat{\epsilon}^\infty + \hat{\mathcal{S}}^\infty(\vec{x})\hat{\epsilon}^*]. \tag{3.13}$$

The result stated in equation (3.10) is also valid for a single anisotropic linear ellipsoid (with stiffness $\hat{\mathcal{C}}^{(2)}$) embedded in an anisotropic linear matrix (with stiffness $\hat{\mathcal{C}}^{(1)}$) [23]. In this case the Eshelby tensor $\hat{\mathcal{S}}$ depends on both the geometry and $\hat{\mathcal{C}}^{(1)}$.

3.1.3. The nonlinear formulation. We generalize the Eshelby theory to the case of a nonlinear inhomogeneity (within the NL–L formalism) described by $\hat{T} = \hat{\mathcal{C}}^{(2)}(\hat{\epsilon})\hat{\epsilon}$, where $\hat{\mathcal{C}}^{(2)}(\hat{\epsilon})$ is any strain-dependent anisotropic stiffness tensor [54, 55]. Equivalently, nonlinear features will be described by an arbitrary energy function $U(\hat{\epsilon})$, as given in equation (2.25). In order to cope with this problem, we suppose we have found a solution for the equation

$$\hat{\epsilon}^{\text{in}} = \{\hat{I} - \hat{\mathcal{S}}[\hat{I} - (\hat{\mathcal{C}}^{(1)})^{-1}\hat{\mathcal{C}}^{(2)}(\hat{\epsilon}^{\text{in}})]\}^{-1}\hat{\epsilon}^{\infty}, \tag{3.14}$$

obtained from equation (3.10). If such a solution $\hat{\epsilon}^{\text{in}}$ exists for a given $\hat{\epsilon}^{\infty}$, then the nonlinear inhomogeneity could be replaced by a linear one with constant stiffness $\hat{\mathcal{C}}^{(2)} = \hat{\mathcal{C}}^{(2)}(\hat{\epsilon}^{\text{in}})$, with no modifications of the elastic fields anywhere. Therefore, if $\hat{\epsilon}^{\text{in}}$ exists, then equation (3.14) exactly describes, through self-consistency, the elastic behavior of the nonlinear anisotropic inhomogeneity.

The existence and uniqueness of a solution $\hat{\epsilon}^{\text{in}}$ for equation (3.14) can be exactly proved under the sole hypothesis of convexity for the strain energy function $U(\hat{\epsilon})$. We rearrange equation (3.14) as follows [54, 55]:

$$\frac{\partial}{\partial\hat{\epsilon}}\left\{\frac{1}{2}\hat{\epsilon}\hat{\mathcal{C}}^{(1)}[\hat{\mathcal{S}}^{-1} - \hat{I}]\hat{\epsilon} - \hat{\epsilon}\hat{\mathcal{C}}^{(1)}\hat{\mathcal{S}}^{-1}\hat{\epsilon}^{\infty} + U(\hat{\epsilon})\right\} = 0. \tag{3.15}$$

The first term represents a symmetric (because of the Betti reciprocal theorem [11]) and positive definite (because of the minimum potential energy principle [48]) quadratic form in $\hat{\epsilon}$, while the second term is a linear function of $\hat{\epsilon}$ [54, 55]. Therefore, the sum of these two terms is a convex functional with relative minimum at $[\hat{I} - \hat{\mathcal{S}}]\hat{\epsilon}^{\infty}$. If $U(\hat{\epsilon})$ is a convex functional (with $U(0) = 0$) as well, the brackets in equation (3.15) contain the sum of two convex terms: they result in an overall convex functional with a minimal extremum at $\hat{\epsilon}^{\text{in}}$. Therefore, a unique solution of equation (3.14) exists under the convexity assumption for $U(\hat{\epsilon})$ [54].

3.2. Atomistic simulations

We aim at replacing over-rich interatomic potentials, as typically used in molecular dynamics simulations, by suitable simplified *constitutive force fields*, paradigmatically accounting for any given elastic behavior and fully exploiting the atomistic features of condensed matter (but still conceiving the continuum description of the relevant elastic phenomena).

We will develop this notion for two-dimensional elastic problems. The reason for that is twofold: on the one hand, the typical boundary conditions considered in the next sections for several three-dimensional nanostructures actually lead to effective two-dimensional mathematical settings; on the other hand, the elasticity of two-dimensional atomic sheets (such as graphene) will be a main concern in this review. In particular, we will adopt a triangular two-dimensional lattice, since it is the only structure which always exhibits an isotropic linear elastic behavior and, therefore, allows us to perform a thorough comparison between atomistic and continuum results.

3.2.1. Building a constitutive force field. If we take into consideration a system of N interacting particles, the potential energy U_{p} (already introduced in section 2.5) is a function of the vector distances $\{\vec{r}_{\alpha\beta}\}_{\alpha,\beta=1,N}$ between each pair of atoms. For further convenience, we cast U_{p} in the form of the following power series:

$$U_{\text{p}} = U_0 + \sum K^{ij}_{\alpha\beta\gamma\delta} r_{\alpha\beta,i} r_{\gamma\delta,j} + \sum K^{ijk}_{\alpha\beta\gamma\delta\zeta\eta} r_{\alpha\beta,i} r_{\gamma\delta,j} r_{\zeta\eta,k} + \cdots \tag{3.16}$$

where $r_{\alpha\beta,i}$ $(i = x, y, z)$ is the ith coordinate of the vector distance between the atom α and the atom β, while U_0, $K^{ij}_{\alpha\beta\gamma\delta}$, $K^{ijk}_{\alpha\beta\gamma\delta\zeta\eta}$, ... and so on are constants. This function must show a minimum at equilibrium: in the following, we will indicate such a reference configuration as $\{\vec{r}^{\,0}_{\alpha\beta}\}_{\alpha,\beta=1,N}$, defined but for an arbitrary roto-traslation of the particles system. For the sake of simplicity, the formal expansion given in equation (3.16) will be arrested at the third-order term in the interatomic distance vectors.

If the system is subjected to a uniform strain field $\hat{\epsilon}$, the vector distance between the atom α and the atom β is given by $\vec{r}_{\alpha\beta} = \vec{r}^{\,0}_{\alpha\beta} + \hat{\epsilon}\,\vec{r}^{\,0}_{\alpha\beta}$ and the corresponding strain energy density is

$$U(\hat{\epsilon}) = \frac{1}{V_0} U_{\text{p}}(\{\vec{r}^{\,0}_{\alpha\beta} + \hat{\epsilon}\,\vec{r}^{\,0}_{\alpha\beta}\}_{\alpha,\beta=1,N}), \tag{3.17}$$

where V_0 is the volume of the reference (unstrained) configuration (see equation (2.33)). Using equation (3.16) in equation (3.17) and by expanding $U(\hat{\epsilon})$ in powers of $\hat{\epsilon}$, it is easy to prove that the linear and nonlinear elastic constants must be linear functions of the parameters $K^{ij}_{\alpha\beta\gamma\delta}$ and $K^{ijk}_{\alpha\beta\gamma\delta\zeta\eta}$. Therefore, it is possible to obtain any elastic behavior by properly setting the K-parameters of the lattice model.

As a useful example, we consider a simple constitutive force field given by harmonic springs between neighboring atoms placed at $\vec{r}_\alpha$ and $\vec{r}_\beta$. The corresponding pair elastic potential energy is

$$U^{2\text{b}}_{\text{h}}(r_{\alpha\beta}; \kappa_{\text{h}}) = \tfrac{1}{2}\kappa_{\text{h}}(r_{\alpha\beta} - r_0)^2, \tag{3.18}$$

where $r_{\alpha\beta} = |\,\vec{r}_{\alpha\beta}\,| = |\,\vec{r}_\alpha - \vec{r}_\beta\,|$, κ_{h} is the spring constant and r_0 is the equilibrium distance. The subscript h stands for *harmonic*. The term $U^{2\text{b}}$ is intended to mimic bond-stretching interactions. If we expand equation (3.18) in the form of equation (3.16), all the coefficients $K^{ij}_{\alpha\beta\gamma\delta}$, $K^{ijk}_{\alpha\beta\gamma\delta\zeta\eta}$, ... will be simply proportional to the spring constant κ_{h}. If the system is subjected to a displacement field $\vec{u}$, so that $\vec{r}_{\alpha\beta} = \vec{r}^{\,0}_{\alpha\beta} + \Delta\vec{u}_{\alpha\beta}$ being $\Delta\vec{u}_{\alpha\beta} = \vec{u}(\vec{r}^{\,0}_\alpha) - \vec{u}(\vec{r}^{\,0}_\beta)$, the potential energy for the α–β pair is

$$U^{2\text{b}}_{\text{h}} = \tfrac{1}{2}\kappa_{\text{h}}(|\,\vec{r}^{\,0}_{\alpha\beta} + \Delta\vec{u}_{\alpha\beta}\,| - r_0)^2. \tag{3.19}$$

We can expand this function in powers of $\vec{u}$, eventually obtaining

$$U^{2\text{b}}_{\text{h}} = \tfrac{1}{2}\kappa_{\text{h}}(\vec{n}_{\alpha\beta}\cdot\Delta\vec{u}_{\alpha\beta})^2 + \mathcal{O}(u^3), \tag{3.20}$$

where $\vec{n}_{\alpha\beta} = (\vec{r}^{\,0}_{\alpha\beta}/r_0)$. If the displacement field corresponds to a uniform strain $\hat{\epsilon}$, it can be expressed as $\Delta\vec{u}_{\alpha\beta} = \hat{\epsilon}\,\vec{r}^{\,0}_{\alpha\beta}$ and equation (3.20) assumes the form

$$U^{2\text{b}}_{\text{h}} = \tfrac{1}{2}\kappa_{\text{h}}(\vec{n}_{\alpha\beta}\cdot\hat{\epsilon}\,\vec{r}^{\,0}_{\alpha\beta})^2 + \mathcal{O}(\epsilon^3). \tag{3.21}$$

We can easily verify that the linear elastic moduli are proportional to the potential parameter κ_h. Moreover, we can see that, through the $\mathcal{O}(\epsilon^3)$ term in equation (3.21), the harmonic interaction also affects the nonlinear behavior, i.e. the nonlinear elastic constants will be proportional to κ_h as well. Therefore, if we are interested in modeling a purely linear elastic regime, we can use just the second-order term in equation (3.20), by obtaining a corresponding ideal linear elastic constitutive model. We name such a linearized potential energy a *linearized spring*, assuming the form

$$U_l^{2b}(r_{\alpha\beta};\kappa_l) = \mathcal{L}_{\mathcal{IN}}\left[\tfrac{1}{2}\kappa_l(r_{\alpha\beta}-r_0)^2\right] = \tfrac{1}{2}\kappa_l(\vec{n}_{\alpha\beta}\cdot\Delta\vec{u}_{\alpha\beta})^2, \tag{3.22}$$

where we have introduced a new spring constant κ_l (l stands for *linear*) and the linearization operator $\mathcal{L}_{\mathcal{IN}}$.

A similar analysis can be performed on the following three-body harmonic potential energy:

$$U_h^{3b}(\theta_{\alpha\beta\gamma};\gamma_h) = \frac{1}{2}\frac{\gamma_h}{r_0{}^2}(\cos\theta_{\alpha\beta\gamma}-\cos\theta_0)^2, \tag{3.23}$$

which is intended to mimic bond-bending interactions. In equation (3.23) $\cos\theta_{\alpha\beta\gamma} = \vec{r}_{\alpha\beta}\cdot\vec{r}_{\alpha\gamma}/|\,\vec{r}_{\alpha\beta}\,||\,\vec{r}_{\alpha\gamma}\,|$ and θ_0 is the equilibrium angle of the 3-body interaction. In this case we obtain

$$\begin{aligned} U_h^{3b} &= \frac{1}{2}\frac{\gamma_h}{r_0{}^4}[\vec{n}_{\alpha\beta}\cdot\Delta\vec{u}_{\alpha\gamma}+\vec{n}_{\alpha\gamma}\cdot\Delta\vec{u}_{\alpha\beta} \\ &\quad -\cos\theta_0(\vec{n}_{\alpha\beta}\cdot\Delta\vec{u}_{\alpha\beta}+\vec{n}_{\alpha\gamma}\cdot\Delta\vec{u}_{\alpha\gamma})]^2+\mathcal{O}(u^3). \end{aligned} \tag{3.24}$$

Similarly to the bond-stretching case, the three-body harmonic interaction introduces both a linear and a nonlinear contribution to the strain energy density. Therefore, a purely linear elastic constitutive model can be obtained by introducing the following *linearized bond-bending energy*:

$$\begin{aligned} U_l^{3b}(\theta_{\alpha\beta\gamma};\gamma_l) &= \mathcal{L}_{\mathcal{IN}}\left[\frac{1}{2}\frac{\gamma_l}{r_0^2}(\cos\theta-\cos\theta_0)^2\right] \\ &= \frac{1}{2}\frac{\gamma_l}{r_0{}^4}\left[\vec{n}_{\alpha\beta}\cdot\Delta\vec{u}_{\alpha\gamma}+\vec{n}_{\alpha\gamma}\cdot\Delta\vec{u}_{\alpha\beta}\right. \\ &\quad \left.-\cos\theta_0\left(\vec{n}_{\alpha\beta}\cdot\Delta\vec{u}_{\alpha\beta}+\vec{n}_{\alpha\gamma}\cdot\Delta\vec{u}_{\alpha\gamma}\right)\right]^2. \end{aligned} \tag{3.25}$$

The potential energy terms given in equations (3.18) and (3.23) and in equations (3.22) and (3.25) are additive and their sum actually describes the resulting elastic behavior of the system of particles.

In order to generalize this conceptual scheme we introduce two *anharmonic* terms (for two-body and three-body interactions, respectively) as

$$U_a^{2b}(r_{\alpha\beta};\kappa_a) = \frac{1}{3}\frac{\kappa_a}{r_0}\left(r_{\alpha\beta}-r_0\right)^3, \tag{3.26}$$

$$U_a^{3b}(\theta_{\alpha\beta\gamma};\gamma_a) = \frac{1}{3}\frac{\gamma_a}{r_0^2}(\cos\theta_{\alpha\beta\gamma}-\cos\theta_0)^3. \tag{3.27}$$

The final resulting potential energy is therefore written as

$$\begin{aligned} U_p &= U_0+\tfrac{1}{2}\sum_{\alpha\beta}[U_l^{2b}(r_{\alpha\beta};\kappa_l)+U_h^{2b}(r_{\alpha\beta};\kappa_h)+U_a^{2b}(r_{\alpha\beta};\kappa_a)] \\ &\quad +\sum_{\alpha\beta\gamma}[U_l^{3b}(\theta_{\alpha\beta\gamma};\gamma_l)+U_h^{3b}(\theta_{\alpha\beta\gamma};\gamma_h)+U_a^{3b}(\theta_{\alpha\beta\gamma};\gamma_a)] \end{aligned} \tag{3.28}$$

where nonlinear features are described through the harmonic and the anharmonic contributions in the constitutive model. Interestingly enough, equation (3.28) can be applied to any kind of lattice.

3.2.2. Definition of the two-dimensional linear and nonlinear elastic moduli. By considering a two-dimensional nonlinear isotropic material, the strain energy density must depend only on the invariants of the tensor $\hat{\epsilon}$, i.e. it must hold that $U(\hat{\epsilon}) = U(\mathrm{Tr}(\hat{\epsilon}),\mathrm{Tr}(\hat{\epsilon}^2))$ [48]. By limiting nonlinear features to the third order, we can write

$$U(\hat{\epsilon}) = \frac{\lambda}{2}\mathrm{Tr}(\hat{\epsilon})^2+\mu\ \mathrm{Tr}(\hat{\epsilon}^2)+\mathsf{e}\ \mathrm{Tr}(\hat{\epsilon})\mathrm{Tr}(\hat{\epsilon}^2)+\mathsf{f}\ \mathrm{Tr}(\hat{\epsilon})^3, \tag{3.29}$$

where λ and μ are the Lamé constants describing the linear elasticity of the system, while the nonlinear behavior is modeled by the two coefficients e and f (nonlinear Landau moduli) [17]. The Lamé constants can be expressed in terms of the two-dimensional Young's modulus E and Poisson's ratio ν (plane strain conditions) or, equivalently, in terms of the stiffness tensor components as

$$\lambda = \frac{\nu E}{1-\nu^2} = C_{12}, \tag{3.30}$$

$$\mu = \frac{E}{2(1+\nu)} = \frac{C_{11}-C_{12}}{2} = C_{44}. \tag{3.31}$$

We note that, since the system is isotropic, the Cauchy relation $2C_{44} = C_{11}-C_{12}$ is always fulfilled. Moreover, the coefficients e and f can be expressed in terms of the standard third-order elastic moduli through the following relations [56, 57]:

$$\mathsf{e} = \tfrac{1}{4}(C_{111}-C_{112}) \qquad \mathsf{f} = \tfrac{1}{4}(C_{112}-\tfrac{1}{3}C_{111}). \tag{3.32}$$

In conclusion, in the case of a fully isotropic medium the nonlinear elasticity is modeled by two independent elastic constants, namely e and f (or, equivalently, C_{111} and C_{112}).

The above system is not related to any crystalline symmetry group since all of them are characterized by an anisotropic nonlinear elastic behavior [56]. Nevertheless, such a fully isotropic model describes the paradigmatic Eshelby configuration of section 3.1. From the atomistic point of view, the most similar crystal class corresponds to a triangular planar lattice, which exhibits an isotropic behavior in the linear elastic regime at least. Therefore, we will develop our atomistic model for such a lattice.

Since the strain energy function is invariant under a rotation of $\pi/3$ about the principal axis (normal to the lattice plane), there exist two linear moduli and three nonlinear independent elastic coefficients hereafter named Λ_1, Λ_2 and Λ_3 [57]. It can be easily proved that

$$\begin{aligned} U(\hat{\epsilon}) &= \frac{\lambda}{2}[\mathrm{Tr}(\hat{\epsilon})]^2+\mu\ \mathrm{Tr}(\hat{\epsilon}^2)+\Lambda_1(\epsilon_{xx}-\epsilon_{yy}) \\ &\quad \times[(\epsilon_{xx}-\epsilon_{yy})^2-12\epsilon_{xy}^2]+\frac{1}{2}\Lambda_2\mathrm{Tr}(\hat{\epsilon}) \\ &\quad \times[2\ \mathrm{Tr}(\hat{\epsilon}^2)-\mathrm{Tr}(\hat{\epsilon})^2]+\frac{1}{2}\Lambda_3\mathrm{Tr}(\hat{\epsilon})^3, \end{aligned} \tag{3.33}$$

Table 1. Contributions to the linear and nonlinear stiffness tensor components (C_{ij} and C_{ijk}) and to the elastic moduli (λ, μ, Λ_1, Λ_2 and Λ_3) of the constitutive force field terms (U^{α}_{β} with $\alpha = 2b$ or 3b and $\beta = l$, h or a) in the case of a planar triangular lattice.

	$U_l^{2b}(r;\kappa_l)$	$U_l^{3b}(\theta;\gamma_l)$	$U_h^{2b}(r;\kappa_h)$	$U_h^{3b}(\theta;\gamma_h)$	$U_a^{2b}(r;\kappa_a)$	$U_a^{3b}(\theta;\gamma_a)$
C_{11}	$+\frac{3\sqrt{3}}{4}\kappa_l$	$+\frac{9\sqrt{3}}{8}\gamma_l$	$+\frac{3\sqrt{3}}{4}\kappa_h$	$+\frac{9\sqrt{3}}{8}\gamma_h$	0	0
C_{12}	$+\frac{\sqrt{3}}{4}\kappa_l$	$-\frac{9\sqrt{3}}{8}\gamma_l$	$+\frac{\sqrt{3}}{4}\kappa_h$	$-\frac{9\sqrt{3}}{8}\gamma_h$	0	0
C_{111}	0	0	$+\frac{9\sqrt{3}}{16}\kappa_h$	$-\frac{189\sqrt{3}}{32}\gamma_h$	$+\frac{9\sqrt{3}}{8}\kappa_a$	$+\frac{27\sqrt{3}}{32}\gamma_a$
C_{222}	0	0	$+\frac{3\sqrt{3}}{16}\kappa_h$	$-\frac{27\sqrt{3}}{32}\gamma_h$	$+\frac{11\sqrt{3}}{8}\kappa_a$	$-\frac{27\sqrt{3}}{32}\gamma_a$
C_{112}	0	0	$-\frac{5\sqrt{3}}{16}\kappa_h$	$+\frac{117\sqrt{3}}{32}\gamma_h$	$+\frac{3\sqrt{3}}{8}\kappa_a$	$-\frac{27\sqrt{3}}{32}\gamma_a$
λ	$+\frac{\sqrt{3}}{4}\kappa_l$	$-\frac{9\sqrt{3}}{8}\gamma_l$	$+\frac{\sqrt{3}}{4}\kappa_h$	$-\frac{9\sqrt{3}}{8}\gamma_h$	0	0
μ	$+\frac{\sqrt{3}}{4}\kappa_l$	$+\frac{9\sqrt{3}}{8}\gamma_l$	$+\frac{\sqrt{3}}{4}\kappa_h$	$+\frac{9\sqrt{3}}{8}\gamma_h$	0	0
Λ_1	0	0	$+\frac{\sqrt{3}}{32}\kappa_h$	$-\frac{27\sqrt{3}}{64}\gamma_h$	$-\frac{\sqrt{3}}{48}\kappa_a$	$+\frac{9\sqrt{3}}{64}\gamma_a$
Λ_2	0	0	$+\frac{\sqrt{3}}{8}\kappa_h$	$-\frac{36\sqrt{3}}{32}\gamma_h$	$+\frac{\sqrt{3}}{4}\kappa_a$	0
Λ_3	0	0	0	0	$+\frac{\sqrt{3}}{6}\kappa_a$	0

where

$$\Lambda_1 = \tfrac{1}{12}(C_{111} - C_{222}), \qquad \Lambda_2 = \tfrac{1}{4}(C_{222} - C_{112}),$$
$$\Lambda_3 = \tfrac{1}{12}(2C_{111} - C_{222} + 3C_{112}). \tag{3.34}$$

The triangular lattice shows a linear isotropic elastic behavior (described by the Lamé coefficients λ and μ) and an anisotropic nonlinear elastic one (described by three independent elastic moduli Λ_1, Λ_2 and Λ_3). Only in the special case with $C_{111} = C_{222}$ we obtain a fully isotropic system, even in the nonlinear regime. In such an isotropic case we obtain $\Lambda_2 = \mathsf{e}$ and $\Lambda_3 - \Lambda_2 = 2\mathsf{f}$, where e and f are the nonlinear elastic constants defined in equation (3.29).

3.2.3. Mapping continuum elasticity onto an atomic lattice. In order to build a constitutive force field for a two-dimensional triangular lattice with any possible linear and nonlinear features, we assume that the corresponding potential energy is composed by two-body (U^{2b}) and three-body (U^{3b}) terms: this is the minimal formulation required to describe bond-stretching and bond-bending phenomena. The resulting potential energy is given in equation (3.28). Consistently, for a mono-component triangular lattice the linear and nonlinear elastic moduli are reported in table 1, after cumbersome algebra. This table must be used as follows: each elastic constant (or modulus) appearing in the first column is determined by adding all the entries in the corresponding row associated with the different constitutive force field terms. For example, the first elastic constant is given by $C_{11} = \frac{3\sqrt{3}}{4}(\kappa_l + \kappa_h) + \frac{9\sqrt{3}}{8}(\gamma_l + \gamma_h)$. We also note that the isotropy condition $C_{44} = (C_{11} - C_{12})/2$ is always satisfied.

We can also calculate the explicit form of Poisson's ratio

$$\nu = \frac{1}{3} - \frac{4(\gamma_l + \gamma_h)}{2(\kappa_l + \kappa_h) + 3(\gamma_l + \gamma_h)} \tag{3.35}$$

and Young's modulus

$$E = \frac{2\sqrt{3}}{3}(\kappa_l + \kappa_h)\left[\frac{(\kappa_l + \kappa_h) + \frac{9}{2}(\gamma_l + \gamma_h)}{(\kappa_l + \kappa_h) + \frac{3}{2}(\gamma_l + \gamma_h)}\right]. \tag{3.36}$$

Equation (3.35) confirms the well-known result [58] that the two-dimensional Poisson's ratio of a system subjected to only two-body interactions is $\nu = 1/3$. Moreover, it is interesting to observe that both ν and E depend only on the sums $\kappa_l + \kappa_h$ and $\gamma_l + \gamma_h$, which, therefore, govern the linear elastic behavior of our system.

Starting from the results given in table 1, we can also obtain the potential parameters for any observed (or just guessed) elastic behavior. To this aim, we first note that we have five elastic constants and six force field parameters: therefore, we have to solve an indeterminate system of simultaneous equations with five unknowns and six equations. The simpler solution is given by fixing the value of one parameter: for example, we choose to fix the value $\gamma_a = 0$, which cancel out the effects of the anharmonic three-body interaction, and we eventually obtain

$$\kappa_l = \frac{\sqrt{3}}{3}C_{11} + \frac{\sqrt{3}}{3}C_{12} + \frac{38\sqrt{3}}{9}C_{111} - 5\sqrt{3}C_{222} + \frac{17\sqrt{3}}{3}C_{112},$$
$$\gamma_l = \frac{2\sqrt{3}}{27}C_{11} - \frac{2\sqrt{3}}{9}C_{12} + \frac{32\sqrt{3}}{81}C_{111} - \frac{4\sqrt{3}}{9}C_{222} + \frac{4\sqrt{3}}{9}C_{112},$$
$$\kappa_h = -\frac{38\sqrt{3}}{9}C_{111} + 5\sqrt{3}C_{222} - \frac{17\sqrt{3}}{3}C_{112},$$

$$\gamma_h = -\frac{32\sqrt{3}}{81}C_{111} + \frac{4\sqrt{3}}{9}C_{222} - \frac{4\sqrt{3}}{9}C_{112},$$
$$\kappa_a = \frac{\sqrt{3}}{3}C_{111} - \frac{\sqrt{3}}{6}C_{222} + \frac{\sqrt{3}}{2}C_{112}. \quad (3.37)$$

These relations provide the design or the determination of the force field parameters, given the macroscopic elastic behavior, provided that it is, respectively, guessed or assigned.

4. Applications

4.1. Isolated inhomogeneity: continuum picture

The Eshelby theory as outlined in section 3.1 provides a fundamental result, namely, the strain field within both a linear [23, 24] or a nonlinear [54, 55] inhomogeneity is uniform (when the matrix is linear). We apply such results to a two-dimensional case with a circular inhomogeneity with linear Lamé coefficients by $\mu^{(2)}$ and $\lambda^{(2)}$ and nonlinear constants e and f (see equation (3.29)). On the other hand, the linear matrix is described by the moduli $\mu^{(1)}$ and $\lambda^{(1)}$; $\hat{\epsilon}^{(2)}$ and $\hat{\epsilon}^{\infty}$ represent the strain within the inhomogeneity and the remotely applied strain, respectively. It is possible to obtain the implicit equation for the internal field $\hat{\epsilon}^{(2)}$ (similarly to equation (4.17)) as

$$\hat{\varepsilon}^{\infty} = A\hat{\epsilon}^{(2)} + B\mathrm{Tr}(\hat{\epsilon}^{(2)})\hat{I} + C\mathrm{Tr}(\hat{\epsilon}^{(2)})\hat{\epsilon}^{(2)} + D\mathrm{Tr}\left[(\hat{\epsilon}^{(2)})^2\right]\hat{I} + E\mathrm{Tr}^2\left(\hat{\epsilon}^{(2)}\right)\hat{I}, \quad (4.1)$$

where

$$A = 1 - \frac{\lambda^{(1)} + 3\mu^{(1)}}{2(\lambda^{(1)} + 2\mu^{(1)})}\left(1 - \frac{\mu^{(2)})}{\mu^{(1)})}\right),$$
$$B = \frac{2(\lambda^{(2)} - \lambda^{(1)}) + \left(1 - \frac{\mu^{(2)}}{\mu^{(1)}}\right)\left(\lambda^{(1)} + \mu^{(1)}\right)}{4(\lambda^{(1)} + 2\mu^{(1)})},$$
$$C = \frac{1}{2\mu^{(1)}}\frac{\lambda^{(1)} + 3\mu^{(1)}}{\lambda^{(1)} + 2\mu^{(1)}}\mathsf{e},$$
$$D = \frac{1}{2}\frac{\mathsf{e}}{\lambda^{(1)} + 2\mu^{(1)}},$$
$$E = \frac{1}{2}\frac{3\mathsf{f}}{\lambda^{(1)} + 2\mu^{(1)}} - \frac{\lambda^{(1)} + \mu^{(1)}}{4\mu^{(1)}}\frac{\mathsf{e}}{\lambda^{(1)} + 2\mu^{(1)}} \quad (4.2)$$

are constant parameters. We eventually obtain the expression of the internal strain field as

$$\hat{\epsilon}^{(2)} = \frac{\hat{\epsilon}^{\infty}}{A} - \frac{B}{A(A+2B)}\mathrm{Tr}(\hat{\epsilon}^{\infty})\hat{I} + \frac{2B(A+B)(C+D) - EA^2}{A^2(A+2B)^3}\mathrm{Tr}^2(\hat{\epsilon}^{\infty})\hat{I} - \frac{1}{A^2(A+2B)}(C\mathrm{Tr}(\hat{\epsilon}^{\infty})\hat{\varepsilon}^{\infty} + D\mathrm{Tr}[(\hat{\epsilon}^{\infty})^2]\hat{I}). \quad (4.3)$$

The applied homogeneous uniaxial elongation is described by the strain tensor

$$\hat{\epsilon}^{\infty} = \begin{pmatrix} \epsilon & 0 \\ 0 & 0 \end{pmatrix}, \quad (4.4)$$

where ϵ is a scalar parameter describing the intensity of the uniaxial deformation (see figure 4). Equation (4.3) assumes the form

$$\hat{\epsilon}^{(2)} = \begin{pmatrix} \epsilon_l & 0 \\ 0 & \epsilon_t \end{pmatrix} = \begin{pmatrix} L^{\mathrm{I}}\epsilon + L^{\mathrm{II}}\epsilon^2 & 0 \\ 0 & T^{\mathrm{I}}\epsilon + T^{\mathrm{II}}\epsilon^2 \end{pmatrix}, \quad (4.5)$$

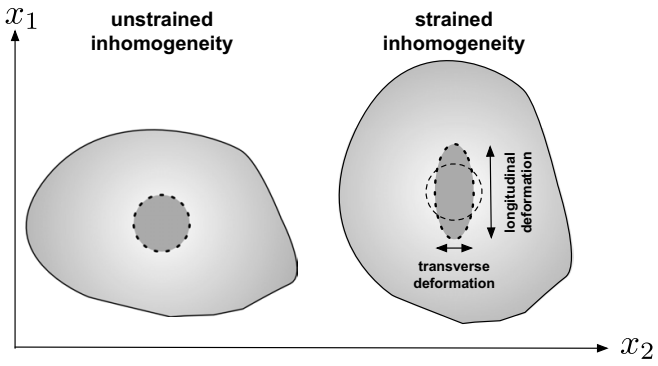

Figure 4. A matrix/inhomogeneity system under uniaxial loading along the x_1 direction. The resulting transverse and longitudinal deformation of the inhomogeneity is shown, while the corresponding strain tensor components are defined in the text.

where we have introduced the simplified notation $\epsilon_l = L^{\mathrm{I}}\epsilon + L^{\mathrm{II}}\epsilon^2$ and $\epsilon_t = T^{\mathrm{I}}\epsilon + T^{\mathrm{II}}\epsilon^2$ to indicate the fractional elongations along the longitudinal and the transverse directions, respectively (see figure 4). Both ϵ_l and ϵ_t are quadratic functions of the remotely applied strain ϵ and the four corresponding coefficients (L^{I} and T^{I} for the linear response and L^{II} and T^{II} for the nonlinear one) are the key quantities of this elastic problem. They are straightforwardly calculated as

$$L^{\mathrm{I}} = \frac{A+B}{A(A+2B)}, \quad (4.6)$$

$$T^{\mathrm{I}} = \frac{-B}{A(A+2B)}, \quad (4.7)$$

$$L^{\mathrm{II}} = \frac{-(C+D)(A^2+2AB+2B^2) - EA^2}{A^2(A+2B)^3}, \quad (4.8)$$

$$T^{\mathrm{II}} = -\frac{A^2(D+E) + 2B(A+B)(D-C)}{A^2(A+2B)^3}. \quad (4.9)$$

If the inhomogeneity is linear (i.e. $\mathsf{e} = 0$ and $\mathsf{f} = 0$), then we obtain $L^{\mathrm{II}} = 0$ and $T^{\mathrm{II}} = 0$ and the original linear Eshelby result is recovered [23, 24].

The trend shown by the parameters L^{I}, T^{I}, L^{II} and T^{II} can be usefully compared with atomistic results, as discussed in section 4.2. Such parameters represent the linear and nonlinear behavior of the longitudinal and transverse components of the internal strain induced by a remote uniaxial load. Therefore, they completely characterize the response of the system and they are well defined both for the atomistic simulations and for the continuum picture. By molecular dynamics simulations we will calculate them for different combinations of matrix and inhomogeneity. This analysis is carried out by plots (see figures 5–11) where the parameters L^{I}, T^{I}, L^{II} and T^{II} are represented (both for the continuum and the atomistic approach) in terms of the elastic contrast between the matrix and the inhomogeneity, as well as in terms of the size of the inhomogeneity. We will be able to identify the scale effects through the different elastic properties.

4.2. Isolated inhomogeneity: atomistic picture

The atomistic counterpart of the isolated inhomogeneity is developed within the constitutive force field framework introduced in section 3.2. We set two different elastic media: a fully isotropic linear material with $C_{111} = C_{222} = C_{112} = 0$ and an isotropic nonlinear one with $C_{111} = C_{222}$ [59]. The linear material is described by the set of parameters $\kappa_l = K$, $\kappa_h = 0$, $\kappa_a = 0$ and $\gamma_i = 0$ for any $i = l, h, a$, where K is a constant governing the elastic stiffness. The resulting elastic behavior is thus given by the following moduli:

$$C^l_{11} = \frac{3\sqrt{3}}{4}K, \qquad C^l_{12} = \frac{\sqrt{3}}{4}K, \qquad C^l_{111} = 0,$$
$$C^l_{222} = 0, \qquad C^l_{112} = 0. \tag{4.10}$$

The nonlinear material is described by setting $\kappa_l = 0$, $\kappa_h = K$, $\kappa_a = \frac{3}{2}K$ and $\gamma_i = 0$ for any $i = l, h, a$. Interactions are therefore composed by a *harmonic* term (affecting both the linear as the nonlinear elastic behavior) and by an *anharmonic* term (affecting only the nonlinear features), tailored to obtain an isotropic behavior. The resulting elastic moduli are

$$C^{nl}_{11} = \frac{3\sqrt{3}}{4}K, \qquad C^{nl}_{12} = \frac{\sqrt{3}}{4}K, \qquad C^{nl}_{111} = \frac{9}{4}\sqrt{3}K,$$
$$C^{nl}_{222} = \frac{9}{4}\sqrt{3}K, \qquad C^{nl}_{112} = \frac{\sqrt{3}}{4}K. \tag{4.11}$$

We have chosen the same equilibrium distance $r_0 = 3.4$ Å and the same crystallographic orientation for both the inhomogeneity and matrix materials. In so doing, we avoid the formation of disordered interfaces, which can appear in more complicated structures [60, 61]; here, we are interested in drawing a comparison with the continuum Eshelby theory which does not contain any information about features induced by possible lattice mismatch. The interaction between atoms belonging to the different phases has been described by a *linearized* spring with a constant given by the geometric mean of the stiffness of the two adjacent materials (Lorentz–Berthelot rule [62]).

The system has been analysed for different values of the *elastic contrast* between the matrix and the inhomogeneity, defined as $\log_2(K_{mat}/K_{inc})$, where K_{mat} and K_{inc} are the elastic stiffness parameters of the matrix and inhomogeneity, respectively, entering in equations (4.10) and (4.11). A positive (negative) contrast means that the matrix is stiffer (softer) than the inhomogeneity. Moreover, all the simulations are repeated for several values of the radius R of the inhomogeneity in order to study the scale effects.

In the present simulations we have described the embedded inhomogeneity by a simulation cell which is a square box of length 120 nm. The system has been relaxed through dumped dynamics in order to allow for the relaxation of the internal degrees of freedom [59].

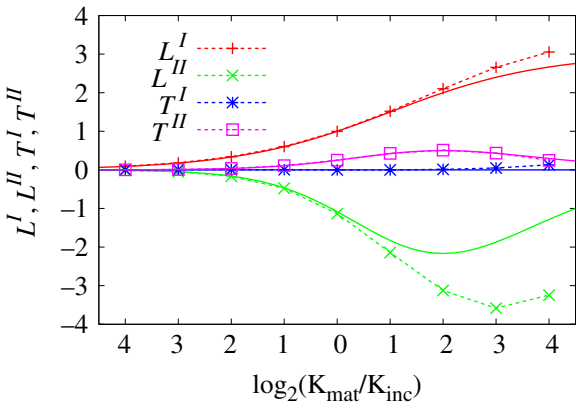

Figure 5. Longitudinal (L^I and L^{II}) and transverse (T^I and T^{II}) coefficients defined in equation (4.5) for an isolated nonlinear inhomogeneity. The solid lines represent the results of the continuum Eshelby theory. Dashed lines with + and × (□ and ∗) symbols represent the atomic result for the longitudinal (transverse) coefficients.

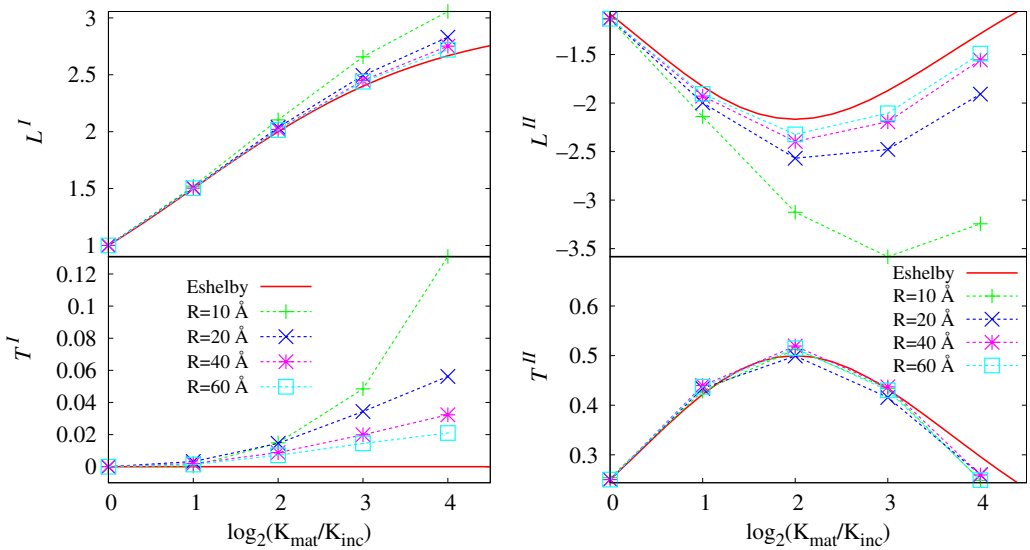

Figure 6. Coefficients L^I, T^I, L^{II} and T^{II} as a function of the elastic contrast, calculated for increasing values of the inhomogeneity radius R. The solid lines represent the Eshelby predictions, while dashed lines with symbols represent the atomistic results.

4.2.1. Nonlinear inhomogeneity in a linear matrix. We have modeled the inhomogeneity by the nonlinear isotropic elastic model represented by equation (4.11) setting $K = K_{\rm inc}$. The matrix is described, in turn, by a linear material with $K = K_{\rm mat}$ (see equation (4.10)) [59]. The inhomogeneity radius is $R = 10$ Å and the resulting internal strain field was found to be uniform.

In figure 5 we report the longitudinal and transverse coefficients of equation (4.5) for several values of the elastic contrast. As for the linear $L^{\rm I}$ and $T^{\rm I}$ coefficients, atomistic data slightly differ from the continuum prediction when the contrast is positive (i.e. when the inhomogeneity is softer than the hosting matrix) , while for negative contrast a perfect agreement between the two approaches is observed. As for the nonlinear $L^{\rm II}$ and $T^{\rm II}$ coefficient, we found once again a perfect agreement between atomistic and Eshelby results under the condition that the inhomogeneity is stiffer than the matrix (negative values of the contrast). On the other hand, atomistic effects are present in the case of positive contrast. We observe that the atomistic transverse nonlinear coefficient is equal to the corresponding continuum one for any value of the contrast. However, sizeable discrepancies have been found for the longitudinal coefficient. The disagreement between the continuum theory predictions and the atomistic results has been further investigated by varying the radius of the inhomogeneity. We have found that the two different pictures reconcile by increasing the radius of the inhomogeneity, as shown in figure 6. It is important to underline that the scale effects vanish for particles with radius larger than ∼10 nm (corresponding to $\sim 30 r_0$), while they are large in smaller particles. Therefore, ∼10 nm can be considered as the threshold for the onset of scale effects. Although this quantitative result holds for the specific case of a triangular lattice here investigated, we guess that a similar order of magnitude for such a threshold (i.e. tens of nanometers) holds as well for different crystals or nanostructures.

This result suggests that L-coefficients could indeed be affected by the actual dimension of the inhomogeneity. It is therefore worth investigating how the longitudinal linear $L^{\rm I}$ and nonlinear $L^{\rm II}$ coefficients vary as a function of R. As shown in figure 7 atomistic data are nicely fitted by a simple power law as

$$\frac{L^{\rm I}(R)}{L^{\rm I}(\infty)} = 1 + \frac{a}{R^{\alpha}} \qquad \text{and} \qquad \frac{L^{\rm II}(R)}{L^{\rm II}(\infty)} = 1 + \frac{b}{R^{\beta}}, \quad (4.12)$$

where a, b, α and β are fitting parameters. This choice implies the relationships

$$\log_{10}[L^{\rm I}(R)/L^{\rm I}(\infty) - 1] = \log_{10} a - \alpha \log_{10} R$$

and

$$\log_{10}[L^{\rm II}(R)/L^{\rm II}(\infty) - 1] = \log_{10} b - \beta \log_{10} R$$

and, therefore, α and β assume the meaning of an angular coefficient when the bi-logarithmic scale is adopted as in figure 7. In order to test if the proposed power laws are appropriate, it is sufficient to check whether the numerical data are represented by straight lines in the bi-logarithmic plane. This can be done through standard statistical techniques. We underline that the scaling exponents α and β represent a

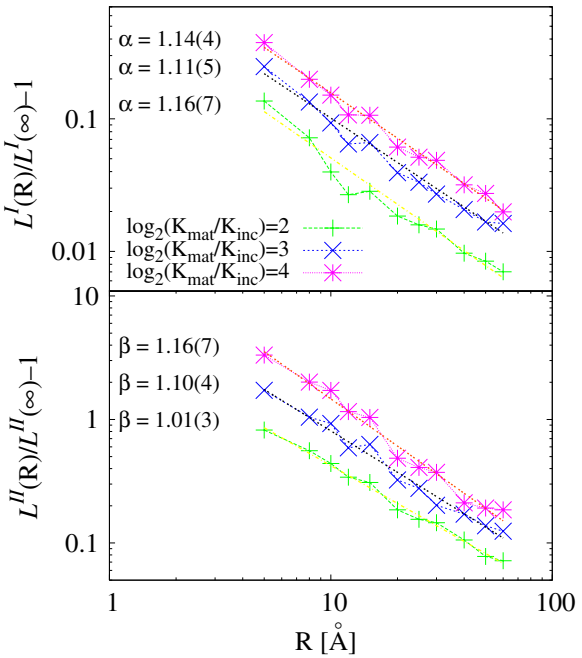

Figure 7. Fitting of equation (4.12) for different elastic contrast between the matrix and the inhomogeneity.

measure of the velocity of convergence toward the macro-scale behaviour by increasing the size R of the embedded particle. In fact, when $R \to \infty$ in equation (4.12) (with $\alpha > 0$ and $\beta > 0$) we obtain $L^{\rm I}(R) = L^{\rm I}(\infty)$ and $L^{\rm II}(R) = L^{\rm II}(\infty)$ which correspond to the case of a very large inhomogeneity without scale effects. We argue that the scaling exponent α and β are the most important parameters describing the scale behavior.

The numerical fits of equation (4.12) provide the same scaling exponent $\alpha \simeq \beta \simeq 1.11 \pm 0.05$ for the linear and nonlinear coefficients. It is important to note that the values of these scaling exponents are independent of the elastic contrast, as shown in figure 7. The above result suggests that the linear and nonlinear behaviors of our lattice system belong to the same universality class. In such a case with $\alpha = \beta$, the overall internal displacement $\epsilon_{\rm l}$ fulfils a similar simple power law $\epsilon_{\rm l}(\epsilon; R) = \epsilon_{\rm l}(\epsilon; \infty) + \Delta(\epsilon) R^{-\alpha}$, where $\Delta(\epsilon) = aL^{\rm I}(\infty)\epsilon + bL^{\rm II}(\infty)\epsilon^2$. As a consequence of such a scaling behavior, the measurement or the computation of the $\epsilon_{\rm l}(\epsilon; \tilde{R})$ curve for a given value of $\tilde{R}$, allows direct knowledge of the same curve for an arbitrary radius R, the latter being simply proportional to the former:

$$\frac{\epsilon_{\rm l}(\epsilon; R) - \epsilon_{\rm l}(\epsilon; \infty)}{\epsilon_{\rm l}(\epsilon; \tilde{R}) - \varepsilon_{l}(\epsilon; \infty)} = \left(\frac{R}{\tilde{R}}\right)^{-\alpha}. \quad (4.13)$$

In other words, because of the relation $\beta = \alpha$, inhomogeneities with different radii exhibit responses to the external load which differ only for a constant scale factor $(R/\tilde{R})^{-\alpha}$ independently of the magnitude ϵ of the applied strain. These conclusions have been proved by varying the radius oh the inhomogeneity within the range 5–60 Å.

Present results can be compared with recent investigations concerning the scale effects in nanostructured materials

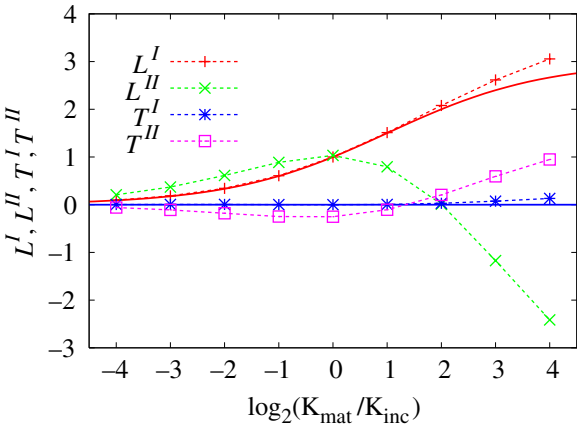

Figure 8. Linear (L^{I} and T^{I}) and nonlinear (L^{II} and T^{II}) coefficients for a linear inohomogeneity embedded in a nonlinear matrix. The solid lines represent the linear results of the continuum Eshelby theory for L^{I} and T^{I}. Dashed lines with + and × (□ and ∗) symbols represent the atomic result for the longitudinal (transverse) coefficients.

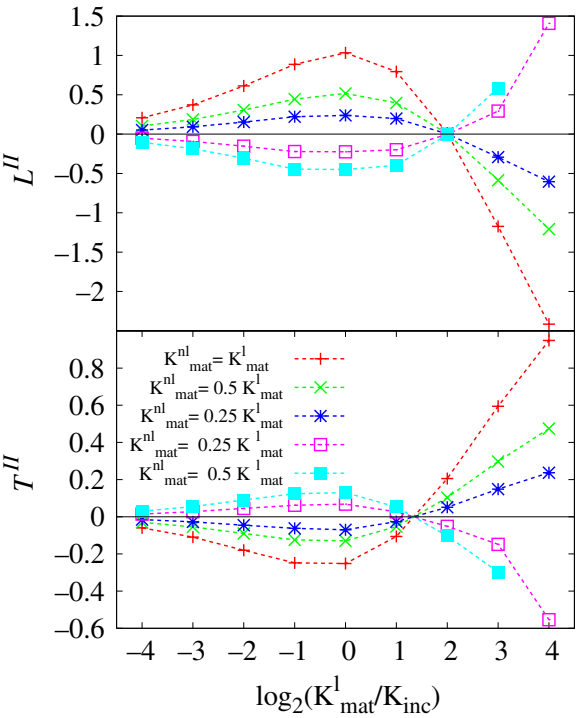

Figure 9. Atomistic results for the nonlinear coefficients L^{II} (top) and T^{II} (bottom) versus the elastic contrast $\log_2(K^{\mathrm{l}}_{\mathrm{mat}}/K_{\mathrm{inc}})$ for different values of the nonlinearity ratio $K^{\mathrm{nl}}_{\mathrm{mat}}/K^{\mathrm{l}}_{\mathrm{mat}}$ in the matrix.

[63–70]. They are all based on the so-called interface stress model (ISM) described by the displacement continuity condition and by the Young–Laplace equation for the stress behavior [71, 72]. Other models introducing scale effects are based upon nonlocal continuum field theories [73]. In [74] the elasticity of a nonideal surface is characterized by two intrinsic length scales. Thus, the size-dependence of any physical property is expected to follow a scaling law with a length scale which is a linear combination of the above two intrinsic length scales. This approach, based on the ISM, leads to the scaling exponent $\alpha = 1$ for the linear properties. This value can be explained through the competition between the elastic surface energy at the interface and the strain energy in the bulk. Our numerically estimated value $\alpha \simeq \beta \simeq 1.11 \pm 0.05$ suggests that the elastic behavior of the inhomogeneity cannot be explained just in terms of the sole competition between surface and volume effects. Rather, we suggest that it should be related to the discretization of the continuum equations at the atomic scale, a feature fully exploited only in the present lattice model, since an interface is generated by only setting different linear and nonlinear spring constants in the internal (inhomogeneity) and external (matrix) regions.

4.2.2. Linear inhomogeneity in a nonlinear matrix. We now consider the case of a linear inhomogeneity embedded in a nonlinear matrix. The elastic behavior of the inhomogeneity is described by equation (4.10) with $K = K_{\mathrm{inc}}$, while the matrix is modeled according to equation (4.11) with $K = K_{\mathrm{mat}}$ [59].

In figure 8 we report the longitudinal and transverse coefficients for several values of the elastic contrast. Even in this case the internal strain field is found to be uniform, although this result is not anticipated by the Eshelby theory. By comparing figures 8 and 5, we can state that when the inhomogeneity is nonlinear then the coefficients L^{II} and T^{II} have constant sign, independently of the contrast. Furthermore, they exhibit a minimum and a maximum, respectively (see figure 5). In contrast, when the matrix is nonlinear it is remarkable to observe that two values of contrast exist which cancel out the second-order nonlinear effects in the longitudinal and transverse direction, respectively (figure 8).

As mentioned above, to the best of the author's knowledge a continuum theory solution of this case is not available. Therefore, we further analyze the elastic behavior of the inhomogeneity/matrix system by varying the nonlinearity of the matrix. To this aim, we have set $\kappa_{\mathrm{l}} = K$, $\kappa_{\mathrm{h}} = K'$ and $\kappa_{\mathrm{a}} = \frac{3}{2}K'$ within the nonlinear matrix, where K and K' are constants, so as to obtain

$$C^{\mathrm{nl}}_{11} = \frac{3\sqrt{3}}{4}K^{\mathrm{l}}_{\mathrm{mat}}, \qquad C^{\mathrm{nl}}_{12} = \frac{\sqrt{3}}{4}K^{\mathrm{l}}_{\mathrm{mat}}, \qquad C^{\mathrm{nl}}_{111} = \frac{9}{4}\sqrt{3}K^{\mathrm{nl}}_{\mathrm{mat}},$$
$$C^{\mathrm{nl}}_{222} = \frac{9}{4}\sqrt{3}K^{\mathrm{nl}}_{\mathrm{mat}}, \qquad C^{\mathrm{nl}}_{112} = \frac{\sqrt{3}}{4}K^{\mathrm{nl}}_{\mathrm{mat}}, \tag{4.14}$$

where $K^{\mathrm{l}}_{\mathrm{mat}} = K + K'$ and $K^{\mathrm{nl}}_{\mathrm{mat}} = K'$ directly affect the linear and nonlinear behavior, respectively. By varing the value of $K^{\mathrm{nl}}_{\mathrm{mat}}$ with respect to $K^{\mathrm{l}}_{\mathrm{mat}}$, we can emphasize the nonlinear regime. In figure 9 we report the atomistic results for the nonlinear coefficients L^{II} (top) and T^{II} (bottom) versus the (linear) elastic contrast for different values of nonlinearity ratio $K^{\mathrm{nl}}_{\mathrm{mat}}/K^{\mathrm{l}}_{\mathrm{mat}}$ in the matrix. We have not reported the results for the linear coefficients L^{I} and T^{I} since they are not affected by the nonlinear features of both inhomogeneity and matrix; indeed, they assume the very same values reported in figure 8. It is interesting to underline that the longitudinal coefficient L^{II} vanishes for a given linear contrast for any possible value of the nonlinear parameter $K^{\mathrm{nl}}_{\mathrm{mat}}$ of the matrix. The same phenomenon has been observed for the transverse coefficient T^{II}.

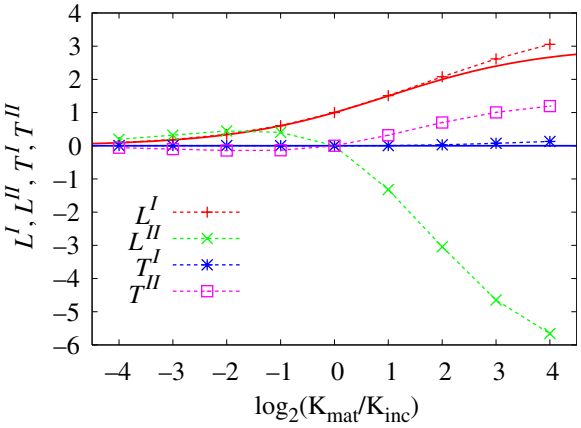

Figure 10. Linear (L^{I} and T^{I}) and nonlinear (L^{II} and T^{II}) coefficients for a nonlinear inhomogeneity embedded in a nonlinear matrix. The solid lines represent the linear results of the continuum Eshelby theory. Dashed lines with + and × (□ and ∗) symbols represent the atomic result for the longitudinal (transverse) coefficients.

4.2.3. Nonlinear inhomogeneity in a nonlinear matrix. We finally consider the case of a nonlinear inhomogeneity embedded in a nonlinear matrix. We start by considering both media as described in equation (4.11) with $K = K_{\mathrm{inc}}$ and $K = K_{\mathrm{mat}}$, respectively in the inhomogeneity and matrix [59]. In figure 10 we report the longitudinal and transverse coefficients for several values of the elastic contrast. In this case the zero contrast value corresponds to a nonlinear but homogeneous material (without inhomogeneity). Therefore, we obtained $L^{\mathrm{II}} = T^{\mathrm{II}} = 0$ and $L^{\mathrm{I}} = 1$ for $K_{\mathrm{mat}} = K_{\mathrm{inc}}$, as expected.

Since, as in the previous case, this configuration is hardly affordable by continuum theory, we performed a more detailed analysis by investigating several nonlinear hosting matrices, all modeled by equation (4.14) but characterized by a different ratio $K^{\mathrm{nl}}_{\mathrm{mat}}/K^{\mathrm{l}}_{\mathrm{mat}}$ between the nonlinear and the linear stiffness coefficients. We have instead set the behavior of the inhomogeneity according to equation (4.11), with $K = K_{\mathrm{inc}}$.

In figure 11 we show the atomistic results for the nonlinear coefficients L^{II} (top) and T^{II} (bottom) versus the elastic contrast for different values of the $K^{\mathrm{nl}}_{\mathrm{mat}}/K^{\mathrm{l}}_{\mathrm{mat}}$ ratio. We have not reported the results for the linear coefficients L^{I} and T^{I} since they are not affected by the nonlinear features of both inhomogeneity and matrix; indeed, they assume the very same values reported in figure 10. Interestingly enough, we observe that there is a value of the (linear) elastic contrast $\log_2(K^{\mathrm{l}}_{\mathrm{mat}}/K_{\mathrm{inc}})$ which generates a constant value of L^{II} (see figure 11, top) for any nonlinearity of the matrix. This result indicates that, in such a specific condition, the nonlinear effects of the matrix are quenched. The same behavior is also observed for the transverse coefficient T^{II} (see figure 11, bottom).

4.2.4. General conclusions. We have proved that our elastic lattice model is in perfect agreement with the continuum Eshelby theory for linear or nonlinear large inhomogeneities embedded in a linear matrix. However, when the radius of the inhomogeneity becomes comparable to the interatomic distance characterizing the selected material, scale effects

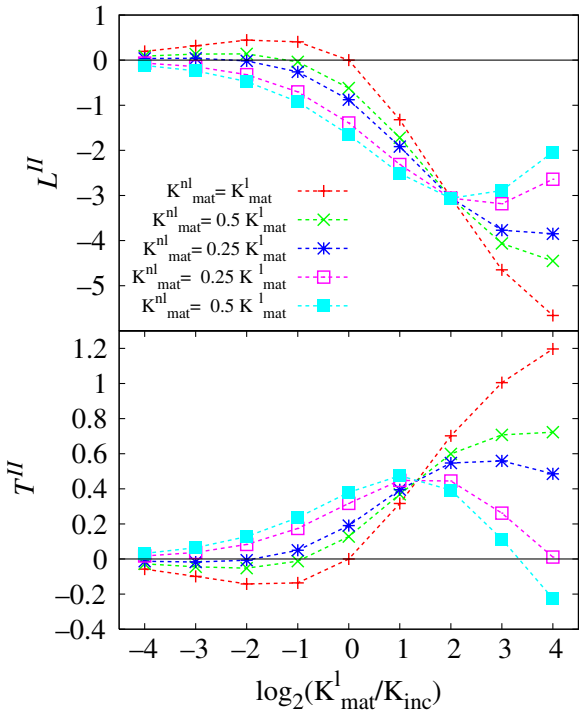

Figure 11. Atomistic results for the nonlinear coefficients L^{II} (top) and T^{II} (bottom) versus the (linear) elastic contrast $\log_2(K^{\mathrm{l}}_{\mathrm{mat}}/K_{\mathrm{inc}})$ for different values of the $K^{\mathrm{nl}}_{\mathrm{mat}}/K^{\mathrm{l}}_{\mathrm{mat}}$ ratio in the matrix.

indeed affect the elastic features, resulting in sizable deviations from the continuum results. More specifically, we have provided evidence that such effects are stronger for a positive elastic contrast, i.e. for a matrix stiffer than the inhomogeneity. The threshold for the onset of possible scale effects can be set at a few tens of nm.

By further investigating the case of a nonlinear matrix embedding a linear inhomogeneity, we have proved that the nonlinear response vanishes for a given linear contrast (for any nonlinearity of the matrix).

Finally, we have proved that linear and nonlinear scale effects are described by the same scaling exponent, independently of the elastic contrast. This suggests that the overall strain or stress field within the inhomogeneity can be described by a similar power law with the same scaling exponent.

4.3. Isolated inhomogeneity: interface effects

The mechanical behavior of nanostructured materials is strongly affected by interface features, occurring at the boundary between phases characterized by different elastic constitutive equations or crystalline structures. These effects can only be described by taking into account the exact atomistic architecture of the two phases and of the interface. Therefore, the elastic lattice model describe above is no longer suitable.

In this section we briefly describe an alternative approach, based on standard molecular dynamics (MD) simulations. As a paradigmatic example, we study the elastic behavior of a silicon nanowire embedded in a silicon matrix. The input configuration is obtained by rotating a cylindrical portion with

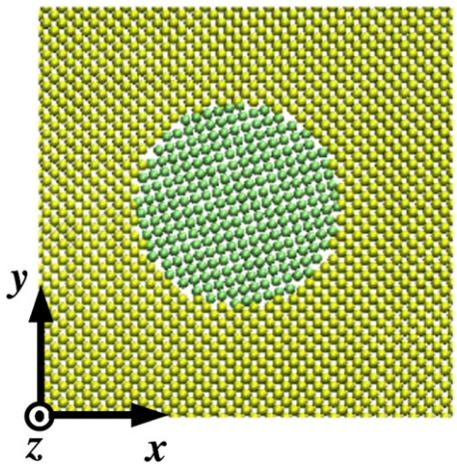

Figure 12. A model of a nanowire embedded in a homogeneous matrix. See text for details about the atomic structure.

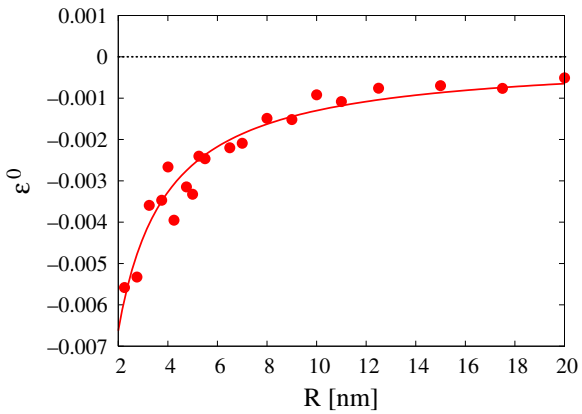

Figure 13. Prestrain within an embedded nanowire as a function of its radius R. Symbols (solid line) represent MD (continuum) results.

radius R of a Si crystal by an angle $\theta = \pi/4$ around the (0 0 1) axis (hereafter referred to as the z-axis), as shown in figure 12. The interface structure is obtained by a careful MD relaxation of the system, based on the realistic Tersoff potential.

Because of the cubic symmetry of the diamond lattice, the rotated cylinder behaves, upon loading along the y-axis, as an inclusion with a different elastic response than the hosting matrix. By generating the input structure as above, we have arranged several samples with $2\,\text{nm} < R < 20\,\text{nm}$ and we have computed the atomic displacement field: the disordered interface generates a uniform hydrostatic compression within the inclusion. Therefore, MD simulations predict that even in the absence of any external load, the inclusions exhibit a state of uniform internal prestrain.

In figure 13 we report the calculated value of the prestrain versus the nanowire radius R: in absolute value the prestrain vanishes for large wires, as expected. By evaluating the atom number density $n_{\text{at}}(r)$ as a function of the distance r from the center of the nanowire, it is found that $n_{\text{at}}(r = R) < n_{\text{at}}^{\text{Si}}$, where $n_{\text{at}}^{\text{Si}}$ is the corresponding quantity for bulk crystalline Si. The interface region effectively behaves as a different material, i.e. a coating of thickness d inserted between the matrix and the inclusion. Therefore, the volume available for the inclusion

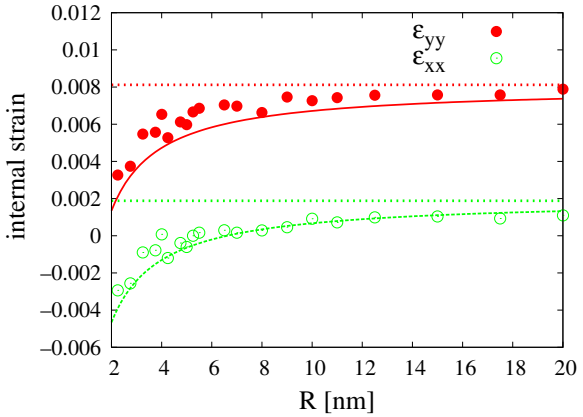

Figure 14. Longitudinal (ϵ_{yy}) and transverse (ϵ_{xx}) strain components within a loaded nanowire as a function of its radius R. Full and dashed lines represent the continuum theory elaborated in [61]. We also show by dotted lines the corresponding asymptotic values approached when the interface-induced prestrain becomes negligible (Eshelby theory).

is reduced with respect to the initial configuration by a factor $((R - d)/R)^2$. When R increases this volume variation and the resulting prestrain tend to zero. A continuum model able to take into consideration this effect is described in [61] and the corresponding result is shown in figure 13.

A uniaxial homogeneous elongation of 1% along the y direction is now applied to the sample and the longitudinal and the transverse strain fields inside the embedded wire are calculated after further MD relaxation; reported in figure 14. For large values of the radius, the effect of the interface-induced prestrain is negligible and the elastic fields become size independent. Moreover, in the limit of vanishing prestrain (or equivalently for $R \to \infty$), the constant values approached by the atomistic data correspond to those predicted by the Eshelby continuum model. Prestrain effects can be taken into account by a specific modification of the continuum theory, as described in [61].

4.4. Dispersions of inhomogeneities

The general result stated in equation (3.14) can be applied (through a suitable homogenization procedure) to model any dispersion of arbitrarily nonlinear and anisotropic inhomogeneities [55]. In particular, we will consider the specific case of a distribution of spherically shaped nanoparticles, as shown in figure 15. Their density is described by the volume fraction $c = V_{\text{e}}/V$, defined as the ratio between the total volume V_{e} of the embedded inhomogeneities and the total volume V of the heterogeneous material.

As for the elastic behavior, we assume that the matrix is described by the linear constitutive equation $\hat{T} = 2\mu_1\hat{\epsilon} + \left(K_1 - \frac{2}{3}\mu_1\right)\text{Tr}(\hat{\epsilon})\hat{I}$, where K_1 and μ_1 are the bulk and shear moduli, respectively. The spherical inhomogeneities, in turn, will be described by the most general isotropic nonlinear constitutive equation expanded up to the second order in the strain components. The corresponding strain energy density

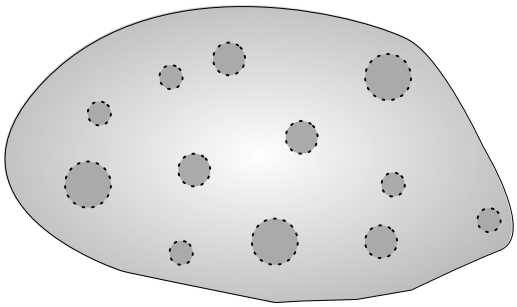

Figure 15. Dispersion of nonlinear spherical inhomogeneities (characterized by linear moduli K_2 and μ_2 and Landau coefficients A, B and C) of total volume V_e, embedded in a linear matrix (characterized by linear moduli K_1 and μ_1). The total volume of the heterogeneous system is V and, therefore, the inhomogeneities' volume fraction is $c = V_e/V$.

$U(\hat{\epsilon})$ is given by

$$U(\hat{\epsilon}) = \mu_2 \mathrm{Tr}\left(\hat{\epsilon}^2\right) + \frac{1}{2}\left(K_2 - \frac{2}{3}\mu_2\right)\left[\mathrm{Tr}\left(\hat{\epsilon}\right)\right]^2 + \frac{A}{3}\mathrm{Tr}\left(\hat{\epsilon}^3\right) + B\mathrm{Tr}\left(\hat{\epsilon}\right)\mathrm{Tr}\left(\hat{\epsilon}^2\right) + \frac{C}{3}\left[\mathrm{Tr}\left(\hat{\epsilon}\right)\right]^3, \quad (4.15)$$

which through equation (2.25) provides the following expression for the stress tensor:

$$\hat{T} = 2\mu_2\hat{\epsilon} + \left(K_2 - \frac{2}{3}\mu_2\right)\mathrm{Tr}\left(\hat{\epsilon}\right)\hat{I} + A\hat{\epsilon}^2 + B\{\mathrm{Tr}(\hat{\epsilon}^2)\hat{I} + 2\hat{\epsilon}\mathrm{Tr}(\hat{\epsilon})\} + C[\mathrm{Tr}(\hat{\epsilon})]^2\hat{I}. \quad (4.16)$$

The parameters A, B and C are the Landau moduli [17] and they represent the deviation from standard linearity. By inserting equation (4.16) and the explicit expression of the Eshelby tensor for a sphere [15] into equation (3.14), it can be proved that

$$L\hat{\epsilon}^{\mathrm{in}} + M\mathrm{Tr}(\hat{\epsilon}^{\mathrm{in}})\hat{I} + N(\hat{\epsilon}^{\mathrm{in}})^2 + O\hat{\epsilon}^{\mathrm{in}}\mathrm{Tr}(\hat{\epsilon}^{\mathrm{in}}) + P\mathrm{Tr}\left[(\hat{\epsilon}^{\mathrm{in}})^2\right]\hat{I} + Q\left[\mathrm{Tr}(\hat{\epsilon}^{\mathrm{in}})\right]^2\hat{I} = \hat{\epsilon}^{\infty} \quad (4.17)$$

defining the explicit relation between the internal strain $\hat{\epsilon}^{\mathrm{in}}$ and the remote deformation $\hat{\epsilon}^{\infty}$, for a single nonlinear spherical inhomogeneity. The parameters

$$L = 1 + \frac{6}{5}\frac{K_1 + 2\mu_1}{3K_1 + 4\mu_1}\left(\frac{\mu_2}{\mu_1} - 1\right), \quad (4.18)$$

$$M = \frac{5K_2 - K_1\left(3 + 2\frac{\mu_2}{\mu_1}\right) - 4(\mu_2 - \mu_1)}{5(3K_1 + 4\mu_1)}, \quad (4.19)$$

$$N = \frac{3}{5}\frac{A}{\mu_1}\frac{K_1 + 2\mu_1}{3K_1 + 4\mu_1}, \quad (4.20)$$

$$O = \frac{6}{5}\frac{B}{\mu_1}\frac{K_1 + 2\mu_1}{3K_1 + 4\mu_1}, \quad (4.21)$$

$$P = \frac{1}{15(3K_1 + 4\mu_1)}\left[15B - A\left(1 + 3\frac{K_1}{\mu_1}\right)\right], \quad (4.22)$$

$$Q = \frac{1}{15(3K_1 + 4\mu_1)}\left[15C - 2B\left(1 + 3\frac{K_1}{\mu_1}\right)\right] \quad (4.23)$$

depend on both linear and nonlinear moduli.

In order to investigate the case shown in figure 15 we will add the approximation of dilute dispersion corresponding to the limit of a small volume fraction, indeed a case of relevant practical interest. Under this assumption, the average value of the strain in the overall system is given by $\langle\hat{\epsilon}\rangle = c\hat{\epsilon}^{\mathrm{in}} + (1-c)\hat{\epsilon}^{\infty}$ [43]. Similarly, the average value of the stress is $\langle\hat{T}\rangle = \hat{\mathcal{C}}^{(1)}\langle\hat{\epsilon}\rangle + c\hat{T}^{\mathrm{in}} - c\,\hat{\mathcal{C}}^{(1)}\hat{\epsilon}^{\mathrm{in}}$ [43]. The average fields $\langle\hat{T}\rangle$ and $\langle\hat{\epsilon}\rangle$, combined through equation (4.17), determine the effective constitutive equation for the heterogeneous system. Basically, it is written as equation (4.16) where, however, a new set of effective linear and nonlinear elastic moduli must be introduced: the linear ones are given by

$$\mu_{\mathrm{eff}} = \mu_1 + c\frac{\mu_2 - \mu_1}{c + (1-c)\left[1 + \frac{6}{5}\left(\frac{\mu_2}{\mu_1} - 1\right)\frac{K_1 + 2\mu_1}{3K_1 + 4\mu_1}\right]}, \quad (4.24)$$

$$K_{\mathrm{eff}} = K_1 + \frac{(3K_1 + 4\mu_1)(K_2 - K_1)c}{3K_2 + 4\mu_1 - 3c(K_2 - K_1)}, \quad (4.25)$$

while the effective counterparts of the Laundau coefficients for the heterogeneous systems are

$$A_{\mathrm{eff}} = c\frac{A}{L'^2} - 2c\frac{N'(\mu_2 - \mu_1)}{L'^3}, \quad (4.26)$$

$$B_{\mathrm{eff}} = 2c\frac{(N'M' - L'P')(\mu_2 - \mu_1)}{L'^3(L' + 3M')} - c\frac{(N' + 3P')\left[K_2 - K_1 - \frac{2}{3}(\mu_2 - \mu_1)\right]}{L'^2(L' + 3M')} + c\frac{B}{L'^2}, \quad (4.27)$$

$$C_{\mathrm{eff}} = \frac{1}{9}\frac{c(9C + 9B + A)}{(L' + 3M')^2} + \frac{1}{9}\frac{c(A - 3B)}{L'^2} + \frac{1}{9}\frac{c(4N' + 6O')(\mu_2 - \mu_1)}{L'^2(L' + 3M')} - \frac{2}{9}\frac{c(3B + A)}{L'(L' + 3M')} + \frac{1}{9}\frac{c(3N' + 9P')(K_2 - K_1)}{L'^2(L' + 3M')} - \frac{4}{9}\frac{N'(\mu_2 - \mu_1)c}{L'^3} - \frac{1}{3}\frac{c(9Q' + 3O' + 3P' + N')(K_2 - K_1)}{(L' + 3M')^3}, \quad (4.28)$$

where we have introduced the parameters $L' = c + (1-c)L$, $M' = (1-c)M$, $N' = (1-c)N$, $O' = (1-c)O$, $P' = (1-c)P$ and $Q' = (1-c)Q$. We note that equations (4.24)–(4.28) hold even in the limiting case of $c = 1$, falling beyond the adopted hypothesis of small volume fraction. Interesting enough, equations (4.26)–(4.28) provide a universal mixing scheme linking the Landau coefficients of the inhomogeneities to the corresponding effective nonlinear elastic moduli of the composite system [54, 55].

In order to discuss a showcase example, we numerically solved equations (4.24)–(4.28), setting $\mu_1 = 1$, $\mu_2 = 4$, $K_1 = 10$, $K_2 = 1$, $A = -3$, $B = 8$, $C = 5$ in arbitrary units. In figure 16 we report the effective moduli versus the volume fraction c. Under the sole hypothesis that $K_1 \gg K_2$, we always observe a remarkable amplification of the nonlinear effective modulus C_{eff}. Such an intriguing feature is obtained for any set of parameters, provided that the matrix is much more incompressible than the inhomogeneities. We point out that this feature occurs well within the range of validity of the present theory, namely for small values of c (see figure 16). More generally, the enhancement of Landau moduli suggests that the nonlinear effective properties can be strongly affected

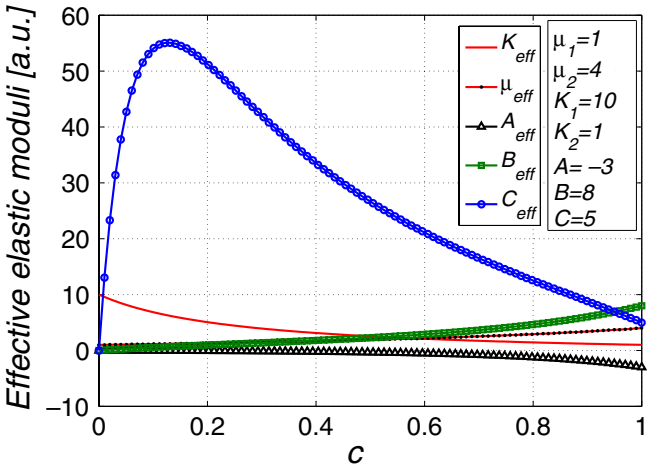

Figure 16. Variation of the linear and nonlinear effective elastic moduli of the composite system shown in figure 12 upon the volume fraction c of the inhomogeneities. The actual values of the linear elastic moduli (in arbitrary units) for the matrix (subscript 1) and for the inhomogeneities (subscript 2) are shown in the top right inset, together with the Laundau coefficients.

by the linear moduli of the constituents of the heterogeneous material [55]. For example, the ratio $C_{\rm eff}/C$ is sensibly modulated by the ratio K_1/K_2.

Finally, we briefly discuss the results concerning the two-dimensional case (dispersion of circular nonlinear inhomogeneities on the plane). The circular inhomogeneities are randomly embedded in a linear matrix with elastic moduli μ_1 and $k_1 = \lambda_1 + \mu_1$ (k_1 is the two-dimensional version of the bulk modulus). As before, we suppose that the volume fraction c of the embedded phase is small (dilute dispersion). The linear matrix is described by $\hat{T}^{(1)} = 2\mu_1\hat{\varepsilon}^{(1)} + (k_1 - \mu_1){\rm Tr}(\hat{\varepsilon}^{(1)})\hat{I}$. If we identify the linear coefficients of the inhomogeneities by μ_2 and $k_2 = \lambda_2 + \mu_2$, and their nonlinear constants by e and f, then equation (3.29) supplies the following stress–strain relation:

$$\hat{T}^{(2)} = 2\mu_2\hat{\varepsilon}^{(2)} + (k_2 - \mu_2){\rm Tr}(\hat{\varepsilon}^{(2)})\hat{I} + 2\mathsf{e}{\rm Tr}(\hat{\varepsilon}^{(2)})\hat{\varepsilon}^{(2)} + \mathsf{e}{\rm Tr}\left[(\hat{\varepsilon}^{(2)})^2\right]\hat{I} + 3\mathsf{f}{\rm Tr}^2(\hat{\varepsilon}^{(2)})\hat{I}. \tag{4.29}$$

As before, we define the average strain $\langle\hat{\epsilon}\rangle$ and average stress $\langle\hat{T}\rangle$ within the overall system. Therefore, the constitutive equation of the whole system is expressed in terms of the effective linear and nonlinear elastic moduli as follows:

$$\langle\hat{T}\rangle = 2\mu_{\rm eff}\langle\hat{\epsilon}\rangle + (k_{\rm eff} - \mu_{\rm eff}){\rm Tr}(\langle\hat{\epsilon}\rangle)\hat{I} + 2\mathsf{e}_{\rm eff}{\rm Tr}(\langle\hat{\epsilon}\rangle)\langle\hat{\epsilon}\rangle + \mathsf{e}_{\rm eff}{\rm Tr}[\langle\hat{\epsilon}\rangle^2]\hat{I} + 3\mathsf{f}_{\rm eff}{\rm Tr}^2(\langle\hat{\varepsilon}\rangle)\hat{I}, \tag{4.30}$$

where the effective linear elastic moduli are given by

$$\mu_{\rm eff} = \mu_1 + c\frac{\mu_2 - \mu_1}{c + (1-c)\left[1 + \frac{1}{2}\left(\frac{\mu_2}{\mu_1} - 1\right)\frac{k_1 + 2\mu_1}{k_1 + \mu_1}\right]},$$
$$k_{\rm eff} = k_1 + c\frac{k_2 - k_1}{c + (1-c)\frac{\mu_1 + k_2}{\mu_1 + k_1}}. \tag{4.31}$$

As for the effective nonlinear elastic moduli, we obtain

$$\mathsf{e}_{\rm eff} = \frac{\mathsf{e}c}{\mathcal{L}^2}\left(1 - \frac{1-c}{\mathcal{L} + 2\mathcal{M}}\frac{k_2 - k_1}{\mu_1 + k_1}\right), \tag{4.32}$$

$$\mathsf{f}_{\rm eff} = -\frac{c(1-c)(k_2 - k_1 - \mu_2 + \mu_1)(2\mathsf{f} + \mathsf{e})}{2(k_1 + \mu_1)(\mathcal{L} + 2\mathcal{M})^3} + \frac{\mathsf{e}c(1-c)(k_2 - k_1 - \mu_2 + \mu_1)}{6\mathcal{L}^2(k_1 + \mu_1)(\mathcal{L} + 2\mathcal{M})} - \frac{\mathsf{e}c}{6\mathcal{L}^2} + \frac{c(1-c)(\mu_1 - \mu_2)(2\mathsf{f} + \mathsf{e})}{2(k_1 + \mu_1)(\mathcal{L} + 2\mathcal{M})^3} + \frac{c(2\mathsf{f} + \mathsf{e})}{2(\mathcal{L} + 2\mathcal{M})^2} + \frac{\mathsf{e}c(1-c)(\mu_2 - \mu_1)(3\mu_1 + k_1)}{6\mu_1(k_1 + \mu_1)\mathcal{L}^2(\mathcal{L} + 2\mathcal{M})} - \frac{\mathsf{e}c}{3\mathcal{L}(\mathcal{L} + 2\mathcal{M})}. \tag{4.33}$$

Here we have defined

$$\mathcal{L} = c + (1-c)\left[1 + \frac{1}{2}\frac{k_1 + 2\mu_1}{k_1 + \mu_1}\left(\frac{\mu_2}{\mu_1} - 1\right)\right], \tag{4.34}$$

$$\mathcal{M} = (1-c)\frac{1}{4(k_1 + \mu_1)} \times \left[2k_2 - k_1\left(1 + \frac{\mu_2}{\mu_1}\right) - 2(\mu_2 - \mu_1)\right] \tag{4.35}$$

which are the two-dimensional counterpart of the parameters $L' = c + (1-c)L$ and $M' = (1-c)M$, where L and M are given in equations (4.18) and (4.19).

4.5. Nanograined composite materials: from uniform to graded structures

Another class of nanostructured materials of large technological interest and paradigmatic conceptual relevance is represented by uniform as well as graded nanograined composite materials. Both systems are described as a mixture of nano-sized grains (having completely haphazard distribution of size, position and shape) made by two (or more) different elastic media. While in uniform systems such a mixture is randomly distributed in space, in graded nanograined materials the composition (i.e. the density and/or size of grains corresponding to a given phase) gradually change along a fixed direction. In figure 17 one can find an example of two random mixtures (made by two different materials, marked by the green and red color) characterized by the same volume fractions for the two phases, but differing as far as the granularity is concerned.

To begin, we take into consideration uniform nanograined materials (of the same kind as those ones shown in figure 17) formed by two different phases having elastic moduli given by $\vec{x}_1 = (\mu_1, k_1)$ and $\vec{x}_2 = (\mu_2, k_2)$, and volume fractions $c_1 = 1 - c$ and $c_2 = c$, respectively. As before, $k_{1,2}$ ($\mu_{1,2}$) are the two-dimensional bulk (shear) moduli. We have combined the two elastic moduli into a two-dimensional vector $\vec{x}_i = (\mu_i, k_i)$ in order to compact and simplify the notation in the following developments. We suppose, in fact, that the mixing rule for this system is given by

$$\vec{x}_{\rm eff} = \vec{G}(\vec{x}_1, \vec{x}_2, c), \tag{4.36}$$

where $\vec{x}_{\rm eff} = (\mu_{\rm eff}, k_{\rm eff})$ effectively describes the elastic features of the grained structure in terms of the bulk and shear moduli of the component materials. We will assume that the only structural information about the mixture is the volume fraction of the second medium, since the overall medium is

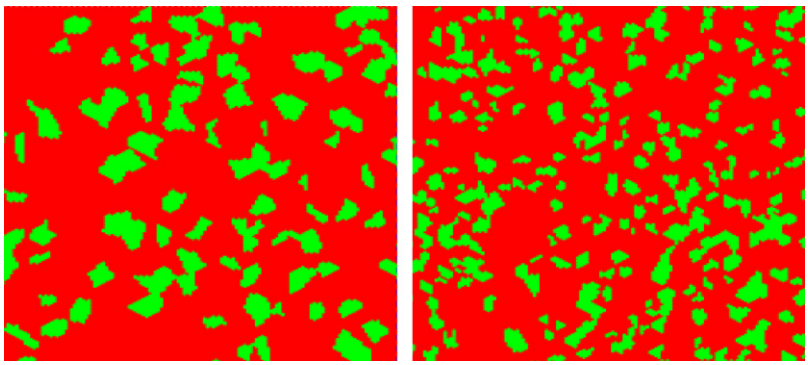

Figure 17. Two examples of $N = 2$ component (red and green) nanograined composite materials with the same volume fractions (red: $c_1 = 0.65$; green: $c_2 = 0.35$), but different granularity $N_0/\mathcal{N} = 50$ (left) and 25 (right).

composed of particles completely randomized in size, position and shape. We note that in this problem we may not distinguish between a 'matrix' and the 'inclusions': accordingly, the concept of 'embedding' so usefully developed in the previous sections is no longer relevant. Nevertheless, it is possible to use equation (4.31) in order to find some properties of a random mixture, i.e. of the function $\vec{G}$ defined in equation (4.36). To this aim, let us examine the situation of the random mixture for very low values of c: we may think that a low value of c is reached when the structure contains only very small elements of the second medium dispersed in the matrix of the first medium. In this limiting case, equation (4.31) (obtained for diluted dispersion of particles) is valid: therefore, the behavior of the function $\vec{G}$ must be described by equation (4.31). Hence, we may write the derivatives of $\vec{G}$ with respect to the volume fraction c (in the limit of vanishingly small c):

$$\frac{\partial G_1}{\partial c} = \frac{\partial \mu_{\text{eff}}}{\partial c} = \frac{2\mu_1 (\mu_1 + k_1)(\mu_2 - \mu_1)}{\mu_1 (k_1 + \mu_2) + \mu_2 (k_1 + 2\mu_1)}, \tag{4.37}$$

$$\frac{\partial G_2}{\partial c} = \frac{\partial k_{\text{eff}}}{\partial c} = \frac{\mu_1 + k_1}{\mu_1 + k_2}(k_2 - k_1). \tag{4.38}$$

Equations (4.37) and (4.38) play a key role in developing a general effective medium theory for the random mixture. Using these expressions, in fact, we may solve the complete problem of a linear random mixture composed by N different homogeneous components randomly mixed together (moduli $\vec{x}_i$ and volume fractions c_i) [75–77]. To this aim we introduce the probability density $f(\vec{x})$ describing the elastic moduli of a given grain (with volume ΔV) of the nanostructure. Such a probability density is normalized on the space Ω, where the properties $\vec{x}$ can range, namely, $\int_\Omega f(\vec{x})\,\mathrm{d}\vec{x} = 1$. In our random mixture we have

$$f(\vec{x}) = \sum_{i=1}^{N} c_i \delta(\vec{x} - \vec{x}_i), \tag{4.39}$$

where $\sum_{i=1}^{N} c_i = 1$. Now, we may think to add to the overall system (with effective properties $\vec{x}_{\text{eff}}$ and volume V) another grain with volume $\Delta V \ll V$ and properties $\vec{x}$, chosen at random through the probability density $f(\vec{x})$. The elastic properties of the resulting new mixture can be described by homogenization, i.e. by describing its average behavior as

$$\vec{x}'_{\text{eff}} = \vec{G}\left(\vec{x}_{\text{eff}}, \vec{x}, \frac{\Delta V}{\Delta V + V}\right), \tag{4.40}$$

where we have considered a two-phase mixture between $\vec{x}_{\text{eff}}$ (the original medium) and $\vec{x}$ (the added grain). Now, the average of $\vec{x}'_{\text{eff}}$ must correspond to the original $\vec{x}_{\text{eff}}$ and therefore we obtain

$$\vec{x}_{\text{eff}} = \int_\Omega \vec{G}\left(\vec{x}_{\text{eff}}, \vec{x}, \frac{\Delta V}{\Delta V + V}\right) f(\vec{x})\,\mathrm{d}\vec{x}. \tag{4.41}$$

Since $\Delta V \ll V$, we can expand $\vec{G}$ up to the first order in $\Delta V/(\Delta V + V)$ and therefore equation (4.41) is approximated (to the linear order) as

$$\begin{aligned}\vec{x}_{\text{eff}} &= \int_\Omega \left[\vec{G}(\vec{x}_{\text{eff}}, \vec{x}, 0) + \frac{\partial \vec{G}}{\partial c}|_{c=0} \frac{\Delta V}{\Delta V + V}\right] f(\vec{x})\,\mathrm{d}\vec{x} \\ &= \vec{x}_{\text{eff}} + \frac{\Delta V}{\Delta V + V} \int_\Omega \frac{\partial \vec{G}}{\partial c}|_{c=0} f(\vec{x})\,\mathrm{d}\vec{x},\end{aligned} \tag{4.42}$$

which implies the most important result of the effective medium theory, namely

$$\int_\Omega \frac{\partial \vec{G}(\vec{x}_{\text{eff}}, \vec{x}, 0)}{\partial c} f(\vec{x})\,\mathrm{d}\vec{x} = 0 \tag{4.43}$$

or, equivalently, by inserting equation (4.39)

$$\sum_{i=1}^{N} c_i \frac{\partial \vec{G}(\vec{x}_{\text{eff}}, \vec{x}_i, 0)}{\partial c} = 0. \tag{4.44}$$

In order to conclude the procedure, we use equations (4.37) and (4.38) by getting the mixing rules for the linear elastic properties of a (two-dimensional) nanograined material or random mixture

$$\frac{1}{k_{\text{eff}} + \mu_{\text{eff}}} = \sum_{i=1}^{N} \frac{c_i}{\mu_{\text{eff}} + k_i}, \tag{4.45}$$

$$\frac{1}{2\mu_{\text{eff}}(k_{\text{eff}} + \mu_{\text{eff}})} = \sum_{i=1}^{N} \frac{c_i}{\mu_{\text{eff}}(\mu_i + k_{\text{eff}}) + \mu_i(\mu_{\text{eff}} + k_{\text{eff}})}. \tag{4.46}$$

While equations (4.45) and (4.46) represent an important result of general validity, they cannot predict how the elastic behavior of a nanoalloy is actually affected by the granularity (see figure 17) or, equivalently, by the real size and shape of grains. Another important atomic-scale detail is omitted, namely the random or gradual character of their space distribution. In order to introduce such relevant information in our theory, we need to switch from the continuum to the fully atomistic picture. In doing that, the first issue to cope with is how to generate a trustworthy model of the mixture nanostructure. A very effective protocol (inspired by the elastic lattice model described in section 3.2) is to proceed as follows: given a rectangular planar region (corresponding to the simulation box of our atomistic simulations):

(i) we construct a perfect triangular lattice containing as many as N_0 points (note that at this stage a lattice point is not yet associated with a given atomic species);
(ii) we then select at random $\mathcal{N} \ll N_0$ sites within the above rectangular region and calculate their corresponding Voronoi cells (each Voronoi cell will contain in average $N_0/\mathcal{N}$ lattice points);
(iii) finally, a given ith material (or, equivalently, atomic species) is randomly assigned (we could possibly have N different materials with $N \ll \mathcal{N}$) so as to realize the above set of volume fractions c_i (such that $\sum_{i=1}^{N} c_i = 1$); whenever two adjacent cells will be filled by the same material atoms, they will be grouped together generating a grain of the final structure.

In figure 17 one can find two examples of uniform nanograined materials with $N = 2$ components (marked by red and green color) and the same volume fractions $c_1 = 0.65$ and $c_2 = 1 - c_1 = 0.35$; the simulation box contains 43 008 atoms placed on a triangular lattice with interatomic distance $r_0 = 3.4$ Å. The two samples have a different granularity defined by $N_0/\mathcal{N} = 50$ (figure 17, left) corresponding to an average Voronoi cell diameter of 25 nm and $N_0/\mathcal{N} = 25$ (figure 17, right) corresponding to an average Voronoi cell diameter of 15 nm.

A second important issue is to verify whether the elastic lattice model of section 3.2 provides elastic moduli values for a random mixture consistent with equations (4.45) and (4.46). This is proved in figure 18 where the linear elastic constants of a two-phase random mixture are calculated atomistically (symbols) and by continuum (dotted lines) for any possible value of the volume fraction of the second phase. We have set the first component material to be a linear one with $C_{11} = 350.11\,\mathrm{N\,m^{-1}}$ and $C_{12} = 59.52\,\mathrm{N\,m^{-1}}$, while the second component material is nonlinear with $C_{11} = 93.40\,\mathrm{N\,m^{-1}}$, $C_{12} = 28.02\,\mathrm{N\,m^{-1}}$, $C_{111} = -450.00\,\mathrm{N\,m^{-1}}$ and $C_{112} = -85.00\,\mathrm{N\,m^{-1}}$. We can draw an important conclusion, namely, the effective linear properties of a nanograined material strongly depend on the average composition.

This result is found to hold for any possible value of granularity we investigated, which therefore appears not to affect the overall linear response of the mixture. Moreover, we note that the atomistic data are in rather good agreement with the effective medium theory above described. It means

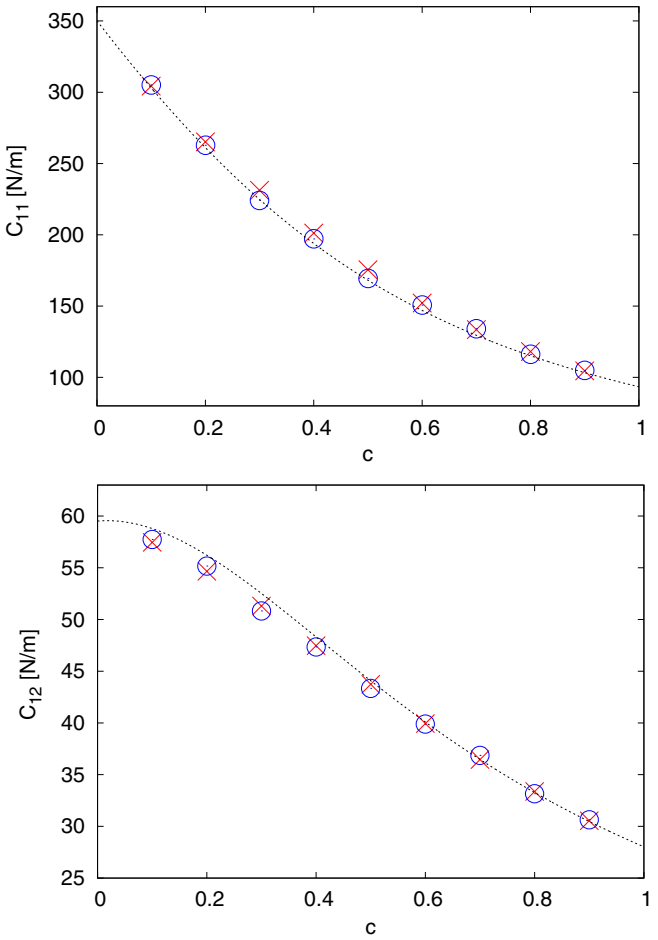

Figure 18. Effective linear constants C_{11} and C_{12} of a two-component nanograined material: comparison between the predictions of continuum (black dotted lines) and atomistic simulations (symbols) obtained with different granularities (red crosses: $N_0/\mathcal{N} = 25$; blue circles: $N_0/\mathcal{N} = 50$).

that the size of the grains is not relevant for the linear elastic response of the nanograined structure, as was indeed assumed for developing the linear effective medium theory.

The nonlinear features are summarized in figure 19 from which we extract a twofold message. On the one hand, the nonlinear effective properties, at variance with their linear counterparts, do depend on the granularity of the structure; in particular, we have found that finer granularities slightly reduce the overall nonlinearity of the grained material, and vice-versa. On the other hand, the effective nonlinear constants are not monotonic functions of the volume fraction of the second material (the nonlinear one). This is a remarkable result providing evidence that there is a value of volume fraction maximizing (in absolute value) a given nonlinear constant. We also note that different moduli are maximized at different c values. This is key issue in tailoring the resulting overall response of a nanograined material: as a matter of fact, we have shown that it is possible to obtain a nonlinear effective property exceeding (always in absolute value) the corresponding nonlinear property of any component phase. In other words, by carefully selecting suitable c values we can obtain an amplification of the nonlinear response of the constituents. Interestingly enough, this feature reflects a

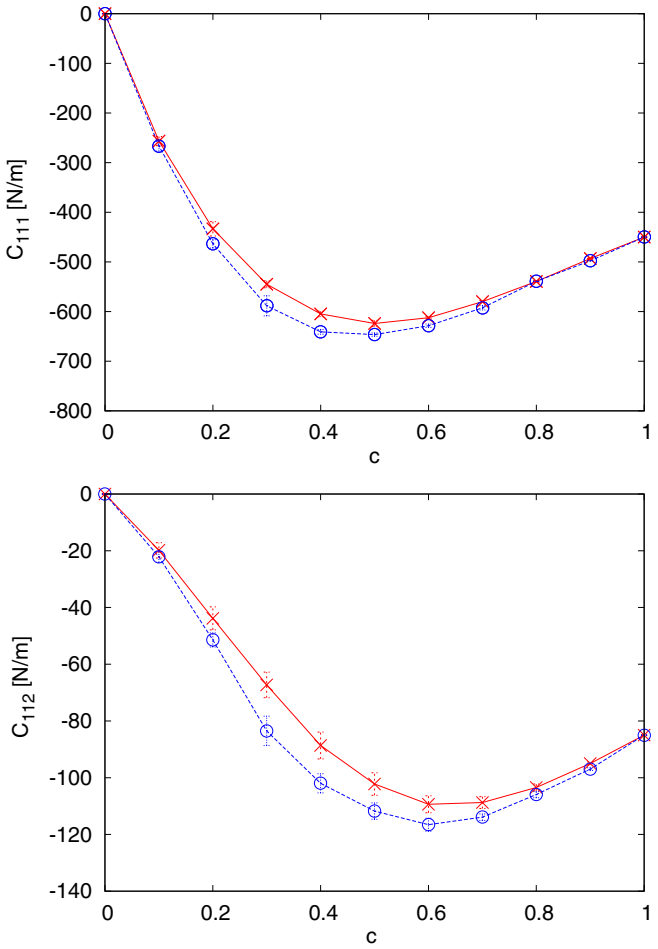

Figure 19. Effective nonlinear constants C_{111} and C_{112} of a two-component nanograined material obtained through atomistic simulations with different granularities $N_0/\mathcal{N} = 25$ (red crosses) and 50 (blue circles). Full and dotted lines are just a guide to the eye.

similar property found for dispersions of inhomogeneities in the previous section.

We now extend our investigations to a graded nanograined material, defined as a material with a gradual composition in a given spatial direction (the z-axis in our case, while we define the orthogonal direction as the y-axis). More specifically, we will consider a nanograined structure with two components having spatial-varying volume fractions $c_1(z) = 1 - c(z)$ and $c_2(z) = c(z)$, where $c(z)$ is a given profile. In order to generate the atomic structure of the graded system corresponding to a given profile $c(z)$, we have adopted a similar protocol as for a random mixture. While the first two steps are basically the same, at the third step we select the ith Voronoi cell with at $z = z_i$ and we assign to it a random number $\xi \in [0, 1]$ with uniform distribution: if $\xi \in [0, c(z_i)]$, then we attribute that cell to the second component material; in contrast, if $\xi \in [c(z_i), 1]$, then the cell is filled out by the first component material. When two adjacent cells correspond to the same material, they are grouped together generating the final grain of the graded structure. At the end, once we fix the granularity $N_0/\mathcal{N}$ and the profile $c(z)$, we are able to generate the atomistic structure of any arbitrary compositionally graded material.

Table 2. Value of the parameter a in terms of the average concentration c_0.

$c_0 = a + a(a-1)\ln\lvert\frac{a-1}{a}\rvert$	a
0.1	−0.043 680 8898
0.2	−0.147 909 5261
0.3	−0.393 982 4571
0.4	−1.196 744 752
0.5	$\pm\infty$
0.6	2.196 744 752
0.7	1.393 982 457
0.8	1.147 909 526
0.9	1.042 994 499

In order to put at work the above machinery on real cases, we have chosen a hyperbolic profile described by a homographic function $c(z) = (az + b)/(z + d)$. Furthermore, by setting $0 \leqslant z \leqslant D$ and placing the pure first (second) component at the boundary $z = 0$ ($z = D$), we simply obtain $b = d$ and $b = -aD$. The parameter D represents the thickness of the space region over which the composition gradually changes (this region is also referred to as the *graded interface* between the two pure phases). In conclusion, the profile is set in the simpler form

$$c(z) = a\frac{z - D}{z - aD}. \tag{4.47}$$

According to this formula, the parameter a controls the shape of the profile. It is possible to calculate the average concentration c_0 for $0 \leqslant z \leqslant D$ in terms of the parameter a. The result is

$$c_0 = \frac{1}{D}\int_0^D a\frac{z - D}{z - aD}dz = a + a(a-1)\ln\left|\frac{a-1}{a}\right| \tag{4.48}$$

and it has been used in table 2 for determining the values of the parameter a corresponding to different values of the average concentration c_0. Of course, for the average concentration c_0 =0.5 we obtain the linear profile $c(z) = 1 - z/D$, which corresponds to $a \to \pm\infty$. With these values we have generated the atomic structure of different graded interfaces, as shown in figure 20, together with the corresponding concentration profile given in equation (4.47).

Once a complete structure is generated, it is possible to evaluate its elastic behavior both in the linear and in the nonlinear regime. It is important to note that the graded structure is anisotropic from the macroscopic point of view and, in fact, it has a different elastic response in the longitudinal and transverse directions. The graded specimen exhibits an orthorhombic symmetry and, therefore, it should be described by four linear elastic constants and by six nonlinear elastic constants. In the following we will evaluate the full linear response described by four constants, but for the sake of brevity we discuss the behavior of only two nonlinear elastic constants. We have chosen two materials as before: the first one is linear with $C_{11} = 350.11\,\mathrm{N\,m^{-1}}$ and $C_{12} = 59.52\,\mathrm{N\,m^{-1}}$; the second one is nonlinear with $C_{11} = 93.40\,\mathrm{N\,m^{-1}}$, $C_{12} = 28.02\,\mathrm{N\,m^{-1}}$, $C_{111} = -450.00\,\mathrm{N\,m^{-1}}$ and $C_{112} = -85.00\,\mathrm{N\,m^{-1}}$. We have used the single granularity $N_0/\mathcal{N} = 50$ corresponding to an average Voronoi cell diameter of 25 nm.

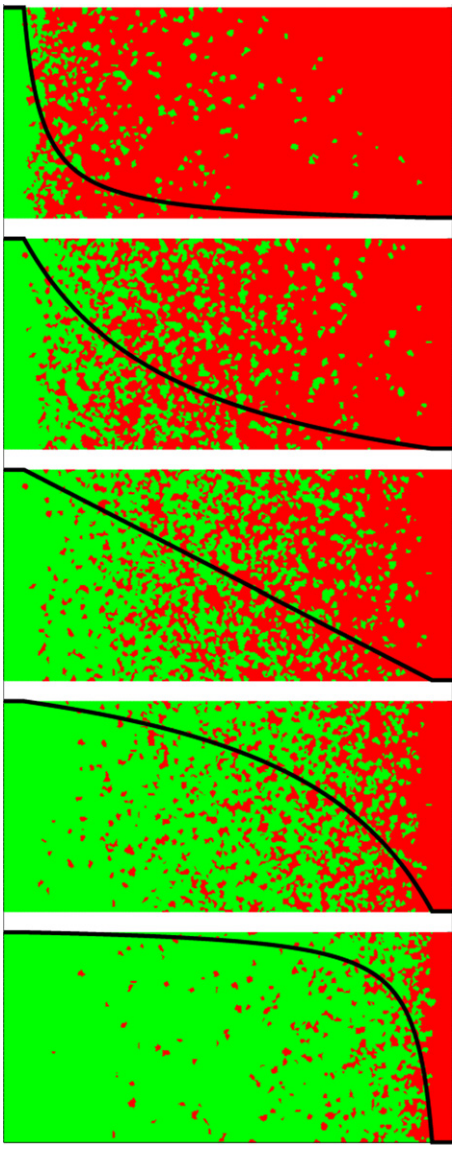

Figure 20. Graded materials with different values of c_0 given by (from top to bottom) 10%, 30%, 50%, 70% and 90%. The black lines represent the profile given in equation (4.47).

Figure 21 shows the behavior of the effective Young's modulus and the effective Poisson's ratio of the graded structure. Both of them have been computed by subjecting the system to transverse (i.e. along y, blue symbols) and longitudinal (i.e. along z, red symbols) deformations versus the average concentration c_0, uniquely characterizing a sample with a given profile (see figure 20 and table 2). The atomistic results are compared with the above described effective medium theory (black dotted–dashed line), corresponding to a nanograined material with the same c_0 composition, but without gradation (i.e. a heterogeneous but isotropic structure). This is equivalent to saying that the continuum theory will not carry any information about the actual atomistic structure of the graded interface material. The unique parameter entering the effective medium theory (in addition to the elastic moduli) is the average concentration c_0 of the components. As for Young's modulus, the atomistic results are very different for the transverse and the longitudinal directions.

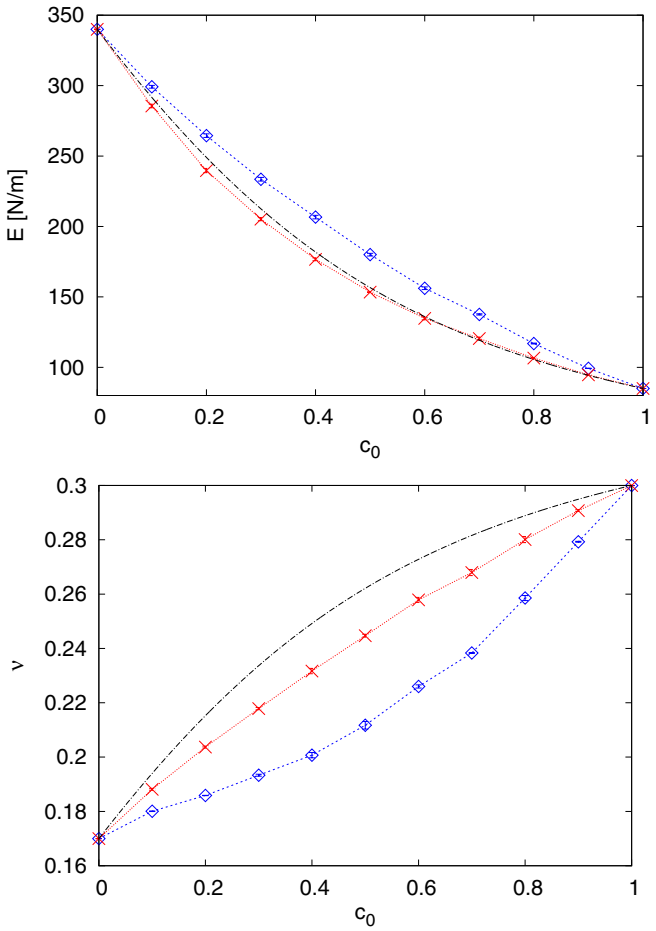

Figure 21. Effective linear moduli E (top) and ν (bottom) of a two-component graded nanograined material versus the average volume fraction c_0. Red: atomistic results for the longitudinal direction; blue: atomistic results for the transverse directions. Black dotted–dashed line: effective medium theory prediction.

More specifically, only the longitudinal behavior is well reproduced by the effective medium theory, which because of its (unrealistic) isotropic character is unable to distinguish between the different response regimes along or normal to the direction of variation of the concentration. Moreover, the longitudinal Young's modulus is always slightly smaller (about 2–3%) than the value predicted by continuum. The maximum disagreement between the two opposite pictures (as large as about 20–25%) can be measured for an approximate average concentration near 50%. On the other hand, neither the longitudinal nor the transverse Poisson's ratio is correctly described by the effective medium theory. Moreover, the results are again very different for the transverse and longitudinal directions.

In figure 22 we finally report the two nonlinear elastic moduli C_{222} and C_{122} of the same graded nanograined material. These two constants can be simultaneously measured (or, in our case, calculated) when the material is subjected to a uniaxial strain ϵ_{zz} along the longitudinal direction z. In fact, in this case the relevant components of the stress are

$$T_{yy} = C_{12}\epsilon_{zz} + \tfrac{1}{2}C_{122}\epsilon_{zz}^2, \qquad T_{zz} = C_{22}\epsilon_{zz} + \tfrac{1}{2}C_{222}\epsilon_{zz}^2. \tag{4.49}$$

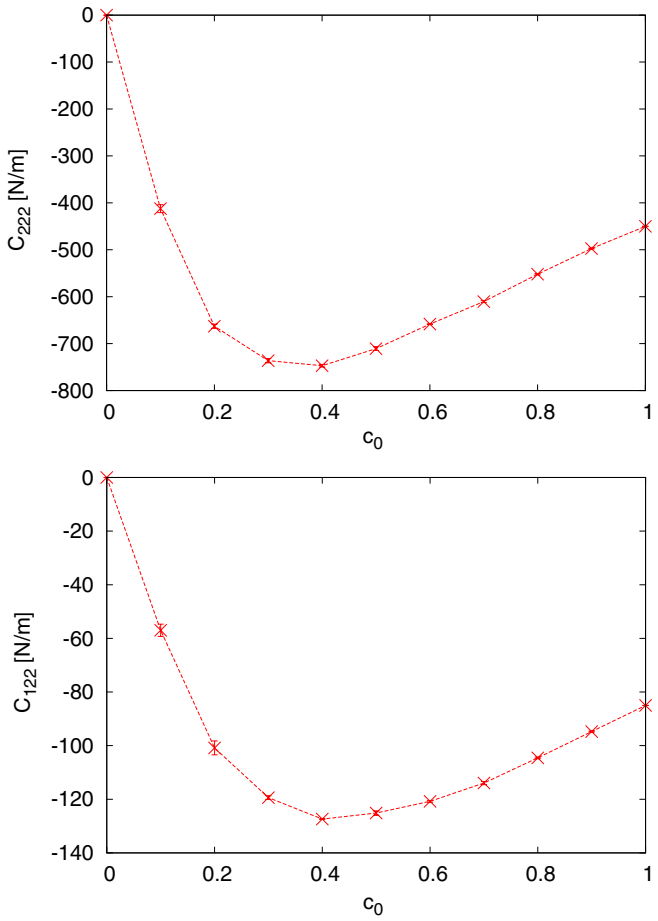

Figure 22. Effective nonlinear constants C_{222} and C_{122} of a two-component graded nanograined material versus the average volume fraction c_0 obtained through atomistic simulations with a fixed granularity $N_0/\mathcal{N} = 50$.

Other nonlinear constants, not discussed here, can be simply obtained by applying different strains to the structure. To conclude, we can draw a comparison between figures 19 and 22 and we understand that the graduation of the composition can further enhance the phenomenon of the amplification of the nonlinearity, already introduced in the previous section.

4.6. Theory versus experimental results

The predictions of homogenization methods have been confirmed by the experimental results in many cases. We briefly report here some examples.

As regards the dispersion of spherical particles, the homogenization method described in section 4.4 has been compared with experimental data corresponding to the bulk modulus of porous P-311 glass measured at room temperature [43]. In the same work a similar comparison has been drawn for Young's modulus of porous polycrystalline monoclinic oxide Gd_2O_3, over a wide range of porosities. In both cases the agreement is very good [43], thus confirming the robustness of these continuum models in predicting the overall elastic features of complex materials.

As regards nanograined materials, the effective medium theory presented here for the linear elastic properties has been compared with experimental data in [77]. In particular, an excellent agreement has been obtained for Young's modulus of sintered glass beads and of different sintered ceramic materials (holmia Ho_2O_3, ytterbia Yb_2O_3, yttria Y_2O_3 and samaria Sm_2O_3) [77].

If we take into consideration the nonlinear elastic properties we must distinguish between homogeneous materials and heterogeneous structures. By focusing on homogeneous materials, one can find several comparisons between the values of the nonlinear elastic moduli obtained by experimental procedures [78, 79] and by computational techniques (e.g. classical MD [80] or first-principles calculations [81]). In this case the computational techniques are currently well suited to reproduce the experimental data.

On the other hand, if we consider the nonlinear elastic properties of heterogeneous or nanostructured systems the comparisons between theory and experiment are rather difficult since experimental data are basically missing. Therefore, the nonlinear models proposed in this review should be better considered as predictive tools, useful to open new lines of research in nonlinear material science.

4.7. Nonlinear elasticity of two-dimensional atomic sheets

Monolayer crystals, as thin as a single atomic sheet, represent a versatile source of novel two-dimensional materials with intriguing physical properties, possibly useful in many front-end technologies such as nano-/opto-electronics, energetics and nanomechanics. The experimental search, synthesis and characterization of such low-dimensional materials, as well as the theoretical investigation of their properties, is a very active and lively field of modern nanoscience (see for instance [82–89] and references therein). Above all, graphene (i.e. a two-dimensional hexagonal lattice of carbon atoms) is playing a role of paramount importance, due to its unique electronic, transport and mechanical properties [90, 91]. In this section, we precisely focus on graphene and its hydrogenated counterparts (also referred to as graphanes) by investigating their linear and nonlinear elastic features.

4.7.1. Nonlinear elasticity of graphene. The graphene atomic scaffold is sketched in figure 23, together with its two nonequivalent high-symmetry 'armchair' and 'zigzag' directions. By the general principles of continuum (small strain) elasticity, we can straightforwardly write down the formal expression, up to third order in strain, for the graphene strain energy density U [92]

$$\begin{aligned} 2U = {} & \frac{E}{1+\nu}\mathrm{Tr}\left(\hat{\epsilon}^2\right) + \frac{E\nu}{1-\nu^2}\left(\mathrm{Tr}\hat{\epsilon}\right)^2 + \frac{1}{3}C_{111}\epsilon_{xx}^3 + \frac{1}{3}C_{222}\epsilon_{yy}^3 \\ & + C_{112}\epsilon_{xx}^2\epsilon_{yy} + (C_{111} - C_{222} + C_{112})\epsilon_{xx}\epsilon_{yy}^2 \\ & + (3C_{222} - 2C_{111} - C_{112})\epsilon_{xx}\epsilon_{xy}^2 \\ & + (2C_{111} - C_{222} - C_{112})\epsilon_{yy}\epsilon_{xy}^2. \end{aligned} \tag{4.50}$$

While any quantity appearing in this equation has been formally defined in section 2, it is important to understand that for the present two-dimensional material U they should be intended as the elastic potential energy per unit area. Also,

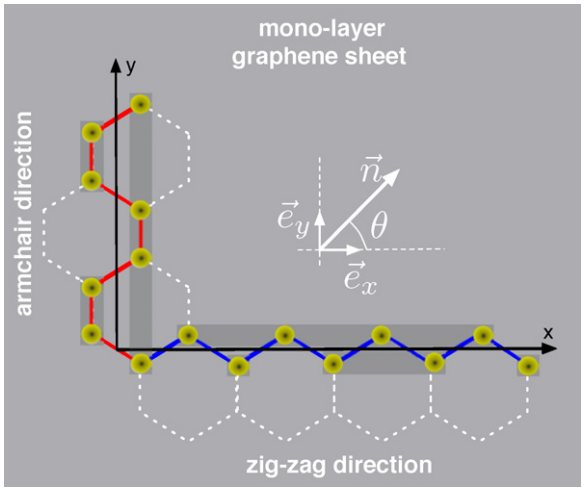

Figure 23. Schematic representation of the graphene scaffold with its armchair and zigzag directions. The central inset defines the set of unit vectors $\vec{e}_{x,y}$ and θ the angle used in the text.

we note that we set $\epsilon_{ii}\epsilon_{jj} = \mathrm{Tr}(\hat{\epsilon}^2)$ and $\epsilon_{ij}\epsilon_{ij} = (\mathrm{Tr}\hat{\epsilon})^2$ to compact the notation. Our primary goal is to work out the stress–strain nonlinear constitutive equation for graphene in-plane stretching according to equation (2.25) and to compare our theoretical predictions to experimental data [44].

We begin by considering very simple in-plane deformations, namely, (i) a uniaxial deformation ζ along the zigzag direction, corresponding to a strain tensor $\epsilon_{ij}^{(\mathrm{zz})} = \zeta\delta_{ix}\delta_{jx}$; (ii) a uniaxial deformation ζ along the armchair direction, corresponding to a strain tensor $\epsilon_{ij}^{(\mathrm{ac})} = \zeta\delta_{iy}\delta_{jy}$; (iii) a hydrostatic planar deformation ζ, corresponding to the strain tensor $\epsilon_{ij}^{(\mathrm{p})} = \zeta\delta_{ij}$ and, finally, (iv) a shear deformation ζ, corresponding to an in-plane strain tensor $\epsilon_{ij}^{(\mathrm{s})} = \zeta(\delta_{ix}\delta_{jy} + \delta_{iy}\delta_{jx})$. In the spirit discussed throughout this review, the continuum picture is now blended to atomistics and, therefore, the energy versus strain curves needed to determine elastic moduli have been calculated atomistically by a suitable tight-binding (TB) model [93, 94] for a periodically repeated square cell containing as many as 400 carbon atoms. For any given applied deformation, full relaxation of the internal degrees of freedom of the simulation cell was performed by zero temperature damped dynamics, until interatomic forces were not larger than 0.5×10^{-11} eV Å^{-1} [92].

For the deformations $\epsilon_{ij}^{(\mathrm{zz})}$, $\epsilon_{ij}^{(\mathrm{ac})}$, $\epsilon_{ij}^{(\mathrm{p})}$ and $\epsilon_{ij}^{(\mathrm{s})}$ the elastic energy of strained graphene can be written in terms of just the single deformation parameter ζ:

$$U(\zeta) = U_0 + \tfrac{1}{2}U^{(2)}\zeta^2 + \tfrac{1}{6}U^{(3)}\zeta^3 + O(\zeta^4), \tag{4.51}$$

where U_0 is the energy of the unstrained configuration. Since the expansion coefficients $U^{(2)}$ and $U^{(3)}$ are related to elastic moduli as summarized in table 3, a straightforward fit of equation (4.51) can provide the full set of linear moduli and TOECs.

The present TB calculation provides a (two-dimensional) Young's modulus value $E = 312\,\mathrm{N\,m^{-1}}$ which is in reasonable agreement with the literature [44, 95–98], while Poisson's ratio value $\nu = 0.31$ is found to be larger than most of the *ab initio* results [97–101]. This disagreement is clearly due to the empirical character of the adopted TB model. It is, however, important to note that the nonlinear elastic features discussed below only weakly depend upon ν: as a matter of fact, by varying its value within the set of values found in the literature, we observed a variation of the effective moduli smaller than 10%. The same fitting of the $U = U(\zeta)$ curve has determined the full set of TOECs as well, which were $C_{111} = -1689.2$, $C_{222} = -1487.7$ and $C_{112} = -484.1$ in units of $\mathrm{N\,m^{-1}}$. We note that C_{111} is different from C_{222}, i.e. a monolayer graphene is isotropic in the linear elasticity approximation (as indeed confirmed by the analysis of the above shear deformation), while it is anisotropic whenever nonlinear features are properly taken into account.

Table 3. Relationship among the energy expansion coefficients $U^{(2)}$ and $U^{(3)}$ of equation (4.51) and the elastic moduli of graphene for four in-plane deformations.

Uniform strain	$U^{(2)}$	$U^{(3)}$
$\hat{\epsilon}^{(\mathrm{zz})} = \begin{pmatrix}\zeta & 0\\ 0 & 0\end{pmatrix}$	$\dfrac{E}{1-\nu^2}$	C_{111}
$\hat{\epsilon}^{(\mathrm{ac})} = \begin{pmatrix}0 & 0\\ 0 & \zeta\end{pmatrix}$	$\dfrac{E}{1-\nu^2}$	C_{222}
$\hat{\epsilon}^{(\mathrm{p})} = \begin{pmatrix}\zeta & 0\\ 0 & \zeta\end{pmatrix}$	$\dfrac{2E}{1-\nu}$	$4C_{111} - 2C_{222} + 6C_{112}$
$\hat{\epsilon}^{(\mathrm{s})} = \begin{pmatrix}0 & \zeta\\ \zeta & 0\end{pmatrix}$	$\dfrac{2E}{1+\nu}$	0

In order to compare our predictions with experimental data, we preliminarily observe that, for any uniaxial deformation along $\vec{n}$ (see figure (23)) the stress field is $\hat{T} = \sigma_{\vec{n}}\vec{n}\otimes\vec{n}$, with in-plane components $T_{xx} = \sigma_{\vec{n}}\cos^2\theta$, $T_{xy} = \sigma_{\vec{n}}\cos\theta\sin\theta$ and $T_{yy} = \sigma_{\vec{n}}\sin^2\theta$. Similarly, we can find the relative variation of length $\epsilon_{\vec{n}} = \vec{n}\cdot\hat{\epsilon}\vec{n}$ along the direction defined by $\vec{n}$. By combining these results, we can elaborate the *effective stress-strain relation* along the arbitrary direction $\vec{n}$ in a very simple form

$$\sigma_{\vec{n}} = E\epsilon_{\vec{n}} + D_{\vec{n}}\epsilon_{\vec{n}}^2, \tag{4.52}$$

where we have introduced the *effective two-dimensional nonlinear modulus*

$$D_{\vec{n}} = \tfrac{3}{2}(1-\nu)^3\Lambda_3 + \frac{3}{2}(1-\nu)(1+\nu)^2\Lambda_2 + 3(2\cos^2\theta - 1)(16\cos^4\theta - 16\cos^2\theta + 1)(1+\nu)^3\Lambda_1 \tag{4.53}$$

describing the overall nonlinear behavior of the carbon sheet. We note that the Λ-parameters are given in equation (3.34). If we set $\vec{n} = \vec{e}_x$ (i.e. $\theta = 0$), we obtain the nonlinear modulus $D^{(\mathrm{zz})}$ for stretching along the zigzag direction

$$D^{(\mathrm{zz})} = 3(1+\nu)^3\Lambda_1 + \tfrac{3}{2}(1-\nu)(1+\nu)^2\Lambda_2 + \tfrac{3}{2}(1-\nu)^3\Lambda_3 \tag{4.54}$$

while, by setting $\vec{n} = \vec{e}_y$ (i.e. $\theta = \pi/2$), we obtain the nonlinear modulus $D^{(\mathrm{ac})}$ for stretching along the armchair direction

$$D^{(\mathrm{ac})} = -3(1+\nu)^3\Lambda_1 + \tfrac{3}{2}(1-\nu)(1+\nu)^2\Lambda_2 + \tfrac{3}{2}(1-\nu)^3\Lambda_3. \tag{4.55}$$

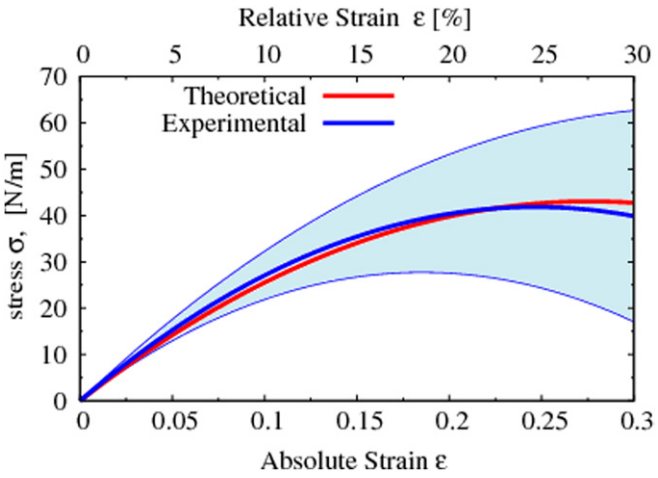

Figure 24. Theoretical (this work) and experimental (see [44]) stress–strain curves. The shaded area represents the experimental error.

In order to perform a meaningful comparison with experimental data, we need to average the expression of $D_{\vec{n}}$ over θ: as a matter of fact, the stress–strain was obtained in [44] by nanoindentation of a suspended monolayer graphene sample, a situation generating a strain field with radial symmetry. This procedure leads to

$$\langle D_{\vec{n}}\rangle = \frac{1}{2\pi}\int_0^{2\pi} D_{\vec{n}}\mathrm{d}\theta = \frac{D^{(\mathrm{zz})}+D^{(\mathrm{ac})}}{2} = \frac{3}{2}(1-\nu)\left[(1+\nu)^2\Lambda_2+(1-\nu)^2\Lambda_3\right]. \quad (4.56)$$

We will consistently assume that the experimentally determined nonlinear modulus of graphene actually corresponds to the average value of the moduli for the zigzag and armchair directions.

Using the TB values for TOECs, we easily obtain $D^{(\mathrm{zz})} = -696.2$, $D^{(\mathrm{ac})} = -469.6$ and $\langle D_{\vec{n}}\rangle = -582.9$ in units $\mathrm{N\,m^{-1}}$. While the negative values for $D^{(\mathrm{zz})}$ and $D^{(\mathrm{ac})}$ indicate that, if the nonlinear behavior of graphene is softening hyperelastic, the value for $\langle D_{\vec{n}}\rangle$ is indeed very close to the experimentally reported value $D = -690\,\mathrm{N\,m^{-1}}$ of [44], thus proving the reliability of the followed procedure. This is convincingly confirmed by figure 24 where the theoretical and experimental graphene stress–strain curves are compared: the agreement is indeed remarkable. We can also determine the failure stress (maximum of the stress–strain curve) $\sigma_{\mathrm{f}} = -E^2/4\langle D_{\vec{n}}\rangle$, corresponding to a predicted failure stress as high as $42.4\,\mathrm{N\,m^{-1}}$. This result is once again in excellent agreement with the experimental value $42\pm4\,\mathrm{N\,m^{-1}}$, reported in [44]. These values correspond to the failure strength of a two-dimensional system. In order to draw a comparison with bulk materials, we define an effective three-dimensional failure stress $\sigma_{\mathrm{f}}^{3\mathrm{D}} = \sigma_{\mathrm{f}}/d$, where d is taken as the interlayer spacing in graphite. By considering $d = 0.335\,\mathrm{nm}$ [102], we obtain $\sigma_{\mathrm{f}}^{3\mathrm{D}} \cong 130\,\mathrm{GPa}$. This very high value, exceeding that of most materials (even including multi-walled nanotubes [103]), motivates the use of one-atom thick carbon layers as possible reinforcement in advanced composites.

4.7.2. Nonlinear elasticity of graphane. Graphane is the hydrogenated form of graphene; it consists of a two-dimensional, periodic, and covalently bonded hydrocarbon with a C : H ratio of 1 [47, 104, 105]. Since hydrogen atoms can bind to carbon atoms on both the top and bottom side, there are three possible decoration schemes, shown in figure 25, generating an equal number of inequivalent conformers: chair (C-), boat (B-) and washboard (W-) graphane. They all fulfil the characterizing conditions of: (i) 1:1 ratio between carbon and hydrogen atoms; (ii) in-plane translational invariance.

The striking difference of graphane with respect to its mother structure graphene is that hydrogenation causes a change in the orbital hybridization which is now sp^3-like. The actual values of elastic moduli are likely to be affected by this major change in chemical bonding. Furthermore, some graphane conformers are not isotropic, at variance with graphene which is so (in the linear approximation): hydrogenation is expected to dramatically affect the overall mechanical behavior of the system by introducing an anisotropic dependence of its response to an external load. Both features are interesting and worthy of investigation. For both we will take full profit of the methods outlined in the previous sections of this review.

While C-graphane has trigonal symmetry (and, therefore, is elastically isotropic in linear regime as hexagonal graphene), the remaining B- and W-conformers show an orthorhombic symmetry, which causes an anisotropic linear elastic behavior. Accordingly, the linear elastic energy density (per unit of area) accumulated upon strain can be expressed as [57]

$$U_{\mathrm{trigo}} = \tfrac{1}{2}C_{11}(\epsilon_{xx}^2+\epsilon_{yy}^2+2\epsilon_{xy}^2)+C_{12}(\epsilon_{xx}\epsilon_{yy}-\epsilon_{xy}^2) \quad (4.57)$$

for the istropic structures and as

$$U_{\mathrm{ortho}} = \tfrac{1}{2}C_{11}\epsilon_{xx}^2+\tfrac{1}{2}C_{22}\epsilon_{yy}^2+C_{12}\epsilon_{xx}\epsilon_{yy}+2C_{44}\epsilon_{xy}^2 \quad (4.58)$$

for the anisotropic ones. Elastic constants are defined as usual and it must be understood that the small-strain tensor is calculated with reference to the planar displacement $\vec{u} = (u_x, u_y)$. It is important to note that U_{trigo} can be obtained from U_{ortho} by simply imposing the isotropy condition $C_{11} = C_{22}$ and the Cauchy relation $2C_{44} = C_{11} - C_{12}$, holding for both the hexagonal and trigonal symmetry. We will take profit of this by focusing just on the elastic behavior of a system described by equation (4.58); when needed, the general results so obtained will be applied to the isotropic structures by fully exploiting the above conditions. The constitutive in-plane stress–strain equations are straightforwardly derived from equation (4.58): $T_{xx} = C_{11}\epsilon_{xx}+C_{12}\epsilon_{yy}$, $T_{yy} = C_{22}\epsilon_{yy}+C_{12}\epsilon_{xx}$ and $T_{xy} = 2C_{44}\epsilon_{xy}$.

We now apply to whichever conformer an axial tension σ along the arbitrary direction $\vec{n} = \cos\theta\vec{e}_x + \sin\theta\vec{e}_y$, where the angle θ identifies the extension direction with respect to the zigzag one (see figure 23, still holding for graphane). By following a similar procedure as in section 4.7.1, we easily obtain both the longitudinal component

$$\epsilon_l = \sigma\left[\frac{C_{11}}{\Delta}s^4+\frac{C_{22}}{\Delta}c^4+\left(\frac{1}{C_{44}}-2\frac{C_{12}}{\Delta}\right)c^2s^2\right] \quad (4.59)$$

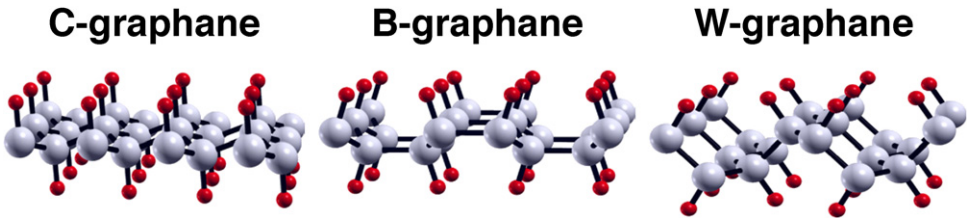

Figure 25. Atomic architecture of the graphane conformers. Gray (red) spheres represent carbon (hydrogen).

Table 4. Graphene and graphane independent elastic constants (units of N m^{-1}). For graphene and C-graphane $C_{11} = C_{22}$ and $2C_{44} = C_{11} - C_{12}$.

	Graphene	C-graphane	B-graphane	W-graphane
C_{11}	354	248	258	280
C_{22}			225	121
C_{12}	60	20	−1.7	14
C_{44}			93	81

and the transverse component

$$\epsilon_t = \sigma\left[\left(\frac{C_{11}+C_{22}}{\Delta} - \frac{1}{C_{44}}\right)c^2s^2 - \frac{C_{12}}{\Delta}\left(c^4+s^4\right)\right] \quad (4.60)$$

of the resulting small-strain tensor along (i.e. longitudinal) or normally to (i.e. transverse) the direction $\vec{n}$ (we set $\Delta = C_{11}C_{22} - C_{12}^2$, $c = \cos\theta$ and $s = \sin\theta$). By means of equations (4.59) and (4.60) we can evaluate, respectively, the θ-dependent Young's modulus

$$E(\theta) = \sigma/\epsilon_l = \frac{\Delta}{C_{11}s^4 + C_{22}c^4 + \left(\frac{\Delta}{C_{44}} - 2C_{12}\right)c^2s^2} \quad (4.61)$$

and the θ-dependent Poisson's ratio

$$\nu(\theta) = -\epsilon_t/\epsilon_l = -\frac{\left(C_{11}+C_{22}-\frac{\Delta}{C_{44}}\right)c^2s^2 - C_{12}\left(c^4+s^4\right)}{C_{11}s^4 + C_{22}c^4 + \left(\frac{\Delta}{C_{44}} - 2C_{12}\right)c^2s^2}. \quad (4.62)$$

Following the same path as for graphene, $E(\theta)$ and $\nu(\theta)$ can be directly obtained by the linear elastic constants C_{ij}, suitably computed through energy versus strain curves for homogeneous in-plane deformations (we refer to [106] for technical details). Table 4 summarizes the numerical results obtained by density functional theory (DFT) as implemented in the Quantum ESPRESSO package [107]. We used such an *ab initio* total energy method since no quantitatively reliable TB or empirical potential models are available for the elasticity of those hydrocarbons here investigated.

We focus on an important new qualitative feature characterizing some graphane conformers, namely, their elastic moduli could depend upon the loading direction. This is shown in figure 26 where we report the polar plots for both Young's modulus (left) and Poisson's ratio (right). It is apparent that graphene and C-graphane are, as expected, characterized by linear elastic moduli independent of θ. On the other hand, it is found that W- and B-graphane are indeed elastically anisotropic, W- being much more anisotropic than the B-conformer. Furthermore, this provides evidence that Poisson's ratio in whichever graphane conformer is much smaller than in pristine graphene. Finally, an intriguing unconventional behavior is observed in figure 26 for B-graphane, namely, for extensions along the zigzag and armchair directions, the corresponding Poisson value is vanishingly small (or even possibly negative, as discussed in [106]).

The intriguing elastic behavior of graphane hydrocarbons is further confirmed by their nonlinear features. The strain energy function U_{trigo} for C-graphane is straightforwardly provided by the continuum theory up to third order in strain

$$\begin{aligned} U_{\text{trigo}} = {} & \tfrac{1}{2}C_{11}(\epsilon_{xx}^2 + \epsilon_{yy}^2 + 2\epsilon_{xy}^2) + C_{12}(\epsilon_{xx}\epsilon_{yy} - \epsilon_{xy}^2) \\ & + \tfrac{1}{6}C_{111}(\epsilon_{xx}^3 + \epsilon_{yy}^3) + \tfrac{1}{2}C_{112}(\epsilon_{xx}^2\epsilon_{yy} + \epsilon_{xx}\epsilon_{yy}^2) \\ & + 2C_{144}(\epsilon_{xx}\epsilon_{xy}^2 + \epsilon_{yy}\epsilon_{xy}^2) + C_{114}(\epsilon_{xx}^2\epsilon_{xy} + \epsilon_{yy}^2\epsilon_{xy}) \\ & + 2C_{124}\epsilon_{xx}\epsilon_{xy}\epsilon_{yy} + \tfrac{4}{3}C_{444}\epsilon_{xy}^3. \end{aligned} \quad (4.63)$$

Although for such a trigonal symmetry $C_{111} = C_{222}$, $C_{112} = C_{122}$ and $C_{144} = C_{244}$, still the overall nonlinear elastic response is truly anisotropic since not all the relevant isotropic conditions are fulfilled. Similarly, the strain energy function U_{ortho} for the B- and W-graphane is given by

$$\begin{aligned} U_{\text{ortho}} = {} & \tfrac{1}{2}C_{11}\epsilon_{xx}^2 + \tfrac{1}{2}C_{22}\epsilon_{yy}^2 + 2C_{44}\epsilon_{xy}^2 + C_{12}\epsilon_{xx}\epsilon_{yy} \\ & + \tfrac{1}{6}C_{111}\epsilon_{xx}^3 + \tfrac{1}{6}C_{222}\epsilon_{yy}^3 + \tfrac{1}{2}C_{112}\epsilon_{xx}^2\epsilon_{yy} \\ & + \tfrac{1}{2}C_{122}\epsilon_{xx}\epsilon_{yy}^2 + 2C_{144}\epsilon_{xx}\epsilon_{xy}^2 + 2C_{244}\epsilon_{yy}\epsilon_{xy}^2. \end{aligned} \quad (4.64)$$

Equations (4.63) and (4.64) can be obtained using the standard tables of the tensor symmetries, found in many crystallography textbooks (see, for instance, [57]). Following our usual protocol, U_{trigo} and U_{ortho} can be computed through energy versus strain curves corresponding to suitable homogeneous in-plane deformations described by just the single parameter ζ:

$$U(\zeta) = U_0 + \tfrac{1}{2}U^{(2)}\zeta^2 + \tfrac{1}{6}U^{(3)}\zeta^3 + O(\zeta^4). \quad (4.65)$$

Since the expansion coefficients $U^{(2)}$ and $U^{(3)}$ are related to elastic constants, as summarized in table 5 for the C-graphane and in table 6 for the B- and W-graphane, a straightforward fit of equation (4.65) can provide the full set of TOECs which are indeed reported in table 7. We also report the graphene moduli for the sake of comparison (these latter are obtained through the *ab initio* method and can also be compared with the corresponding TB results of the previous section).

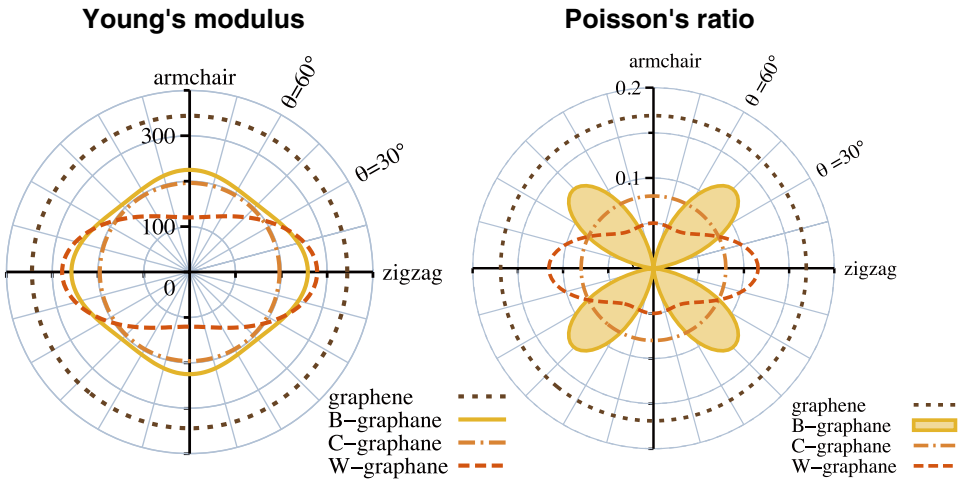

Figure 26. Polar diagram for Young's modulus E (left) in units N m^{-1} and Poisson's ratio (right) of graphene and all graphane conformers. The angle θ identifies the extension direction with respect to the zigzag one. Isotropic (anisotropic) behavior is associated with a circular (non-circular) shape of the polar plot. The special case of B-graphane (as for the Poisson ratio) is highlighted by shading.

Table 5. Strain fields applied to compute the linear (C_{ij}) and nonlinear (C_{ijk}) elastic constants of C-graphane. The relation between such constants and the fitting terms $U^{(2)}$ and $U^{(3)}$ of equation (4.65) is reported as well.

Uniform strain	$U^{(2)}$	$U^{(3)}$
$\begin{pmatrix}\zeta & 0\\ 0 & 0\end{pmatrix}$	C_{11}	C_{111}
$\begin{pmatrix}\zeta & 0\\ 0 & \zeta\end{pmatrix}$	$2\,(C_{11}+C_{12})$	$2C_{111}+6C_{112}$
$\begin{pmatrix}0 & \zeta\\ \zeta & 0\end{pmatrix}$	$2\,(C_{11}-C_{12})$	$8C_{444}$
$\begin{pmatrix}\zeta & \zeta\\ \zeta & 0\end{pmatrix}$	$3C_{11}-2C_{12}$	$C_{111}+12C_{144}+6C_{114}+8C_{444}$
$\begin{pmatrix}0 & \zeta\\ \zeta & -\zeta\end{pmatrix}$	$3C_{11}-2C_{12}$	$-C_{111}-12C_{144}+6C_{114}+8C_{444}$
$\begin{pmatrix}\zeta & \zeta\\ \zeta & -\zeta\end{pmatrix}$	$4\,(C_{11}-C_{12})$	$12C_{114}-12C_{124}+8C_{444}$

We note that $C_{111} < C_{222}$ for graphene and $C_{222} > C_{111}$ for B-graphane or, equivalently, graphene and B-graphane are characterized by an inverted anisotropy. In contrast, W-graphane has the same anisotropy of graphene ($C_{111} < C_{222}$), but a larger $|C_{111} - C_{222}|$ difference. This means that the different distribution of hydrogen atoms can induce strong qualitative variations for the nonlinear elastic behavior of the different conformers. We note that necessarily $C_{444} = 0$ in B- and W-graphane because of the orthorhombic symmetry. On the other hand, this nonlinear shear modulus could assume any value for the trigonal lattice. Interestingly enough, we have verified that $C_{444} = 0$ also for C-graphane. This is due to the additional (with respect to the trigonal symmetry) mirror symmetry of C-graphane.

Similarly to the case of graphene, an effective direction-dependent nonlinear stress-strain relation can also be derived for the three graphane conformers, having the same form given in equation (4.52) with $E = E(\theta)$ taken from equation (4.61).

Table 6. Strain fields applied to compute the linear (C_{ij}) and nonlinear (C_{ijk}) elastic constants of the B- and W-graphane. The relation between such constants and the fitting terms $U^{(2)}$ and $U^{(3)}$ of equation (4.65) is reported as well.

Uniform strain	$U^{(2)}$	$U^{(3)}$
$\begin{pmatrix}\zeta & 0\\ 0 & 0\end{pmatrix}$	C_{11}	C_{111}
$\begin{pmatrix}0 & 0\\ 0 & \zeta\end{pmatrix}$	C_{22}	C_{222}
$\begin{pmatrix}\zeta & 0\\ 0 & \zeta\end{pmatrix}$	$C_{11}+C_{22}+2C_{12}$	$C_{111}+C_{222}+3C_{112}+3C_{122}$
$\begin{pmatrix}0 & \zeta\\ \zeta & 0\end{pmatrix}$	$4C_{44}$	0
$\begin{pmatrix}\zeta & \zeta\\ \zeta & 0\end{pmatrix}$	$C_{11}+4C_{44}$	$C_{111}+12C_{144}$
$\begin{pmatrix}0 & \zeta\\ \zeta & \zeta\end{pmatrix}$	$C_{22}+4C_{44}$	$C_{222}+12C_{244}$
$\begin{pmatrix}\zeta & 0\\ 0 & -\zeta\end{pmatrix}$	$C_{11}+C_{22}-2C_{12}$	$C_{111}-C_{222}-3C_{112}+3C_{122}$

The nonlinear elastic modulus $D_{\vec{n}}^{(\mathrm{trigo})}$ for the C-graphane (as well as for any trigonal 2D lattice) is given by [106]

$$\begin{aligned}D_{\vec{n}}^{(\mathrm{trigo})} = \tfrac{1}{2}\big[&\nu\,(1-\nu)\,(C_{111}-3C_{112})\\ &+(1-\nu)\left(1+\nu^2\right)C_{111}\\ &+6cs\,(1+\nu)\left(1+\nu^2\right)C_{114}-12cs\,(1+\nu)\,\nu C_{124}\\ &+3c^2s^2\,(1-\nu)\left(1+\nu^2\right)(-C_{111}+4C_{144}+C_{112})\\ &+4c^3s^3\,(1+\nu)\left(1+\nu^2\right)(-3C_{114}+2C_{444}+3C_{124})\\ &+8c^3s^3\,(1+\nu)\,\nu\,(-6C_{114}+5C_{444}+6C_{124})\big],\end{aligned} \tag{4.66}$$

while the corresponding modulus $D_{\vec{n}}^{(\mathrm{ortho})}$ for B- and W-graphane is

$$\begin{aligned}D_{\vec{n}}^{(\mathrm{ortho})} = \frac{1}{2\Delta^3 E_{\vec{n}}^3}\big[&C_{111}(C_{22}c^2-C_{12}s^2)^3\\ &+C_{222}(C_{11}s^2-C_{12}c^2)^3\end{aligned}$$

Table 7. Graphene and graphane independent nonlinear elastic constants (units of Nm^{-1}).

	Graphene	C-graphane	B-graphane	W-graphane
C_{111}	-1910 ± 11	-1385 ± 18	-1609 ± 31	-1756 ± 33
C_{222}	-1764 ± 3		-1827 ± 7	-487 ± 85
C_{112}	-341 ± 35	-195 ± 41	-20 ± 14	-75 ± 54
C_{122}			-55 ± 22	-296 ± 36
C_{124}		-411 ± 17		
C_{114}		530 ± 12		
C_{144}		568 ± 7	-161 ± 4	-143 ± 17
C_{244}			-159 ± 3	-287 ± 10
C_{444}		0.0 ± 10^{-5}		

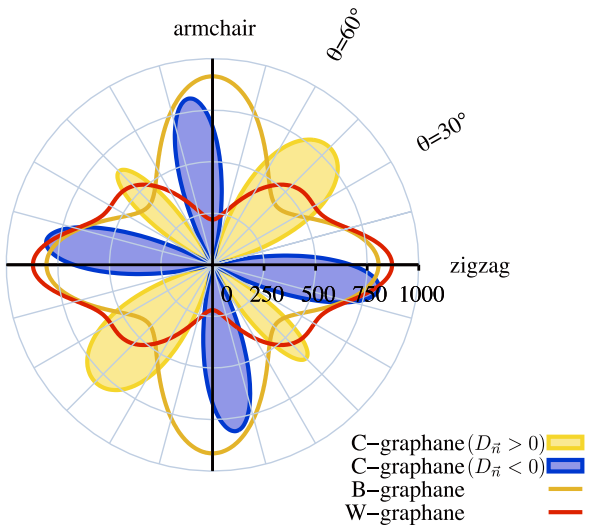

Figure 27. Polar representation of the nonlinear elastic moduli $D_{\vec{n}}$ of the three graphane conformers. In the B- and W-graphane cases, $D_{\vec{n}} \equiv D$ are everywhere negative (softening hyperelasticity), while in the C-graphene one the $D_{\vec{n}}$ alternates negative and positive values (hardening hyperelasticity).

$$
\begin{aligned}
&+3C_{112}(C_{11}s^2 - C_{12}c^2)(C_{22}c^2 - C_{12}s^2)^2 \\
&+3C_{122}(C_{22}c^2 - C_{12}c^2)(C_{11}s^2 - C_{12}c^2)^2 \\
&-3C_{166}c^2s^2(C_{22}c^2 - C_{12}s^2)(\Delta/C_{44})^2 \\
&-3C_{266}c^2s^2(C_{11}s^2 - C_{12}c^2)(\Delta/C_{44})^2\big]. \qquad (4.67)
\end{aligned}
$$

They are shown in figure 27 as a function of θ.

Since all $C_{ijk} < 0$, as shown in table 7, $D_{\vec{n}}^{(\mathrm{ortho})}$ are negative for stretching along any direction and, correspondingly, B- and W-graphane are characterized by a hyperelastic softening behavior. The trigonal C-graphane behaves in a very different way. Since the C_{114} and C_{144} are positive, a hyperelastic hardening behavior in the angular sectors $5/12\pi + k\pi < \theta < 1/12 + k\pi$ and $8/12\pi + k\pi < \theta < 10/12 + k\pi$ ($k \epsilon \mathbb{Z}$) is, in fact, predicted. We can conclude that C-graphane admits both softening and hardening hyperelasticity, depending on the direction of the applied strain. This unusual nonlinear property makes graphane a very intriguing material with potentially large technological impact in nanomechanics.

5. Conclusions

5.1. Synopsis of the key concepts and main results discussed in this review

This review was basically organized into two parts.

In the first part we briefly outlined the elementary continuum theory of elasticity in the small deformation regime. The resulting framework formally defined the strain energy function and the constitutive equation for any arbitrary nonlinear elastic material. Nevertheless, such a continuum picture was recognized to be inherently unable to exploit the real atomic-scale structure of condensed matter and, therefore, unable to predict important length-scale phenomena in nanostructured systems.

The next part was devoted to a major conceptual step, namely, blending continuum and atomistic theories. We have, in particular, elaborated an elastic lattice model designed (i) to map continuum elasticity onto a discrete lattice; (ii) to introduce the notion of interatomic distance which, in turn, naturally drives to the notion of length scale and, therefore, to the possible onset of scale effects and (iii) to cast any arbitrary (either linear or nonlinear) continuum constitutive law in the form of a suitable atomic interaction potential, eventually put at work on the above lattice.

This two-step procedure has been extensively applied to investigate several key issues in the theory of the elastic response of nanostructured materials, namely:

- *nonlinearity*; since the Eshelby model is affordable by continuum methods for a few selected combinations of nonlinear matrix or inhomogeneity, we applied the elastic lattice model for investigating several heterogeneous structures, taking into account any such combinations found in real composite materials.
- *scale effects*; we provided evidence of some elastic features falling out of reach of continuum theory, typically when the nanostructure displays at a length scale smaller 10 nm. This length scale can be therefore assumed as the lower boundary for continuum theory. We have also verified the emergence of some power laws and their universality, driving the scale effects in the range 5–60 Å. In our approach, no educated guess on the actual constitutive behavior for the interface (or nonlocal continuum model) is assumed. Rather, we have directly deduced the scale effects from atomic-scale features. In other words, the sale effects we have observed are directly related to the discretization of the mass on the real atomic lattice.
- *correspondence between nanoscale structure and elastic moduli*; the lattice model was defined through a set of interatomic parameters, predicting the macroscopic behavior on the basis of linear and nonlinear elastic moduli. We have obtained the universal relations providing the *analysis* of the linear and nonlinear behavior of a lattice with a given set of parameters, namely, the determination of the macroscopic elastic constants when the interatomic parameters are given. On the other hand, we have also provided the *synthesis* of the lattice with an

arbitrary desired elastic behavior, namely, the design or the determination of the interatomic parameters starting from the macroscopic elastic behavior. This approach has been developed for a two-dimensional triangular lattice (but several generalizations are straightforward).

- *scaling exponent*; we have proved that linear and nonlinear scale effects are described by the same scaling exponent, independently of the elastic contrast. This suggests that the overall strain or stress field within an inhomogeneity can be described by a similar power law with a universal scaling exponent.
- *evaluation of linear and nonlinear elastic moduli*; for specific complex materials promising new properties of possibly large technological impact. We have described the case of graphene and its hydrogenated conformers. In particular, we have shown that B-graphane has a vanishingly small (possibly negative) Poisson's ratio along the armchair and zigzag principal directions (axially auxetic elastic behavior). Moreover, we observed that C-graphane admits both softening and hardening hyperelasticity, depending on the direction of applied load.

5.2. *Perspective on possible future research directions*

While this review presented quite a few situations of paradigmatic importance and some conclusions valid for most nanomaterials, several issues worthy of investigation still remain open.

To begin, we take in consideration once again the Eshelby theory for nonlinear particles embedded in a linear matrix. In this review we have limited the treatment of nonlinear features to the second order in strain. As a matter of fact, it is possible to extend the theory to any order of nonlinearity, an issue of formal relevance. Moreover, while we have only shown the results for spherically shaped inhomogeneities, the Eshelby method could be generalized (indeed a non-trivial task) to arbitrarily shaped (in general, ellipsoidal) nanoparticles, thus approaching some important configuration of technological relevance, e.g. the one corresponding to fiber-reinforced nanomaterials. Finally, the classical Eshelby theory can be used to investigate an inhomogeneity with a different shape than the hosting cavity; in this configuration a prestrain is generated in order to create the perfect bonding between the external surface of the particle and the internal surface of the cavity.

Another important open problem that should be taken into consideration by continuum theory is the Eshelby configuration with a nonlinear matrix, a situation that, to the best of the author's knowledge, has not yet been investigated. This case can be most likely solved only numerically, for example with the lattice model discussed in the present review. Finally, the continuum theory should be extended in order to consider nanostructured materials undergoing large deformations (such as complex elastomers): in fact, L–NL and NL–NL problems (see section 1.1) are relevant for several applications as, for instance, nondestructive testing of materials and ultrasound techniques, where finite deformations and corresponding stress states can influence wave propagation and hence interpretation of data. Modeling wave propagation in biological materials is also important in ultrasound techniques and biological soft tissues are often in a largely deformed state due to growth and remodeling.

As for atomistic modeling, an obvious step forward with respect to the present review consists of the generalization of our consititutive force field approach to three-dimensional lattices (at least for those ones characterized by high symmetry). The extension to amorphous structures is also useful for many applications. In particular, the results of the analysis and synthesis approach can be straightforwardly extended to both crystalline or amorphous structures such as nanocomposites, polycrystals and multi-layered systems. Atomistic modeling could be particularly important for investigating the elastic properties of nonideal or tailor-structured interfaces.

Another important direction for future investigation is that of including into atomistic models the coupling among different physical fields. As a matter of fact, there is a large interest in determining the magnetic, electric and elastic fields in composite structures with piezoelectric and magnetoelastic phases. Typically, such heterogeneous materials are assembled at the nanoscale and, therefore, the method based on constitutive force fields is very promising. The coupling between the elastic and thermal fields is important as well, especially in technological applications where a large range of temperatures must be taken into account. Therefore, the generalization of the discussed atomistic models to finite temperature defines yet another different research enterprise.

Acknowledgments

The authors acknowledge computational support by CYBERSAR (Cagliari, Italy) and CASPUR (Roma, Italy) supercomputing centers. They also acknowledge financial support by 'Regione Autonoma della Sardegna (RAS)' under project 'Modellazione Multiscala della Meccanica dei Materiali Compositi (M4C)'. SG acknowledges financial support by Fondation Centrale Initiatives under project 'Continuum approach for studying the static and dynamic behavior of piezo-magneto-elastic composite materials'.

References

[1] Moriarty P 2001 Nanostructured materials *Rep. Prog. Phys.* **64** 297–381
[2] Gleiter H 2000 Nanostructured materials: basic concepts and microstructure *Acta Mater.* **48** 1–29
[3] Konstantatos G and Sargent E H 2010 Nanostructured materials for photon detection *Nature Nanotechnol.* **5** 391–400
[4] Aricò A S, Bruce P, Scrosati B, Tarascon J M and Van Schalkwijk W 2005 Nanostructured materials for advanced energy conversion and storage devices *Nature Mater.* **4** 366–77
[5] Sahimi M 2003 *Heterogeneous Materials I, Linear Transport and Optical Properties* (New York: Springer)
[6] Sahimi M 2003 *Heterogeneous Materials II, Nonlinear and Breakdown Properties and Atomistic Modeling* (New York: Springer)
[7] Atkin R J and Fox N 1980 *An Introduction to the Theory of Elasticity* (New York: Dover)

[8] Novozhilov V V 1999 *Foundations of the Nonlinear Theory of Elasticity* (New York: Dover)
[9] Gurtin M E 1981 *An Introduction to Continuum Mechanics* (New York: Academic)
[10] Gurtin M E 1983 *Topics in Finite Elasticity* (Philadelphia: SIAM)
[11] Love A E H 2002 *A Treatise on the Mathematical Theory of Elasticity* (New York: Dover)
[12] Graff K F 1991 *Wave Motion in Elastic Solids* (New York: Dover)
[13] Broberg K B 1999 *Cracks and Fracture* (London: Academic)
[14] Hirth J P and Lothe J 1991 *Theory of Dislocations* (Malabar, FL: Krieger)
[15] Mura T 1987 *Micromechanics of Defects in Solids* (Dordrecht: Kluwer)
[16] Asaro R J and Lubarda V A 2006 *Mechanics of Solids and Materials* (Cambridge: Cambridge University Press)
[17] Landau L D and Lifschitz E M 1986 *Theory of Elasticity* (Oxford: Butterworth Heinemann)
[18] Amenzade Y A 1979 *Theory of Elasticity* (Moscow: MIR)
[19] Den Hartog J P 1987 *Advanced Strength of Materials* (New York: Dover)
[20] Lubliner J 1998 *Plasticity Theory* (New York: Macmillan)
[21] Frenkel D and Smit B 2002 *Understanding Molecular Simulation* (London: Academic)
[22] Finnis M 2003 *Interatomic Forces in Condensed Matter* (Oxford: Oxford University Press)
[23] Eshelby J D 1957 The determination of the elastic field of an ellipsoidal inclusion and related problems *Proc. R. Soc. Lond.* A **241** 376–96
[24] Eshelby J D 1959 The elastic field outside an ellipsoidal inclusion *Proc. R. Soc. Lond.* A **252** 561–9
[25] Eshelby J D 1961 Elastic inclusions and inhomogeneities *Progress in Solid Mechanics* vol 2, ed I N Sneddon and R Hill (Amsterdam: North-Holland) pp 89–140
[26] Xiao S and Belytschko T 2004 A bridging domain method for coupling continua with molecular dynamics *Comput. Methods Appl. Mech. Eng.* **193** 1645–69
[27] Li X and W. E 2005 Multiscale modeling of the dynamics of solids at finite temperature *J. Mech. Phys. Solids* **53** 1650–85
[28] Ghoniem N M, Busso E P, Kioussis N and Huang H 2003 Multiscale modeling of nano and micro-mechanics: an overview *Phil. Mag.* **83** 3475–528
[29] Miller R E and Tadmor E B 2002 The quasicontinuum method: overview, applications and current directions *J. Comput.-Aided Mater. Des.* **9** 203–39
[30] Sharma P and Ganti S 2002 Interfacial elasticity corrections to the elastic state of quantum dots *Phys. Status Solidi* b **234** R10
[31] Yang M, Sturm J C and Prevost J 1997 Calculation of band alignments and quantum confinement effects in zero- and one-dimensional pseudomorphic structures *Phys. Rev.* B **56** 1973–80
[32] Zhang X and Sharma P 2005 Size dependency of strain in arbitrary shaped, anisotropic embedded quantum dots due to nonlocal dispersive effects *Phys. Rev.* B **72** 195345
[33] Sharma P and Ganti S 2004 Size-dependent Eshelby's tensor for embedded nano-inclusions incorporating surface/interface energies *J. Appl. Mech.* **71** 663–71
[34] Sharma P, Ganti S and Bhate N 2003 The effect of surfaces on the size-dependent elastic state of (nano) inhomogeneities *Appl. Phys. Lett.* **82** 535–7
[35] Suresh S 2001 Graded materials for resistance to contact deformation and damage *Science* **292** 2447–51
[36] Lin D S, Wu J L, Pan S Y and Chiang T C 2003 Atomistics of Ge deposition on Si(1 0 0) by atomic layer epitaxy *Phys. Rev. Lett.* **90** 046102
[37] Hwang H Y 2006 Tuning interface states *Science* **313** 1895–6
[38] Erdélyi Z, Sladecek M, Stadler L M, Zizak I, Langer G A, Kis-Varga M, Beke D L and Sepiol B 2004 Transient interface sharpening in miscible alloys *Science* **306** 1913–5
[39] Bertoldi K, Bigoni D and Drugan W J 2007 Structural interfaces in linear elasticity: I. Nonlocality and gradient approximations *J. Mech. Phys. Solids* **55** 1–34
[40] Bertoldi K, Bigoni D and Drugan W J 2007 Structural interfaces in linear elasticity: II. Effective properties and neutrality *J. Mech. Phys. Solids* **55** 35–63
[41] Christensen R M 2005 *Mechanics of Composite Materials* (New York: Dover)
[42] Ajayan P M, Schadler L S and Braun P V 2003 *Nanocomposite Science and Technology* (Weinheim: Wiley-VCH)
[43] Giordano S 2003 Differential schemes for the elastic characterization of dispersions of randomly oriented ellipsoids *Eur. J. Mech. A/Solids* **22** 885–902
[44] Lee C, Wei X, Kysar J W and Hone J 2008 Measurement of the elastic properties and intrinsic strength of monolayer graphene *Science* **321** 385–8
[45] Cocco G, Cadelano E, Colombo L 2010 Gap opening in graphene by shear strain *Phys. Rev.* B **81** 241412(R)
[46] Cadelano E, Giordano S and Colombo L 2010 Interplay between bending and stretching in carbon nanoribbons *Phys. Rev.* B **81** 144105
[47] Elias D C *et al* 2009 Control of graphene's properties by reversible hydrogenation: evidence for graphane *Science* **323** 610–13
[48] Marsden J E and Thomas J R 1983 *Mathematical Foundations of Elasticity* (New York: Dover)
[49] Goldstein H 1959 *Classical Mechanics* (London: Addison-Wesley)
[50] Polizzotto C 2001 Nonlocal elasticity and related variational principles *Int. J. Solids Struct.* **38** 7359–80
[51] Triantafyllidis N and Bardenhagen S 1996 The influence of scale size on the stability of periodic solids and the role of associated higher order gradient continuum models *J. Mech. Phys. Solids* **44** 1891–928
[52] Lam D C C, Yang F, Chong A C M, Wang J and Tong P 2003 Experiments and theory in strain gradient elasticity *J. Mech. Phys. Solids* **51** 1477–508
[53] Ciarletta M and Iesan D 1993 *Non-Classical Elastic Solids* (Harlow: Longman Scientific and Technical)
[54] Giordano S, Palla P L and Colombo L 2008 Nonlinear elastic Landau coefficients in heterogeneous materials *Eur. Phys. Lett.* **83** 66003
[55] Giordano S, Palla P L and Colombo L 2009 Nonlinear elasticity of composite materials *Eur. Phys. J.* B **68** 89–101
[56] Nye J F 1985 *Physical Properties of Crystals* (Oxford: Oxford University Press)
[57] Huntington H B 1958 *The Elastic Constants of Crystals* (New York: Academic)
[58] Giordano S, Mattoni A and Colombo L 2011 Brittle fracture: from elasticity theory to atomistic simulations *Rev. Comput. Chem.* **27** 1–83
[59] Palla P L, Giordano S and Colombo L 2010 Lattice model describing scale effects in nonlinear elasticity of nanoinhomogeneities *Phys. Rev.* B **81** 214113
[60] Palla P L, Giordano S and Colombo L 2008 Interfacial elastic properties of *a*-Si and *c*-Si *Phys. Rev.* B **78** 012105
[61] Palla P L, Giordano S and Colombo L 2009 The role of interface elasticity in nanostructured silicon *Phys. Rev.* B **80** 054105
[62] Schnabel T, Vrabec J and Hasse H 2007 Unlike Lennard-Jones parameters for vapor-liquid equilibria *J. Mol. Liq.* **135** 170–8
[63] Duan H L, Wang J, Huang Z P and Karihaloo B L 2005 Size-dependent effective elastic constants of solids

containing nano-inhomogeneities with interface stress *J. Mech. Phys. Solids* **53** 1574–96
[64] Duan H L, Wang J, Huang Z P and Luo Z Y 2005 Stress concentration tensors of inhomogeneities with interface effects *Mech. Mater.* **37** 723–36
[65] Duan H L, Yi X, Huang Z P and Wang J 2007 A unified scheme for prediction of effective moduli of multiphase composites with interface effects: I. Theoretical framework *Mech. Mater.* **39** 81–93
[66] Duan H L, Yi X, Huang Z P and Wang J 2007 A unified scheme for prediction of effective moduli of multiphase composites with interface effects: II. Application and scaling laws *Mech. Mater.* **39** 94–103
[67] Duan H L, Wang J, Huang Z P and Karihaloo B L 2005 Eshelby formalism for nano-inhomogeneities *Proc. R. Soc. Lond.* A **461** 3335–53
[68] Duan H L, Wang J and Karihaloo B L 2009 Theory of elasticity at the nano-scale *Adv. Appl. Mech.* **42** 1–68
[69] Duan H L, Karihaloo B L, Wang J and Yi X 2006 Strain distributions in nano-onions with uniform and non-uniform compositions *Nanotechnology* **17** 3380–7
[70] Duan H L, Karihaloo B L, Wang J and Yi X 2006 Compatible composition profiles and critical sizes of alloyed quantum dots *Phys. Rev.* B **74** 195328
[71] Gurtin M E and Murdoch A I 1975 A continuum theory of elastic material surfaces *Arch. Ration. Mech. Anal.* **57** 291–323
[72] Gurtin M E and Murdoch A I 1978 Surface stress in solids *Int. J. Solids Struct.* **14** 431-440
[73] Eringen A C 2002 *Non-Local Continuum Field Theories* (New York: Springer)
[74] Wang J, Duan H L, Huang Z P and Karihaloo B L 2006 A scaling law for properties of nano-structured materials *Proc. R. Soc. Lond.* A **462** 1355–63
[75] Giordano S 2005 Disordered lattice networks: general theory and simulations *Int. J. Circ. Theor. Appl.* **33** 519–40
[76] Giordano S 2007 Two-dimensional disordered lattice networks with substrate *Physica* A **375** 726–40
[77] Giordano S 2007 Relation between microscopic and macroscopic mechanical properties in random mixtures of elastic media *J. Eng. Mater. Technol.* **129** 453–61
[78] Hughes D S and Kelly J L 1953 Second-order elastic deformation of solids *Phys. Rev.* **92** 1145–9
[79] Bateman T, Mason W P and McSkimin H J 1961 Third-order elastic moduli of germanium *J. Appl. Phys.* **32** 928–36
[80] Cain T and Ray J R 1988 Third-order elastic constants from molecular dynamics: theory and an example calculation *Phys. Rev.* B **38** 7940–6
[81] Zhao J, Winey J M and Gupta Y M 2007 First-principles calculations of second- and third-order elastic constants for single crystals of arbitrary symmetry *Phys. Rev.* B **75** 094105
[82] Novoselov K S, Jiang D, Schedin F, Booth T J, Khotkevich V V, Morozov S V and Geim A K 2005 Two-dimensional atomic crystals *Proc. Natl. Acad. Sci. USA* **102** 10451–3
[83] Sahin H, Cahangirov S, Topsakal M,Bekaroglu E, Akturk E, Senger R T and Ciraci S 2009 Monolayer honeycomb structures of group-IV elements and III–V binary compounds: first-principles calculations *Phys. Rev.* B **80** 155453
[84] Zhi C, Bando Y, Tang C, Kuwahara H and Golberg D 2009 Large-scale fabrication of boron nitride nanosheets and their utilization in polymeric composites with improved thermal and mechanical properties *Adv. Mater* **21** 2889–93
[85] Lee C, Li Q, Kalb W, Liu X-L, Berger H, Carpick R W and Hone J 2010 Frictional characteristics of atomically thin sheets *Science* **328** 76–80
[86] March N H and Rubio A 2011 Structural and electronic properties of low-dimensional C-nanoassemblies and possible analogues for Si (and Ge) *J. Nanomater.* **2011** 932350
[87] Coleman J N *et al* 2011 Two-dimensional nanosheets produced by liquid exfoliation of layered materials *Science* **331** 568–71
[88] Dimiev A, Kosynkin D V, Sinitskii A, Slesarev A, Sun Z, Tour J M 2011 Layer-by-layer removal of graphene for device patterning *Science* **331** 1168–72
[89] Kotakoski J, Krasheninnikov A V, Kaiser U and Meyer J C 2011 From point defects in graphene to two-dimensional amorphous carbon *Phys. Rev. Lett.* **106** 105505
[90] Wu Y H, Yu T and Shen Z X 2010 Two-dimensional carbon nanostructures: fundamental properties, synthesis, characterization, and potential applications *J. Appl. Phys.* **108** 071301
[91] Gómez-Navarro C, Burghard M and Kern K 2008 Elastic properties of chemically derived single graphene sheets *Nano Lett.* **8** 2045–9
[92] Cadelano E, Palla P L, Giordano S and Colombo L 2009 Nonlinear elasticity of monolayer graphene *Phys. Rev. Lett.* **102** 235502
[93] Colombo L 2005 Tight-binding molecular dynamics: a primer *Riv. Nuovo Cimento* **28** 1–59
[94] Xu C H, Wang C Z, Chan C T and Ho K M 1992 A transferable tight-binding potential for carbon *J. Phys.: Condens. Matter* **4** 6047–54
[95] Wei X, Fragneaud B, Marianetti C A and Kysar J W 2009 Nonlinear elastic behavior of graphene: *ab initio* calculations to continuum description *Phys. Rev.* B **80** 205407
[96] Michel K H and Verberck B 2008 Theory of the elastic constants of graphite and graphene *Phys. Status. Solidi.* b **245** 2177–80
[97] Kudin K N, Scuseria E and Yakobson B I 2001 C_2F, BN, and C nanoshell elasticity from *ab initio* computations *Phys. Rev.* B **64** 235406
[98] Liu F, Ming P and Li J 2007 *Ab initio* calculation of ideal strength and phonon instability of graphene under tension *Phys. Rev.* B **76** 064120
[99] Gui G, Li J and Zhong J 2008 Band structure engineering of graphene by strain: first-principles calculations *Phys. Rev.* B **78** 075435
[100] Senchez-Portal D, Artacho E, Soler J M, Rubio A and Ordejen P 1999 *Ab initio* structural, elastic and vibrational properties of carbon nanotubes *Phys. Rev.* B **59** 12678
[101] Zhou G, Duan W, Gu B 2001 First-principles study on morphology and mechanical properties of single-walled carbon nanotube *Chem. Phys. Lett.* **333** 344–9
[102] Al-Jishi R and Dresselhaus G 1982 Lattice-dynamical model for graphite *Phys. Rev.* B **26** 4514–22
[103] Peng B, Locascio M, Zapol P, Li S, Mielke S L, Schatz G C and Espinosa H D 2008 Measurements of near-ultimate strength for multiwalled carbon nanotubes and irradiation-induced crosslinking improvements *Nature Nanotechnol.* **3** 626–31
[104] Sofo J O, Chaudhari A S, and Barber G D 2007 Graphane: a two-dimensional hydrocarbon *Phys. Rev.* B **75** 153401
[105] Boukhvalov D W, Katsnelson M I, and Lichtenstein A I 2008 Hydrogen on graphene: electronic structure, total energy, structural distortions and magnetism from first-principles calculations *Phys. Rev.* B **77** 035427
[106] Cadelano E, Palla P L, Giordano S and Colombo L 2010 Elastic properties of hydrogenated graphene *Phys. Rev.* B **82** 235414
[107] Giannozzi P *et al* 2009 Quantum ESPRESSO: a modular and open-source software project for quantum simulations of materials *J. Phys.: Condens. Matter* **21** 395502